EULER-LAGRANGE MODELING OF DISPERSED GAS-LIQUID REACTORS

Dissertation

to obtain the academic degree of "Doktor der technischen Wissenschaften"

at the Graz University of Technology

by Radompon Sungkorn, MSc

Graz, March 2011

Institute for Process and Particle Engineering

Graz University of Technology

Graz, Austria

Radompon Sungkorn

Euler-Lagrange modeling of dispersed gas-liquid reactors

Dissertation

First assessor and Supervisor

Univ.-Prof. Dipl.-Ing. Dr.techn. Johannes G. Khinast

Institute for Process and Particle Engineering

Graz University of Technology

and

Research Center Pharmaceutical Engineering GmbH

Second assessor

Univ.-Prof. Dipl.-Ing. Dr.techn. Christoph Herwig

Institute of Chemical Enigneering

Division Biochemical Engineering

Vienna University of Technology

Co-Supervisor

Prof. Dr. Jos Derksen

Department of Chemical and Materials Engineering

University of Alberta

EIDESSTATTLICHE ERKLÄRUNG

Ich erkläre an Eides statt, dass ich die vorliegende Arbeit selbstständig verfasst, andere als die angegebenen Quellen/Hilfsmittel nicht benutzt, und die den benutzten Quellen wörtlich und inhaltlich entnommene Stellen als solche kenntlich gemacht habe.

Graz, am …………………… …………………………………………..

(Unterschrift)

STATUTORY DECLARATION

I declare that I have authored this thesis independently, that I have not used other than the declared sources / resources, and that I have explicitly marked all material which has been quoted either literally or by content from the used sources.

…………………………… …………………………………………..

date (signature)

To my parents

แด่ ป๊า ม๊า และ น้องเฟิร์น

CONTENTS

ABSTRACT

Large variety of processes in chemical and biochemical industries involve with dispersion of gas into a continuous liquid phase. A thoroughly understanding of the underlying physics is necessary for design, optimization and scale-up of such processes. This understanding can lead to increases in process performance, improvement of safety, reduction of cost as well as reduction of environmental impact.

Computational fluid dynamics (CFD) is an attractive alternative to gain insights into these processes. An attempt has been made in this thesis to explore the feasibility of using CFD for engineering of high performance gas-liquid reactors. Approaches based on elementary physics principles were employed in the simulations such that they can be used for a wide range of reactor scales. Furthermore, it is becoming clear that multiple-processors computing hardware will set the standard of scientific computing, either in academia or in industry. Hence, parallel computational potential was also an important criterion in choosing the approaches. The goal of this thesis is to enable large-scale simulations with a sophisticated level of accuracy and reasonable computational time.

The capability of the presented modeling technique was explored by validating against cases ranging from simple (e.g., a bubble column operating in dilute dispersion regime) to complex underlying physics (e.g., a gas-liquid stirred reactor). In addition, simplifications and assumptions have been made to be able to model an extremely complex gas-liquid flow in a stirred reactor with pseudoplastic liquids. Detailed information of flow hydrodynamics as well as evolution of the dispersed phase has been achieved.

This thesis contributes to establishing the framework for high-fidelity, high-parallel performance modeling of gas-liquid flows in industrial-relevant scale reactors. The presented modeling technique also provides great flexibility with respect to incorporating models for additional phenomena or to improving its accuracy.

ACKNOWLEDGEMENT

1

INTRODUCTION TO GAS-LIQUID FLOW MODELING

1.1   Introduction

Many processes in chemical and biochemical industries involve with dispersion of gas into a continuous liquid phase. Typical examples include industrial hydrogenations or oxidization, as well as aerobic fermentation processes. One of the most challenging tasks, for example, in biotechnological process, is to create adequate liquid mixing with large interfacial contact while avoiding shear damage on microorganisms cause by hydrodynamic effects (Gogate et al., 2000; Arlov et al., 2008).

Bubble columns or stirred reactors are typically used in these processes. The phenomena encountered in these reactors are highly complex. In a single liquid-phase stirred reactor, the flow structure are known to be highly complex associated with time-dependent, three-dimensional phenomena covering a wide range of spatiotemporal scales (Derksen & Van den Akker, 1999). The complexity increases drastically when a gas phase is introduced to the process. Additional effects include the interaction between phases in terms of mass, energy and momentum exchange, the interaction between the second phase and the reactor (e.g., the impeller), and bubble breakage and coalescence. A detailed knowledge concerning hydrodynamics of the continuous liquid phase and the evolution of the dispersed phase may lead to increases of performance, improvement of safety, reduction in cost and reduction in environmental impact.

Traditionally, engineering of gas-liquid dispersed flows is based on empirical correlations derived from experiments. The information obtained from this approach is typically described in global parametric form and applicable within a narrow window of geometry configurations and operating conditions. Computational fluid dynamics (CFD) is being widely perceived as an attractive alternative to gain a detailed insight into such processes. Significant progress has been made over the last decades in fields of turbulence and multiphase flow modeling, numerical methods as well as computing hardware. Consequently, time-dependent, three-dimensional simulations of gas-liquid dispersed flows with a sophisticated level of detail and accuracy are feasible today.

1.2 Gas-Liquid Flows Modeling

Gas-liquid flows can be roughly classified as dispersed flows, mixed flows and separated flows (Ishii, 1975). In the first regime, one discontinuous phase is dispersed in another continuous phase, e.g., bubbly flows. Dispersed flows presented in a number of industrially important reactors including bubble column and stirred reactors (Ranade, 2002). In separated flow regime, both phases appear in a semi-continuous mode with interfaces between the different phases, e.g., film flow, annular flow and jet flow. In the last regime, dispersed particles as well as semi-continuous interface coexist. Examples of flows in this regime include droplet annular flow where liquid flows in the form of an annular film and, at the same time, suspended droplets in the gas core.
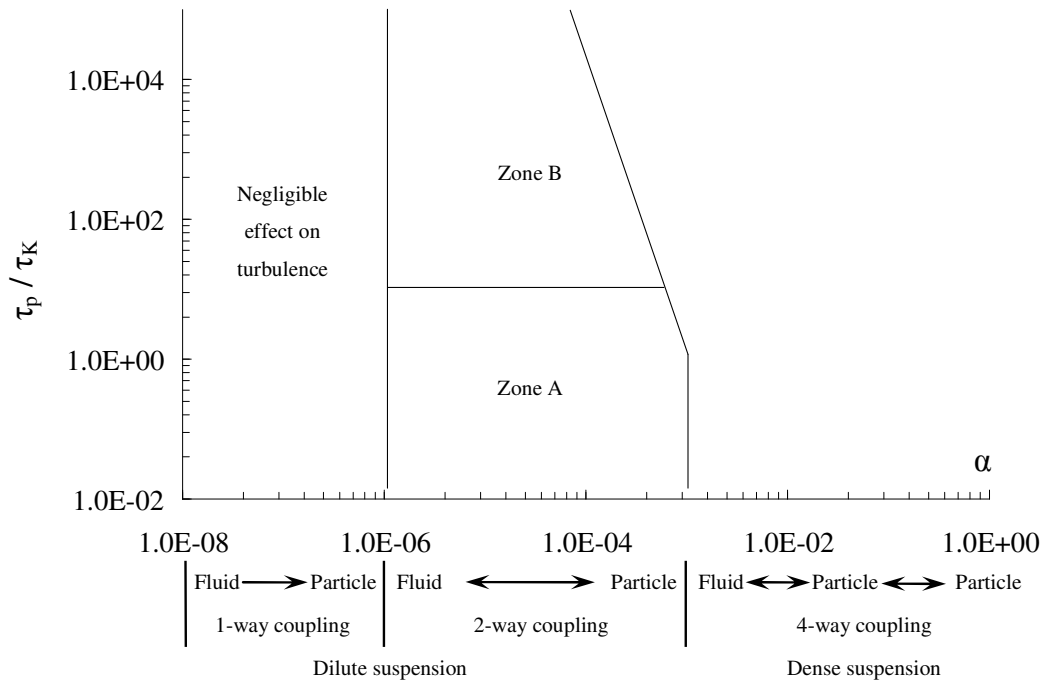
Figure 1.1. Classification map of dispersed two-phase flows (Loth et al., 2006).

Enormous efforts have been directed at establishing a framework for modeling multiphase flows. Delnoij (2001) proposed the hierarchy-of-models concept where three levels of modeling are identified based on the spatial resolution of the model. At the finest level, where relevant scales include individual dispersed bubbles, small-scale vortices behind bubbles and bubble-bubble interactions, the volume-of-fluid (VOF) approach of Hirt & Nichols (1981) or the front tracking (FT) approach of Unverdi & Tryggvason (1992) may be employed. Due to their intensive computational cost, these approaches are suitable for study of interfacial closure

relations or study of phenomena under bubble-scale of a single bubble or a few interacting bubbles. At intermediate resolution, each individual bubble or a parcel of bubbles is represented by a single point. Its trajectory is tracked by solving its equation of motion. This approach is known as the Euler-Lagrange (EL) approach. The approach requires closure relations to account for the inter-phase forces, which can be obtained from empirical relations or from simulations with higher resolution, i.e., VOF or FT. The EL approach offers high flexibility with respect to incorporating microscopic and bubble-level phenomena, such as bubble-bubble interactions, coalescence or breakup of bubbles (Ranade, 2002; Van den Hengel et al., 2005).The EL approach becomes infeasible for simulations of industrial relevant-scale due to its moderate computational requirement. For such cases, the coarsest level of modeling, i.e., the Euler-Euler (EE) approach, is typically employed. In the EE approach, both phases are treated as interpenetrating continua. The interactions between phases are modeled via the phase interaction terms that appear in the conservation equations describing the dynamics of the system. Despite its lack of detail at the bubble-level, it has been widely used in the past decades for the engineering modeling of industrial relevant-scale reactors.

Since this thesis focuses on the EL approach, it is therefore important to examine the level of interaction between phases, i.e., degree of coupling between phases. Generally, the level of interation can be separated between dilute and dense two-phase flows based on the dispersed phase fraction (Loth et al., 2006). The classification map (Figure 1.1) relates the level of interaction (i.e., coupling between phases) using the dispersed volume fraction α, the particle (bubble) response time $\tau_p = \rho_p d_p^2 / 18 \rho_l \nu$ and the Kolmogorov time scale $\tau_K = (\nu \varepsilon)^{1/2}$. In these definition, ρ_p, ρ_l, d_p, ν and ε represent dispersed and liquid phase density, particle (bubble) diameter, liquid phase viscosity and energy dissipation rate, respectively. For a α value lower than 10^{-6}, the so-called one-way coupling can be employed. That is, the presence of dispersed phase has negligible effect on the continuous phase and vice versa. In the range of $10^{-6} < \alpha \le 10^{-3}$, the momentum exchange between phases becomes important and has to be taken into account. This interaction is called two-way coupling. With increasing α value, referred to as the dense suspension regime, the interactions within the dispersed phase, i.e., collision, coalescence and breakup, are increasingly significant to the flow structure and have to be accounted for. This calculation is referred to as four-way coupling.

1.3   This Thesis

The object of this thesis is to develop a modeling technique for modeling of dispersed flows in industrial-scale relevant reactors covering dilute and dense dispersion regimes. The time-dependent, three-dimensional phenomena down to bubble-scale are resolved using the EL approach. The bubble-bubble interactions (i.e., collision, coalescence and breakup) as well as bubble-reactor components interactions (e.g., bubble-impeller and bubble-wall) are taken into account. The modeling technique is based on elementary physical principles which valid for a wide range of scales. Therefore, its applicability is not limited only to laboratory-scale reactors but also valid for large-scale reactors. Additionally, the presented modeling technique offers an attractive parallel efficiency as will be shown in the next chapter.

Chapter 2 discusses the modeling of turbulent gas-liquid bubbly flows. The EL approach with two-way coupling is introduced. The lattice-Boltzmann scheme for discretizing the conservation equations of the liquid continuous phase and the stochastic Lagrangian model for inter-particle collision are presented and discussed in detail. The presented modeling technique is validated by carrying out simulations of a bubble column. The predicted results are compared with experimental data from the literature.

Chapter 3 further discusses the extension of the modeling technique presented in the chapter 2. Coalescence, breakup of bubbles, and the interaction between bubbles and reactor components are included and presented in detail. Simulations of gas-liquid stirred reactor with Newtonian liquid are performed and validated against data from the literature. The chapter demonstrates the feasibility of using CFD as a tool to gain insights into a gas-liquid stirred reactor.

Chapter 4 presents an attempt to model gas-liquid flow in stirred reactors with pseudoplastic liquids. Assumptions have been made to simplify the underlying physics within the reactors. Despite the lack of fundamental knowledge concerning turbulence in non-Newtonian liquids, the simulations provide a sophisticated level of accuracy and valuable information concerning the phenomena within the reactors.

General conclusions and outlook on future research is discussed in Chapter 5. The main elements of the presented work will be briefly summarized. Achievements that have been made in this work are presented. Challenges for future research are pointed out.

1.4 References

1   Arlov D, Revstedt J, Fuchs L. Numerical simulation of gas-liquid Rushton stirred reactor – LES and LPT. *Computers & Fluids*. 2008;37:793-301.

2   Delnoij E. Fluid dynamics of gas-liquid bubble columns: A theoretical and experimental study. PhD Thesis. 2001. Twente University. The Netherlands.

3   Derksen JJ, Van den Akker HEA. Large eddy simulations of the flow driven by a Rushton turbine. *AIChE J*. 1999;45:209-221.

4   Gogate PR, Beenackers AACM, Pandit AB. Multiple-impeller systems with a special emphasis on bioreactors: A critical review. *Biochem. Eng. J*. 2000;6:109-144.

5   Hirt CW, Nichols BD. Volume of fluid (VOF) method for the dynamics of free boundaries. *Journal of Computational Physics*. 1981;39:201.

6   Ishii M. Thermo-fluid dynamics theory of two phase flow. Eyrolles. 1975.

7   Loth E, Tryggvason G, Elgobashi SE, Crowe CT, Berlemont A, Reeks M, Simonin O, Frank Th, Onishi Y, Van Wachem B. Modeling. In: Crowe CT. Multiphase Flow Handbook. CRC Press, Boca Raton, 2006.

8   Ranade VV. Computational flow modeling for chemical reactor engineering. Academic Press. San Diego. 2002.

9   Unverdi SO, Tryggvason G. A front-tracking method for viscous, incompressible multi-fluid flow. *Journal of Computational Physics*. 1992;200:25-37.

10   Van den Hengel EIV, Deen NG, Kuipers JAM. Application of coalescence and breakup models in a discrete bubble model for bubble columns. *Industrial and Engineering Chemistry Research*. 2005;44:5233-5245.

2

MODELING OF TURBULENT GAS-LIQUID BUBBLY FLOWS[1]

*In this paper we present detailed, three-dimensional and time-resolved simulations of turbulent gas-liquid bubbly flows. The continuous phase is modeled using a lattice-Boltzmann (LB) scheme. The scheme solves the large-scale motions of the turbulent flow using the filtered conservation equations, where the Smagorinsky model has been used to account for the effects of the sub-filter scales. A Lagrangian approach has been used for the dispersed, bubbly phase. That is we update the equations of motion of individual bubbles. It is shown that the incorporation of the sub-filter scale fluid fluctuations along the bubble trajectory improves the predictions. Collisions between bubbles are described by the stochastic inter-particle collision model based on kinetic theory developed by Sommerfeld (Int. J. Multiphase Flow **2001**, 27, 1829-1858). It has been found that the collision model not only dramatically decreases computing time compared to the direct collision method, but also provides an excellent computational efficiency on parallel platforms. Furthermore, it was found that the presented modeling technique provides very good agreement with experimental data for mean and fluctuating velocity components.*

---

[1] This chapter is based on Sungkorn R, Derksen JJ, Khinast JG. Modeling of turbulent gas-liquid bubbly flows using stochastic Lagrangian model and lattice-Boltzmann scheme. Accepted for publication in *Chemical Engineering Science* (2011).

2.1   Introduction

Many processes in the chemical and pharmaceutical industry involve turbulent gas-liquid flows. The phenomena encountered in these processes are highly complex, such as those in bubble column reactors (Joshi, 2001; Ranade, 2002). In a bubble column reactor, the flow patterns are generated not only by the interactions between the phases on a macroscopic scale, but also relate to small scale flows such as the wakes behind individual rising gas bubbles. The various scales interact and create complex, turbulent flow. It exhibits unsteady (time-dependent), three-dimensional turbulent behavior characterized by a wide range of time and length scales, from small vortices shed by bubbles to macroscopic circulation patterns with the size of the reactor. These flow patterns relate to the operating and design variables. Therefore, a descriptive engineering model which provides thorough understanding of the hydrodynamics in gas-liquid bubbly flows is essential for analyzing, optimizing, designing and scaling-up of these processes.

Over the past decades, computational fluid dynamics (CFD) have been adopted by large numbers of researchers to study the underlying physics of turbulent gas-liquid bubbly flows. Accordingly, enormous efforts have been directed at establishing a framework for modeling multiphase flows, including the development of closures for inter-phase forces. Using the "hierarchy-of-models" concept introduced by Delnoij (2001), three levels of modeling can be identified based on the spatial and temporal resolution of the model. At the finest level, where relevant scales include individual bubbles, small-scale vortices behind bubbles and bubble-bubble interactions, the volume-of-fluid (VOF) approach of Hirt and Nichols (1981) or the front tracking (FT) approach of Unverdi and Tryggvason (1992) may be employed. However, these approaches are restricted to a single bubble or a few interacting bubbles due to the extensive computational requirements (Deen et al., 2004). At the intermediate level each individual bubble or a parcel of bubbles is represented by a single point, and its trajectory is tracked by solving its equation of motion. This approach is known as the Euler-Lagrange (EL) approach. In contrast to the VOF and FT approach, the EL approach requires closure relations to account for the inter-phase forces, which can be obtained from empirical relations or from simulations with a more sophisticated level of resolution (i.e., VOF or FT). Nevertheless, the EL approach is highly flexible with respect to incorporating microscopic and bubble-level phenomena, such as bubble-bubble interactions, coalescence or break-up of bubbles (Ranade, 2002; Van den Hengel et al., 2005). Due to the significant computational resources required, the EL approach becomes infeasible for simulations of large industrial-scale bubble columns or stirred tanks which may contain tens of millions of bubbles. For such cases, the coarsest level of modeling, i.e., the

Euler-Euler (EE) approach (also called two-fluid model), which treats both phases as interacting continua, is applied. Despite its lack of detail at the bubble-level, it has been widely used in the past decade for the engineering modeling of large-scale industrial bubble column reactors due to the relatively limited computational resources needed. However, a detailed understanding of multiscale phenomena, including large-scale mixing patterns, as well as breakup and coalescence of bubbles, is crucial for analyzing, designing and scaling of processes, especially for processes that are critical in terms of mass transfer and chemical reactions. As may be clear from the above, limitations of the currently available modeling techniques and computational resources makes resolution of bubbly flow hydrodynamics down to the bubble-scale not practical.

The goal of this study is to introduce a novel approach which allows the modeling of turbulent gas-liquid bubbly flows using the EL approach to obtain detailed information of the hydrodynamics down to the bubble-scale with only moderate computational resource requirements. The modeling technique used in this study includes the following elements:

- The continuous liquid phase is modeled using a variation of the lattice-Boltzmann (LB) scheme due to Somers (1993) and Eggels & Somers (1995).We use the scheme to solve for the large-scale motions of the turbulent flow using the filtered conservation equations, where the Smagorinsky subgrid-scale model (Smagorinsky, 1963) has been used to model the effects of the sub-filter scales. It has been demonstrated that the LB scheme can accurately represent turbulent flow hydrodynamics, including single phase flows (Derksen and Van den Akker, 1999), as well as multiphase flows (Derksen et al., 2008; Derksen, 2003, 2010). Due to the locality of operations, lattice-Boltzmann schemes have high computational efficiency, especially on parallel platforms (Derksen and Van den Akker, 1999).

- For the dispersed gas phase, the trajectories of the individual bubbles are computed in the Lagrangian manner taking into account the sum of net gravity force, forces due to stress gradients, drag force, lift and added mass forces. The force coupling between the fluid phase and the bubbles, i.e., the two-way coupling between the phases, is achieved by the "cheap clipped fourth-order polynomial mapping function" introduced by Deen et al. (2004). A set of closure relations for these inter-phase forces were carefully chosen from literature data (Hu, 2005; Joshi, 2001; Loth, 2000). It should be noted that the EL approach does not resolve the gas-liquid interface and the size of the bubbles considered in this work is smaller than the grid-spacing. The impact of turbulence on the bubbles, i.e., the fluctuations of the

sub-filter or residual fluid velocity along the bubble trajectory, is computed using the Langevin equation model introduced by Sommerfeld et al. (1993). Collisions of bubbles are governed by the so-called stochastic inter-particle collision model of Sommerfeld (2001). Although the model was originally proposed for solid particle-laden flows, it has also been successfully applied to modeling of bubbly flow (Sommerfeld et al., 2003).

Although various elements of this approach have been reported in the literature, the presented EL model, for the first time assesses the feasibility of using the LB scheme with the stochastic particle model to obtain a fast, yet detailed understanding of turbulent bubbly flows. Thus, the combination of these two techniques constitutes a novel development in the simulation of bubbly multiphase flows.

This paper is organized in the following manner: In the next section, the modeling approach for turbulent bubbly flows in the EL framework will be discussed in more detail. In the subsequent section, the model validation, including the impact of the modeling techniques and choices on the predicted results, will be presented. The computational performance of the presented modeling technique will be discussed as well, followed by a summary and conclusions.

2.2 Modeling of Gas-Liquid Bubbly Flows

2.2.1 Liquid phase hydrodynamics

In our work the lattice-Boltzmann (LB) method is used for modeling the continuous liquid phase. The LB method is based on a simple form of the Boltzmann kinetic equation, which can be used to recover the macroscopic hydrodynamic behavior of fluids (Bernaschi et al., 2010). The specific LB scheme employed here is due to Somers (1993) (see also Eggels & Somers (1995) and Derksen & Van den Akker (1999)). It provides a second-order discretization in space and time for the incompressible Navier-Stokes equations on a uniform, cubic lattice. This scheme was chosen because of its robustness for turbulence simulations and its inherently high parallelization efficiency. The robustness results from its explicit treatment of the higher-order terms leading to enhanced stability at low viscosities. This allows us to reach relatively low viscosities and thus high Reynolds numbers and makes the scheme suitable for turbulence simulations (Derksen, 2010). The inherent parallelism of the LB method is due to the locality of its arithmetic operations. Thus, the communication between processors requires only limited amounts of overlapped-boundary data, resulting in an efficient parallel structure.

In this paper, we limit ourselves to a flow configuration in which the motion of the continuous liquid phase is solely driven by the dispersed gas bubbles. Bubble collisions are expected to have a significant effect on the hydrodynamics. However, coalescence and breakup of bubbles are neglected in the present study as we consider a dilute system. In this flow, the turbulent stress can be divided into two components, i.e., one component due to bubble buoyancy leading to liquid velocities above the turbulence onset, and one component due to the so-called pseudo-turbulence, caused by the fluctuations of the bubbles (i.e., the motion of bubbles relative to the liquid which results in turbulent-like flows) (Hu and Celik, 2008).

A filtering process with a filter width equal to the grid space was applied to the conservation equations of the liquid phase to resolve only the evolution of the large-scale motions. The resolved flow can be interpreted as a low-pass filtered representation of the real flow. The impact of the residual motion that resides at scales smaller than the filter width, i.e., the subgrid-scale (SGS), is modeled using the Smagorinsky SGS model (Smagorinsky, 1963). In the Smagorinsky model, the SGS motion is considered to be purely diffusive, and the model only drains energy from the resolved motions without feed-back. For finer grid spacing, a larger fraction of the eddies and more of the energy contained in the flow field are resolved. However, the choice of the grid spacing in the present work is also restricted by the requirements of the EL approach, i.e., the point-volume assumption that the interfacial details are not resolved. Therefore, the grid spacing should be larger than the (physical) bubble diameter. In the case where the bubble diameter is larger than the grid spacing, the bubble's interfacial detail becomes important and should be resolved (Nicěno et al., 2009). This is also consistent with the grid size considerations discussed in the work of Milelli et al. (2001). Based on considerations of the energy spectra and modeling closures for the inter-phase forces, they stated that the grid space should be at least 50% larger than the bubble diameter, i.e., the ratio between the grid spacing h and the bubble diameter d_p should be larger than 1.5.

In the present paper, the ratio between h and d_p was chosen to be 1.25, similar to that in the work of Nicěno et al. (2009), and clearly smaller than the criterion proposed by Milelli et al. (2001). However, it can be argued that it is known *a priori* that the flow pattern of the bubble column is dominated by a bubble plume which meanders from one side of the bubble column to the other side. Therefore, it can be concluded that the largest scale, which contains most energy, will be of the size of the domain cross-section (Nicěno et al., 2009). The grid resolution employed here is a compromise between sufficiently fine to capture the most energetic eddies, and sufficiently coarse to stay close to the Milelli criterion (Milelli et al., 2001).

The SGS model used in the present work is the Smagorinsky model adopted directly from the single-phase SGS model. In this model, the eddy viscosity ν_t concept is used to represent the impact of the SGS motion as

$$\nu_t = \left(C_S \Delta\right)^2 \sqrt{S^2} \, , \tag{2.1}$$

with the Smagorinsky constant C_S, the filter width Δ (with size equal to the grid spacing h) and the resolved deformation rate $\sqrt{S^2}$. As pointed out in the work of Hu and Celik (2008) the so-called pseudo (or bubble-induced) turbulence possesses a universal energy spectrum with identifiable power-law decay. This, however, is different from the classical -5/3 decay. Therefore, the residual motion arising from both turbulence and pseudo-turbulence could (in principle) be captured using a dedicated subgrid-scale model acting on the continuous phase. However, such a (reliable and accurate) SGS model for multiphase flows is not readily available (Hu, 2008), so that we reverted to the use of the Smagorinsky model for our simulations of gas-liquid flows, justified by favorable results as will be shown later in this paper.

Since the simulations discussed here are restricted to the dilute dispersion condition (global gas void fraction up to 2%), we assume that the void fraction term in the conservation equations for the continuous phase only has a relatively small effect on the flow field, and can be neglected. Therefore, the filtered conservation equations (equipped with momentum source terms representing the bubbles) for single-phase flows are approximately valid. This assumption has been tested successfully by some researchers, e.g., Hu and Celik (2008) and Hu (2005), for a relatively dilute void fraction gas-liquid bubbly flow (up to 1%) and Derksen (2003) for dilute suspensions (solid volume fractions up to 3.6%).

In the present paper, the forces imposed by a bubble on the continuous phase and vice versa (i.e., two-way coupling) are considered. These local interactions are represented via the inter-phase force terms in the conservation equations, i.e., the drag force $\mathbf{F}_D$, lift force $\mathbf{F}_L$ and added mass force $\mathbf{F}_A$. Expressions for these forces are discussed in the following section.

2.2.2 *Bubble dynamics*

Each individual bubble is treated as a single, point-volume particle/bubble with constant mass and has three degrees of freedom associated to it, i.e., three spatial coordinates. Its trajectory is tracked based on Newton's equation of motion:

$$d_t \mathbf{x}_p = \mathbf{u}_p \tag{2.2}$$

$$\rho_p V_p d_t \mathbf{u}_p = \mathbf{F}_p \tag{2.3}$$

where $\mathbf{x}_p$, $\mathbf{u}_p$, ρ_p, V_p and $\mathbf{F}_p$ represent the center position of the bubble, the velocity, the bubble density, the bubble volume and the net force, respectively. Here, the net force $\mathbf{F}_p$ acting on each individual bubble is the sum of net gravity force $\mathbf{F}_G$, forces due to stress gradients $\mathbf{F}_S$, drag force $\mathbf{F}_D$, net transverse lift force $\mathbf{F}_L$ (i.e., the sum of shear- and wake-induced lift forces), added mass force $\mathbf{F}_A$ and Basset history force $\mathbf{F}_H$:

$$\mathbf{F}_p = \mathbf{F}_G + \mathbf{F}_S + \mathbf{F}_D + \mathbf{F}_L + \mathbf{F}_A + \mathbf{F}_H. \tag{2.4}$$

Force	Closure
$\mathbf{F}_G = (\rho_p - \rho_l) V_p \mathbf{g}$	-
$\mathbf{F}_S = \rho_l V_p D_t \mathbf{u}$	-
$\mathbf{F}_D = -\dfrac{1}{2} C_D \rho_l \pi r_p^2 \lvert \mathbf{u}_p - \mathbf{u} \rvert (\mathbf{u}_p - \mathbf{u})$	$C_D = \max \left[\min \left[\dfrac{24}{\mathrm{Re}_p}(1 + 0.15\mathrm{Re}_p^{0.687}), \dfrac{48}{\mathrm{Re}_p} \right], \dfrac{8}{3}\dfrac{\mathrm{Eo}}{\mathrm{Eo}+4} \right]$
$\mathbf{F}_L = -C_L \rho_l V_p (\mathbf{u}_p - \mathbf{u}) \times \nabla \times \mathbf{u}$	$C_L = \begin{cases} \min[0.288\tanh(0.121\mathrm{Re}_p), f(\mathrm{Eo}_d)], & \mathrm{Eo}_d < 4 \\ f(\mathrm{Eo}_d), & 4 < \mathrm{Eo}_d \le 10 \\ -0.29, & \mathrm{Eo}_d > 10 \end{cases}$ $\mathrm{Eo}_d = \dfrac{\mathrm{Eo}}{E^{2/3}}, \quad E = \dfrac{1}{1 + 0.163\mathrm{Eo}^{0.757}}$ $f(\mathrm{Eo}_d) = 0.00105\mathrm{Eo}_d^3 - 0.0159\mathrm{Eo}_d^2 - 0.0204\mathrm{Eo}_d + 0.474$
$\mathbf{F}_A = -C_A \rho_l V_p (D_t \mathbf{u}_p - D_t \mathbf{u})$	$C_A = 0.5$

Table 2.1. Expressions for the forces acting on a bubble.

It has been reported by Loth (2000) that the Basset history force is negligible when time-averaged or when integral quantities in a turbulent fluid velocity field are of interest. Thus, the Basset history force is neglected in this work. Formulations of the forces acting on a bubble have been discussed in detail by a number of researchers, see for example, Loth (2000), Joshi

(2001) and Hu (2005). With the expressions summarized in Table 2.1 and substituting Eq. (2.4) into Eq. (2.3), the following set of equations is solved in order to keep track of individual bubbles:

$$
\begin{aligned}
\rho_p V_p d_t \mathbf{u}_p = \left(\rho_p - \rho_l\right) V_p \mathbf{g} + \rho_l V_p D_t \mathbf{u} - \frac{1}{8} C_D \rho_l \pi d_p^2 \left|\mathbf{u}_p - \mathbf{u}\right|\left(\mathbf{u}_p - \mathbf{u}\right) \\
- C_L \rho_l V_p \left(\mathbf{u}_p - \mathbf{u}\right) \times \nabla \times \mathbf{u} - C_A \rho_l V_p \left(D_t \mathbf{u}_p - D_t \mathbf{u}\right)
\end{aligned}
\tag{2.5}
$$

with ρ_l being the liquid phase density, $\mathbf{u}$ the liquid velocity, and C_D, C_L and C_A the drag, lift and added mass force coefficients, respectively. The drag and lift coefficients depend on the bubble Reynolds number $Re_p = \left|\mathbf{u}_p - \mathbf{u}\right| d_p / \nu_l$ and the Eötvös number $Eo = \left(\rho_l - \rho_p\right)\left|\mathbf{g}\right| d_p^2 / \sigma$. It should be noted that the drag coefficient does not have a local void-fraction dependency because the gas volume-fractions considered here are sufficiently low not to include a dependency of the drag coefficient on the local void-fraction. Similar considerations apply to the buoyancy term.

The liquid velocity at the bubble position $\mathbf{u}$ introduced in Eq. (2.5) is composed of the resolved liquid velocity and a (residual) liquid fluctuating component $\mathbf{u}'$. The latter component is recovered using the so-called Langevin equation model introduced by Sommerfeld (1993). In this model, a correlation function $R_p\left(\Delta t, \Delta r\right)$ (see Appendix) is used to correlate the fluctuation velocity from the old to the new bubble location:

$$
\mathbf{u}'_{n+1} = R_p\left(\Delta t, \Delta r\right) \mathbf{u}'_n + \sigma_{SGS} \sqrt{1 - R_p\left(\Delta t, \Delta r\right)} \, \xi ,
\tag{2.6}
$$

where σ_{SGS} is the characteristic residual motion, and ξ a Gaussian random number with a mean value of zero and a standard deviation of one. Based on the assumption that the residual turbulent motion is locally homogeneous and isotropic, the characteristic residual motion was estimated by $\sigma_{SGS=}\sqrt{2/3 k_{SGS}}$. The SGS kinetic energy k_{SGS} was approximated based analysis of the energy spectrum as (Pozorski and Apte, 2009):

$$
k_{SGS} = \left(\frac{\nu_t}{0.067\Delta}\right)^2 .
\tag{2.7}
$$

The interpolation of the liquid properties on the Eulerian grid to the bubble centroid on the Lagrangian reference frame is achieved using a mapping function ς described by the so-called cheap clipped fourth-order polynomial proposed by Deen et al. (2004):

$$\varsigma(\mathbf{x}-\mathbf{x}_p) = \frac{15}{16}\left[\frac{(\mathbf{x}-\mathbf{x}_p)^4}{n^5} - 2\frac{(\mathbf{x}-\mathbf{x}_p)^2}{n^3} + \frac{1}{n}\right] \text{ with } |\mathbf{x}-\mathbf{x}_p| \le n \,, \qquad (2.8)$$

where $\mathbf{x}$ is the position of a neighboring grid node, and n is half of the predefined influence diameter (set to $2d_p$ in this work). With this mapping function, a property, such as the liquid velocity at the bubble centroid $\mathbf{u}(\mathbf{x}_p)$, is evaluated by the integration of the liquid velocity at the neighboring grid nodes (that is located inside the influence diameter) $\mathbf{u}(\mathbf{x})$. The forces exerted on the continuous phase by the bubbles are treated as a point force and distributed to the continuous phase using a similar mapping function. A further discussion concerning mapping techniques can be found in the work of Deen et al. (2004), and Hu & Celik (2008).

For turbulent bubbly flow simulations, numerical instabilities can be induced by many factors, for instance, the evolution of bubbles with a very small mass, and/or strong fluctuations generated by forces exerted from the bubbles on the liquid. In order to avoid these instabilities, we used a very small time step to maintain the velocity update due to the inter-phase force (in lattice units) within the compressible limit of the LB scheme. We under-relax the distributed force with a relaxation factor of 0.25. Additionally, the mapping technique with the influence diameter concept discussed above also helps to prevent high concentration of forces exerted by a bubble.

2.2.3 *Stochastic inter-particle collision model*

Collisions between bubbles are considered using the stochastic inter-particle collision model introduced by Sommerfeld (2001). Instead of direct collision calculation, where a large amount of information from surrounding bubbles is required, only a fictitious collision partner and a collision probability according to kinetic theory are generated for each bubble at each time step of the trajectory calculation. In this model, the size and the velocity of the fictitious collision partner is sampled from the local distribution functions stored at each grid node. Since the bubble size used is relatively large, in order to obtain representative properties, the distribution functions is computed from a set of nodes that reside in the influence diameter of the bubble using a similar mapping technique as in the previous section. Hence, in this work, the so

generated fictitious bubble can be considered as representative for the bubbles in its direct vicinity.

The velocity components of the fictitious bubble consist of the local mean velocity $\mathbf{u}_{fict}$ and the fluctuating component $\mathbf{u}'_{fict}$ which also compose of three degrees of freedom. The first component is obtained from the method discussed above. The latter component is obtained via a correlation proposed by Sommerfeld (2001)

$$\mathbf{u}'_{fict} = R(St)\mathbf{u}'_{real} + \boldsymbol{\sigma}_p \sqrt{1 - R(St)^2}\, \xi, \tag{2.9}$$

with $\mathbf{u}'_{real}$ being the fluctuating velocity components of the real bubble which are evaluated based on the ensemble-averaged bubble velocity and the instantaneous bubble velocity. $R(St)$ is the correlation function based on the bubble Stokes number St, and $\boldsymbol{\sigma}_p$ is the local rms value of the bubble velocity components. The bubble Stokes number St is defined as the ratio of bubble response time τ_p and the Lagrangian integral time scale T_L, as suggested by Ho (2004) (see Appendix). As can be seen in Eq. (2.9), the degree to which the bubble fluctuating velocities are correlated depends on their response to turbulent fluctuations, which is characterized by the Stokes number. Based on the calculations obtained from large eddy simulations, Sommerfeld (2001) reports the dependence of the correlation function on the Stokes number as

$$R(St) = \exp(-0.55St^{0.4}). \tag{2.10}$$

The occurrence of a collision is determined by the collision probability P_{coll} given by kinetic theory,

$$P_{coll} = \frac{\pi}{4}(d_{p,i} + d_{p,j})^2 |\mathbf{u}_{p,i} - \mathbf{u}_{p,j}| n_p \Delta t, \tag{2.11}$$

where $d_{p,i}$ and $d_{p,j}$ are the bubble diameters, $|\mathbf{u}_{p,i} - \mathbf{u}_{p,j}|$ the instantaneous relative velocity between the considered and the fictitious bubble, and n_p the number of bubbles per unit volume in the respective grid nodes. A collision takes place when a random number RN, generated by a uniform distribution in the interval [0,1], becomes smaller than the collision

probability, i.e., $RN < P_{coll}$. In the case of a collision, the point of impact on the bubble surface is statistically determined based on a collision cylinder (see Sommerfeld (2001) and Ho (2004) for a detailed description). In this work, the bubble-bubble collisions are assumed to be fully elastic.

2.2.4 Parallelization aspects

As mentioned previously, the lattice-Boltzmann (LB) scheme has an inherently high parallelization potential due to its locality of operations, e.g., data required for the calculation and parallelization are obtained from the neighbors and the stress tensor is explicitly obtained from the data stored in a single node. In the present implementation, parallelization of the continuous phase is achieved by axially dividing the computational domain into subdomains. In contrast to the conventional parallelization strategy used in single-phase LB schemes where only boundary values are communicated, the present multiphase (EL) numerical scheme requires the communication of a number of grid layers, depending on the bubble diameter and the influence diameter. For instance, a bubble with a diameter of $0.8h$ and an influence diameter of $2d_p$ located near the boundary between subdomains would require data not only from the nodes at the boundary but also from the other three rows behind the boundary for the distribution and redistribution of properties between the bubble and the liquid phase (see Figure 2.1). It should be noted that although information from two rows behind the boundary is used in the mapping function, one additional row (the third row) is required for the evaluation of the curl of the fluid velocity $\nabla \times \mathbf{u}$. It will be shown in the next section that despite the larger amount of data being communicated between the subdomains, the speedup for the continuous phase calculation is still excellent.

Generally, the parallelization of the dispersed phase is significantly more complicated than that of the continuous phase. The first complication is due to the handling of bubble-bubble collisions in the vicinity of subdomain borders. For direct collisions handling, large amounts of information of bubbles crossing borders as well as bubbles close to the border need to be communicated. This is overcome by employing the stochastic inter-particle collision model described above. Since the model requires only information stored at the Eulerian grid nodes, only a limited amount of information concerning bubbles crossing borders is communicated. Another complication arises from the dynamical nature of bubbles, which makes their spatial distribution non-uniform. In order to achieve high parallel performance, a load-balancing strategy needs to be considered. In our case, unbalanced loading occurred only at the initial

stages of the simulation. After the onset of aeration, the loading at each processor was approximately balanced. Hence, a static domain decomposition is considered efficient enough for the parallelization of the dispersed phase.
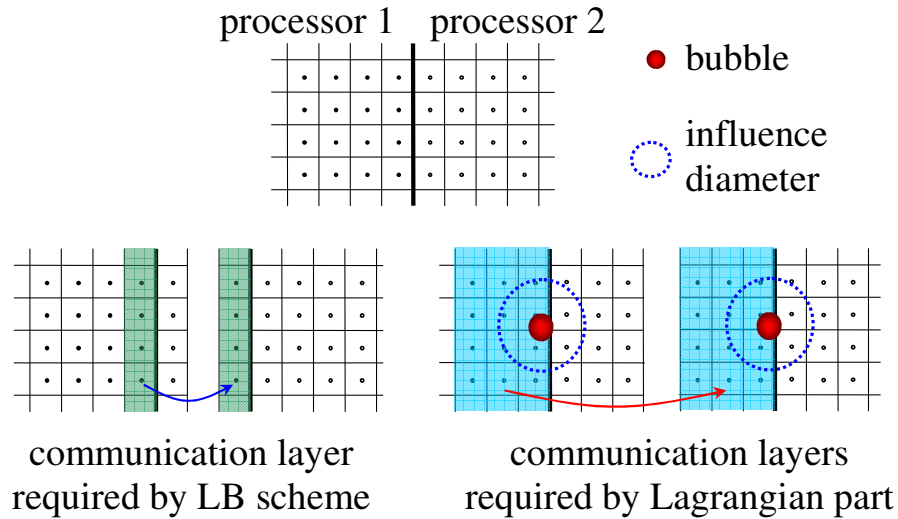
Figure 2.1. Parallelization strategy (left) single communication layer required by the LB scheme and (right) three co mmunication layers required by the Lagrangian part.

2.2.5   *The Deen bubble column experiment*

In the present study, the bubble column experiment performed by Deen et al. (2001), hereafter called the Deen case, was used as a reference for validating the simulations. Their three-dimensional rectangular bubble column has a width, depth and height of 0.15, 0.15 and 0.45 m, respectively. Air bubbles were introduced at the bottom-center plane with an area of 0.03×0.03 m^2 and a superficial gas velocity of 4.9 mm/s. A bubble mean diameter in the order of 4 mm was observed in their experiments using digital image analysis. It was assumed to have that uniform size with spherical shape in the simulations presented in this paper.

2.2.6   *Numerical implementation*

In all the following simulations, the fluid domain is discretized by a uniform cubic grids of 30×30×90 lattices in width, depth and height, respectively. This results in a bubble size of 0.8 times the lattice distance. An influence diameter is set to $2d_p$. The criteria for the selection of the grid spacing have been described previously. A no-slip, i.e., a bounce-back, boundary condition is applied at every sides of the computational domain except for the top where a free-

slip boundary condition is applied. Bubbles are injected at the bottom of the column through 49 inlet positions. Once a bubble (with its physical surface) touches the top surface of the column, it will be discarded from the simulation. From our simulations, it has been observed that a maximum number of 7,000 bubbles were tracked. The calculation starts with the quiescent liquid and proceeds with a time step for the liquid phase of 10 μs for 150 s. The time step used in this work has the same order of magnitude as used for a solid suspension simulation in a stirred tank by Derksen (2003). Using 8 processors, the simulation time (i.e., the real clock time) is approximately 100 hours for case number 0 to 3. A sub-time step of 1 μs is used for the calculation of the dispersed gas phase. The reason for this small time step used in this work is to obtain stability of the LB scheme as well as Newton's equation of motion (Eq. (2.5)).

2.3   Results and Discussion

In this study the gas-liquid flow from the Deen case is simulated using the modeling technique described in the previous sections. The gas-liquid flow hydrodynamics of the Deen case will be discussed first, followed by a study of the sensitivity of the SGS fluctuations, as well as the Smagorinsky constant C_S. The parallelization performance of our code will also be assessed. Six different cases were considered and Table 2.2 summarizes the characteristics of these simulations.

Case	SGS velocity	Collision	C_S	h/d_p
0	Eq. (2.6)	Eq. (2.11)	0.10	1.25
1	-	Eq. (2.11)	0.10	1.25
2	Eq. (2.6)	Eq. (2.11)	0.08	1.25
3	Eq. (2.6)	Eq. (2.11)	0.12	1.25
4	Eq. (2.6)	Eq. (2.11)	0.10	1.50
5	Eq. (2.6)	Eq. (2.11)	0.10	1.10

Table 2.2. Overview of the different simulation cases.

2.3.1   Two-phase flow

A series of snapshots of the evolving bubble plume for the standard case (case 0) are shown in Figure 2.2(a)-(d). These snapshots are taken at consecutive points in time of 20, 50, 100 and 150 s. As can be seen, the lower part of the plume fluctuates within a small range, while the upper part fluctuates strongly around the bubble column in a random manner. This behavior was also observed in the experiments by Deen (2000) and Deen et al. (2001). The corresponding instantaneous liquid flow fields at the vertical mid-depth plane are shown in Figure 2.3(a)-(d). Several large and small vortices can be observed in the liquid phase. These vortices interact with each other and significantly change their size, shape and position randomly with time. The random velocity fluctuation of the liquid phase can be seen clearly in the plot of the velocity at an arbitrary point in the column, as shown in Figure 2.4. These results illustrate the strong coupling between the fluctuation of the bubble plume and the turbulent flow field in the liquid phase.
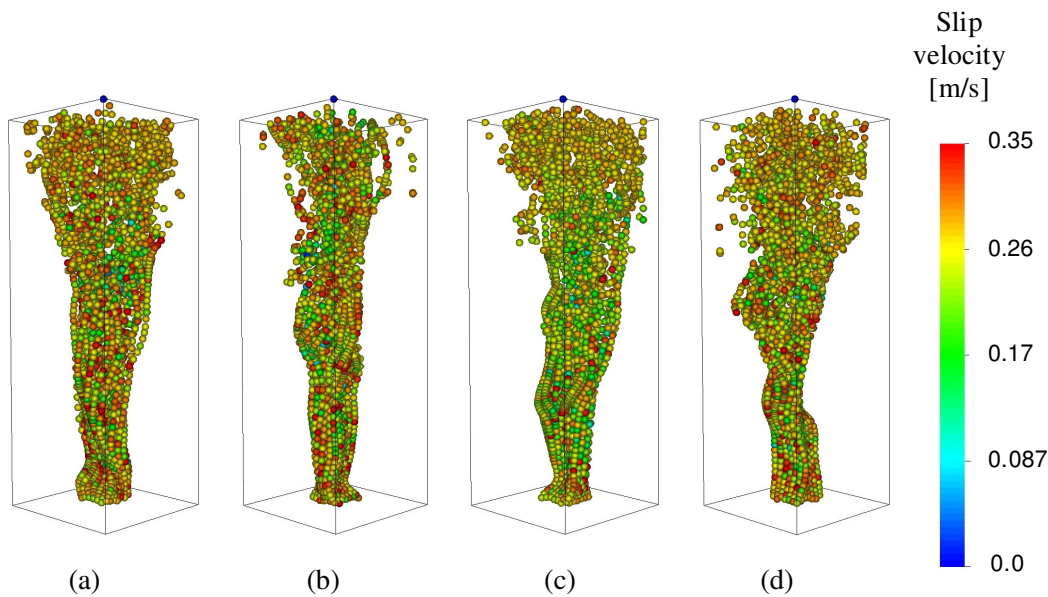
Figure 2.2. Snapshots of the bubble dispersion pattern after 20, 50, 100 and 150 s. The bubbles are colored by the magnitude of bubble's slip velocity. Note that the bubbles are magnified for visualization purpose, not to scale.
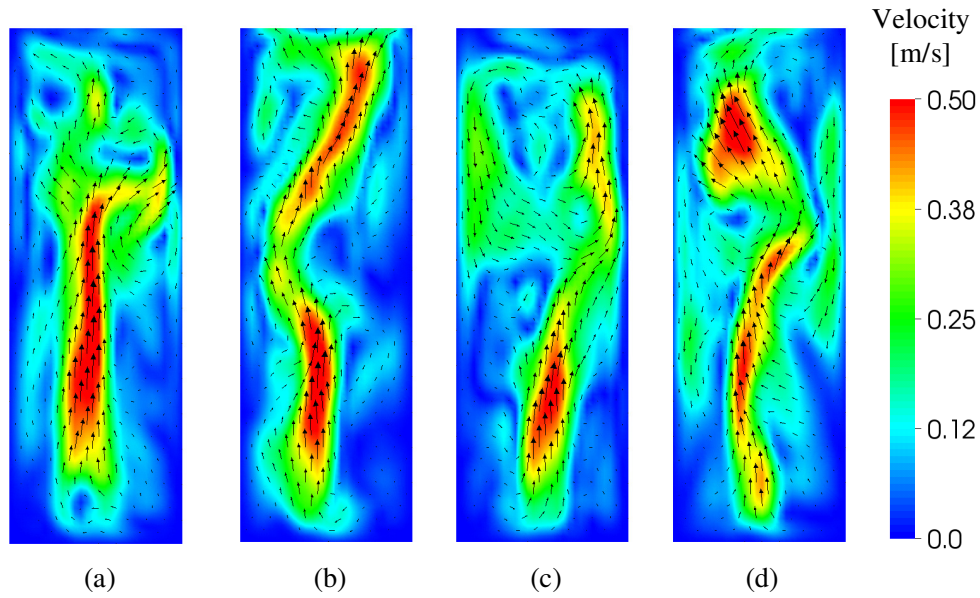
Figure 2.3. Snapshots of the liquid phase velocity at the mid-plane after 20, 50, 100 and 150 s.
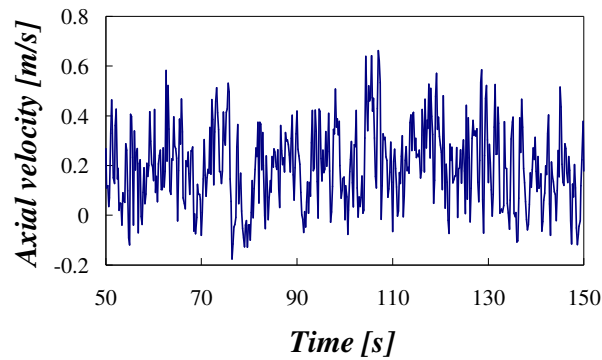
Figure 2.4. Axial liquid velocity as a function of time at the centerline of the column and a height of 0.28 m.

A quantitative comparison of the time-averaged hydrodynamics between predicted results and experimental data is required for the validation of the presented modeling technique. In order to obtain statistically meaningful results, a sufficiently long simulation period has to be considered. Since the fluctuation of the bubble plume was only observed after the onset of aeration, the time-averaged quantities were calculated starting from 20 s. The average liquid velocity and velocity fluctuations at various simulation times are shown in Figure 2.5. It can be seen that all quantities are converged after the simulation time of approximately 125 s.
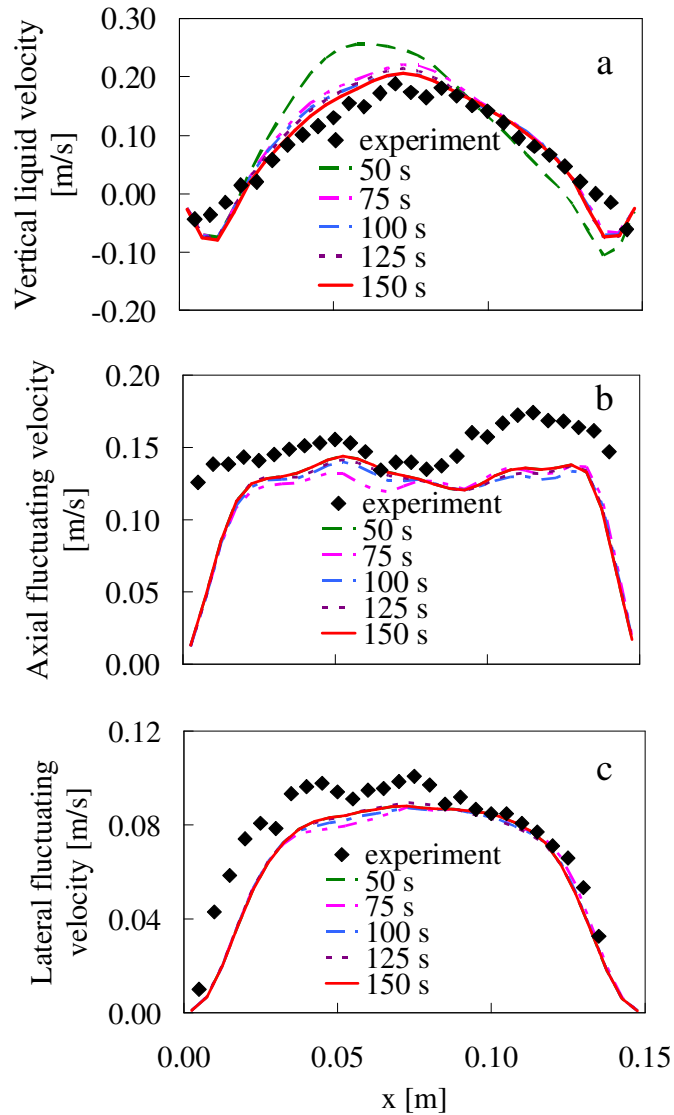
Figure 2.5. Comparison of the predicted and experimental liquid velocity and fluctuating velocity components for the standard case (case 0) at a height of 0.28 m and a depth of 0.075 m after different averaging periods.

A comparison of the predicted mean vertical velocity with experimental data in Figure 2.5(a) shows excellent agreement between simulation and experiment. The magnitude and the position of the local maximum are accurately predicted. The overall velocity profile is correctly reproduced quantitatively and qualitatively. Only a small deviation of the velocity near the wall region can be noticed. This might be attributed to an insufficient resolution of the near-wall structures, which may be resolved by introducing a wall function or an adaptive grid refinement at the near wall region (with some computational expenses). In Figure 2.5(b) and (c), the second-order statistics related to the turbulence quantities, i.e., the fluctuating components of

the resolved flow field, predicted by the simulations are compared with the experimental data. This comparison is necessary to obtain confidence in the prediction of problems involving turbulent flows. The vertical component of the resolved fluctuating liquid velocity is shown in Figure 2.5(b). The twin-peaked shape observed in the experiments is correctly reproduced. Quantitatively, the magnitude of the vertical fluctuating component is slightly under-predicted, except at the near-wall regions where larger deviations can be noticed. Figure 2.5 (c) shows the resolved lateral fluctuating liquid velocity. It should be noted that in order to compare simulation results to the experimental data which are measured in two dimensions, only one horizontal velocity component (on the measured plane) is used throughout this work, unless otherwise stated. Again, the predicted profile agrees very well with the experimental data. Additionally, it is apparent that the fluctuations in the vertical direction are larger than in the lateral direction, which implies that the turbulence is anisotropic.

A long-term average of the liquid flow fields is shown in Figure 2.6. The flow is dominated by the upward flow induced by the bubble plume. Two thin circulation zones close to the wall region can be observed over the height of the bubble column. The long-term average of the liquid flow field at the upper part of the column is compared with the experimental data in Figure 2.7. The flow field, i.e., the upwards flow in the middle and thin circulation zones close to the wall, is correctly reproduced by the simulation. A contour plot of the resolved liquid phase turbulent kinetic energy TKE in the mid-plane is given in Figure 2.8. Two regions of high turbulent activity (i.e., high TKE) separated by the center line of the bubble plume can be observed. It can be further seen that, due to the injection of the bubbles, TKE increases from the bottom, and has maximum at about half the height of the column. Consequently, since the top surface dampens the fluctuation of the liquid phase, the TKE decreases from the middle to the top of the column. A comparison between the predicted TKE at the upper part of the column with the experimental data is shown in Figure 2.9. The simulation underpredicts the measured TKE. Additionally, the gas void-fraction profiles at different height levels are shown in Figure 2.10. The distribution of the gas void-fraction from Lagrangian to Eulerian reference frame is calculated using the mapping function introduced in the previous section. It can be seen that at the bottom of the column, where the bubble inlet is located, the profile has a high concentration of gas only near the center line of the column, while the profile tends to broaden towards the top of the column.
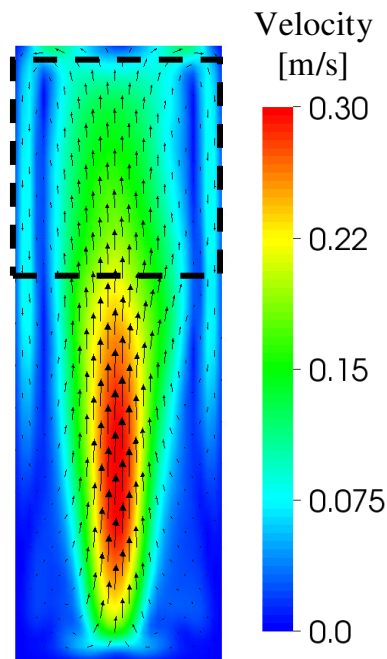
Figure 2.6. Long-term average of the liquid velocity field in the mid-depth plane.
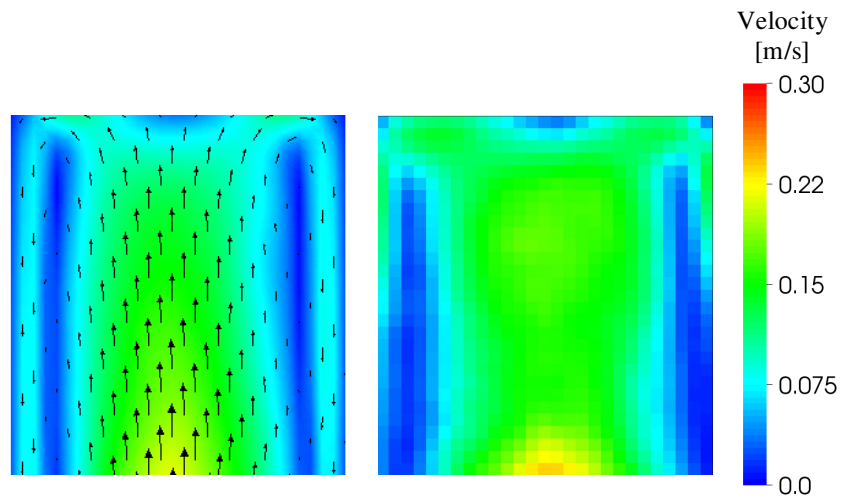
Figure 2.7. Predicted and experimental long-term average of the liquid velocity field in the mid-depth plane at the upper part of the bubble column.
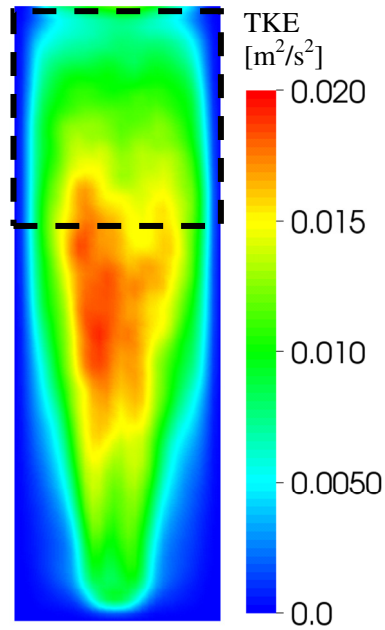
Figure 2.8. Long-term average of the turbulent kinetic energy contour in the mid-depth plane.
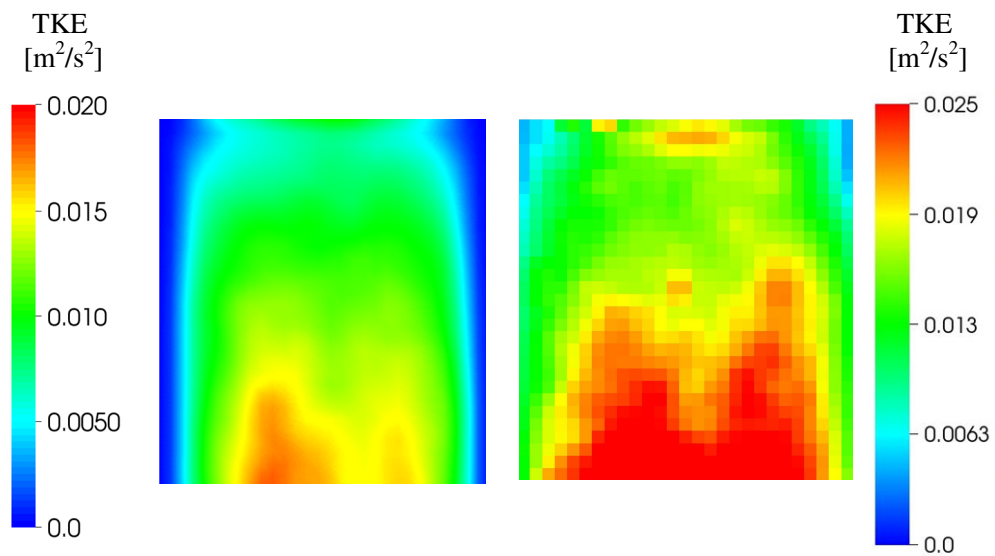
Figure 2.9. Predicted and experimental long-term average of the turbulent kinetic energy in the mid-depth plane at the upper part of the bubble column.
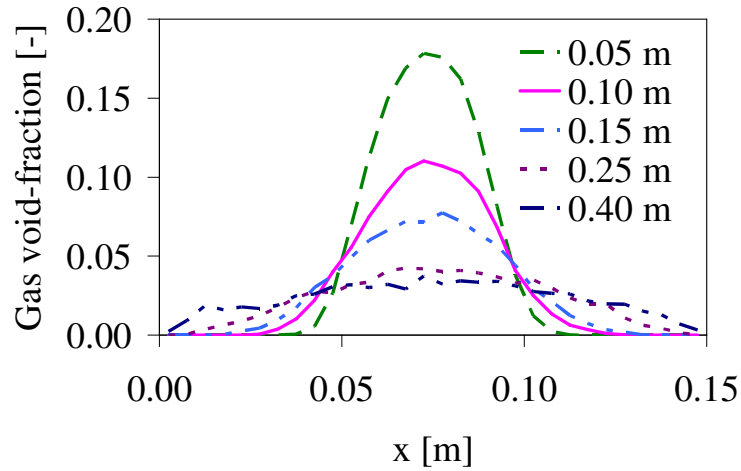
Figure 2.10. Long-term average of the gas void-fraction at various height levels in the mid-depth plane.

2.3.2 Subgrid-scale velocity

The influence of the subgrid-scale (SGS) velocity, i.e., the residual liquid fluctuations at the bubble position, was assessed by comparing cases 0 and 1. A series of snapshots of the evolving bubble plume colorized by magnitude of bubble's slip velocity and liquid fluctuations at its position for Case 0 are shown in Figure 2.2(a)-(d) and Figure 2.11(a)-(d), respectively. The bubble's slip velocity varies only within a small range throughout the column (mostly between 0.2 and 0.35 m/s). The magnitude of the liquid fluctuations at bubbles' position, which is approximately one order of magnitude lower than the slip velocity, varies throughout the column and decreases from the bottom towards the top of the column.

It can be seen in Figure 2.12(a) that the predicted average liquid velocity with and without the incorporation of the SGS velocity are quantitatively different. The position of the local maximum was shifted away from the center of the column with a lower velocity magnitude (about 0.02 m/s) than that predicted by the case 0. It might be that, without the SGS velocity, the fluctuation of the plume can not be correctly predicted. In Figure 2.12 (b) and (c), the vertical and the lateral component of the resolved fluctuating liquid velocity obtained from the cases 0 and 1 are shown. Similar qualitative and quantitative deviations can be observed in the resolved fluctuating components. These results point out that the inclusion of the SGS velocity has some effect on the dispersion pattern of the bubbles which can be seen in the predicted results. It can be anticipated that the inclusion of the SGS velocity is beneficial for an accurate prediction of the motion of the bubbles, and hence, the mean velocity profile. A

significant improvement should be obtained when a simulation of denser gas void-fraction is realized. It is important to note that the stochastic inter-particle collision model also produces fluctuations due to its stochastic nature. Therefore, larger differences between the simulations with and without SGS velocity might be obtained when the direct collision model for bubbles is used.
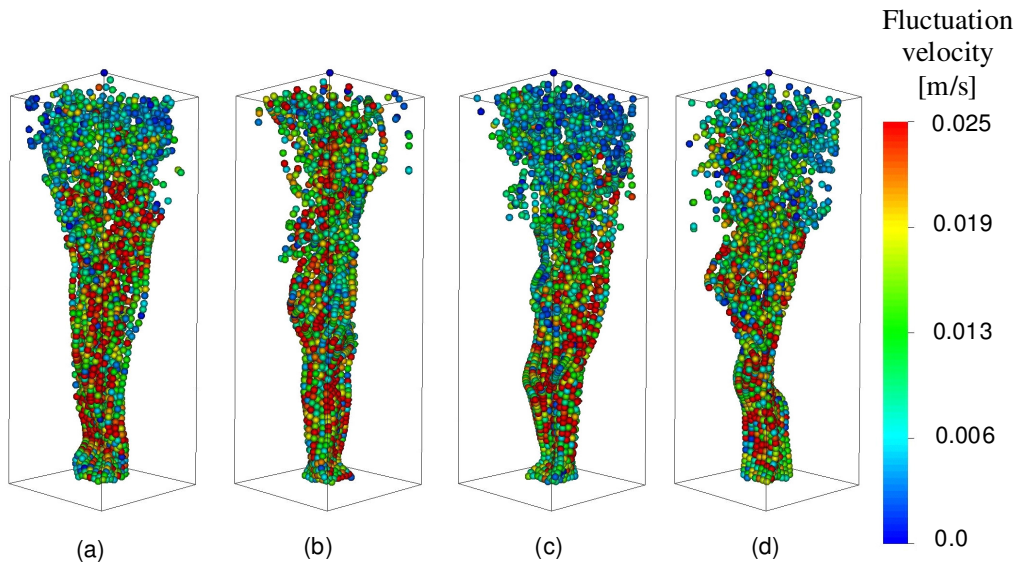
Figure 2.11. Snapshots of the bubble dispersion pattern after 20, 50, 100 and 150 s. The bubbles are colored by the magnitude of the liquid fluctuations at its position. Note that the bubbles are magnified for visualization purpose, not to scale.

2.3.3   Effect of the Smagorinsky constant C_S

In the present study, the turbulence generated by bubbles, i.e., the so-called "bubble-induced turbulence", is not specifically modeled. Hence, the impact of the Smagorinsky constant C_S was studied by varying its value. The analysis is carried out based on the case with $C_S = 0.10$ (i.e., case 0) in comparison to a lower $C_S = 0.08$ (case 2) and a higher $C_S = 0.12$ (case 3). Figure 2.13(a)-(c) shows the comparison between the experimental and predicted profiles of the mean vertical velocity and fluctuating velocity components of the liquid phase. It can be seen that in the case with higher C_S, the predicted mean profile is almost equal to the case of $C_S = 0.10$, while a lower C_S provides the least good agreement between experiment and simulation. This is due to the fact that with a decrease of C_S, the turbulent viscosity is also decreased. Consequently, the fluctuations of the bubble plume get stronger, resulting in a higher

collision frequency and lower average velocity profiles. This phenomenon only slightly influences the flow field in the case with higher C_S. It can also be seen that, both vertical and lateral fluctuating components are affected by the choice of C_S in the similar manner. We conclude that the variation of C_S has only marginal effect to the predicted flow fields and an improvement can be made by incorporating a reliable multiphase turbulence model.
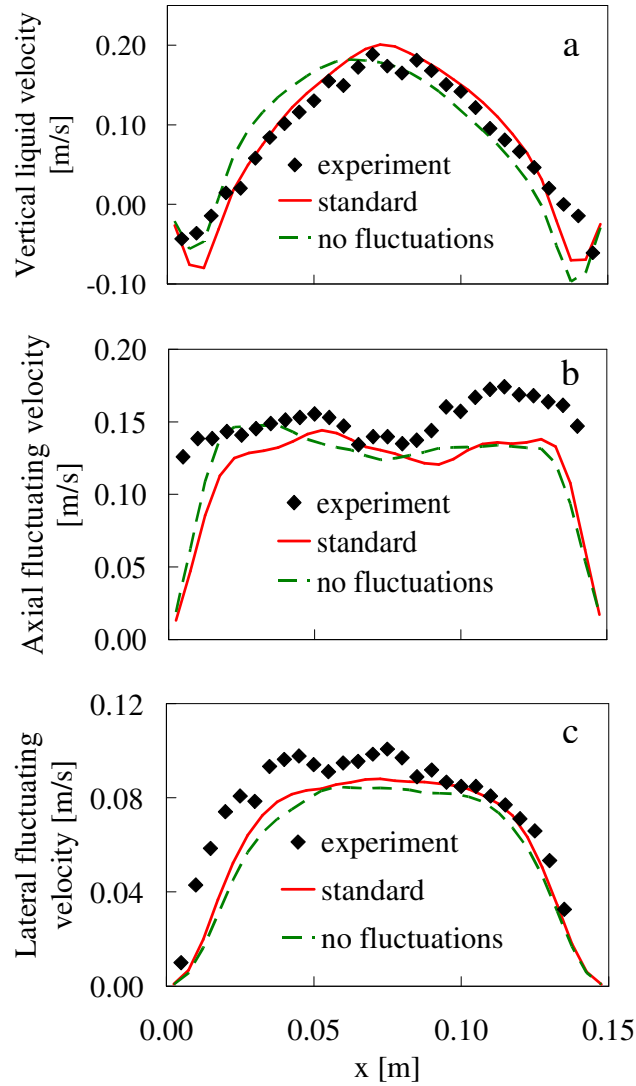
Figure 2.12. Comparison of the predicted and experimental average liquid velocity and the fluctuating velocity components for the standard case (case 0) and the case without subgrid-scale fluctuations (case 1) at a height of 0.28 m and a depth of 0.075 m.
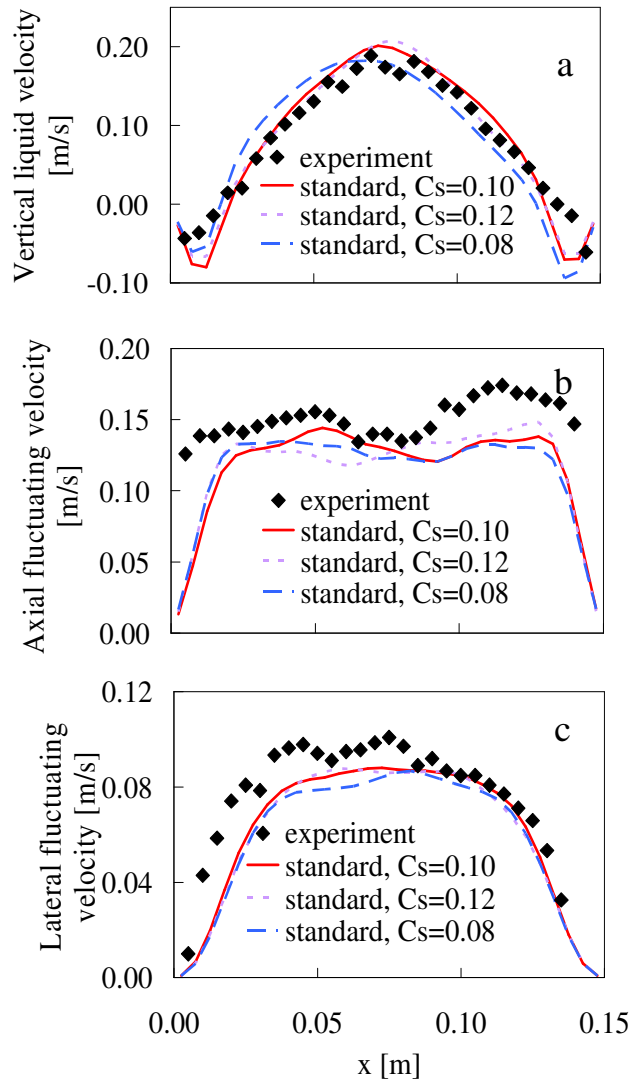
Figure 2.13. Comparison of the predicted and experimental average liquid velocity and fluctuating velocity components for the standard case (case 0) with various values of the Smagorinsky constant (case 2 and 3) at a height of 0.28 m and a depth of 0.075 m.

2.3.4 Sensitivity of the grid size ratio to the bubble diameter

As discuss earlier that, the grid size ratio to the bubble diameter, h/d_p ratio, should compromise between a sufficiently fine grid resolution to capture the most energetic eddies, and a sufficiently coarse grid resolution to stay close to the Milelli criterion, here we studied the influence of the h/d_p ratio by carry out simulations with a h/d_p ratio equal to 1.25 (the standard case, case 0), 1.50 (case 4), and 1.10 (case 5). Figure 2.14(a)-(c) shows the comparison of the predicted profiles of the mean vertical velocity and fluctuating velocity components of the liquid phase with various h/d_p ratios. As expected, the simulation with the highest h/d_p ratio, i.e.,

the coarsest grid size, provides large deviation from the experimental data. Albeit the h/d_p ratio is closet to the Millelli criterion, the grid size is too coarse for resolving the flow field and correctly coupling between phases. Decreasing the h/d_p ratio from 1.25 to 1.10 slightly improves the prediction with an expense of computational resources. Therefore, we concluded that, in this work, the h/d_p ratio of 1.25 provides a sophisticated level of accuracy along with reasonable computational expenses.
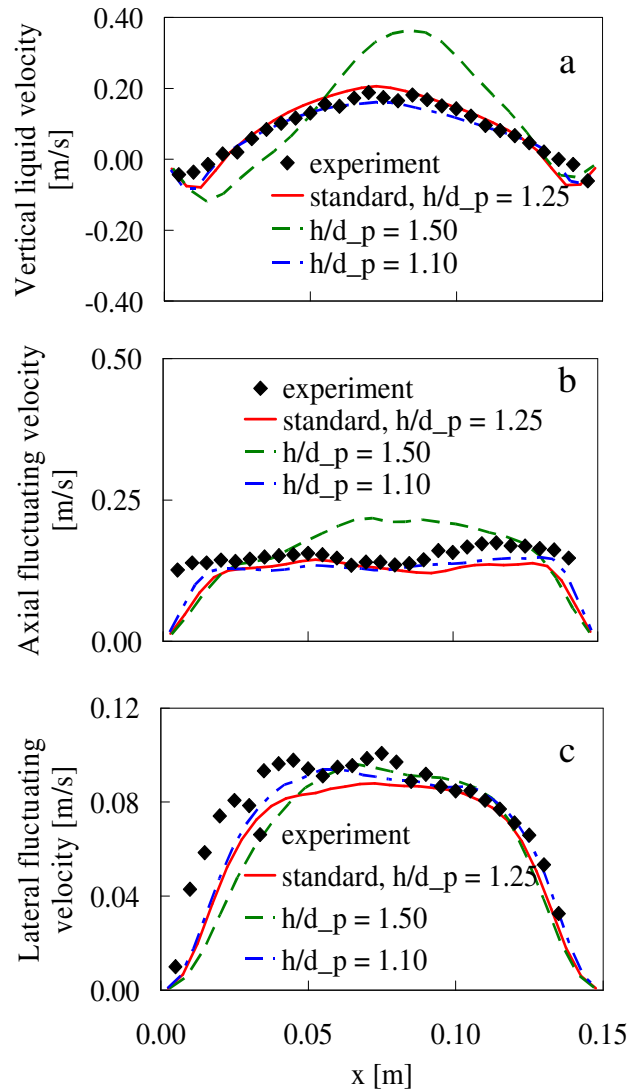
Figure 2.14. Comparison of the predicted and experimental average liquid velocity and fluctuating velocity components for the standard case (case 0) with various grid size ratio to the bubble diameter (h/d_p) (case 4 and 5) at a height of 0.28 m and a depth of 0.075 m.

2.3.5   Speedup and scalability on parallel platforms

In order to analyze the parallelization performance of the presented modeling technique, the concepts of speedup and scalability are employed. The speedup concept represents the relative reduction of execution time when a parallel execution on p processors is performed. According to Rauber and Rünger (2009), the speedup $S_p(n)$ of a parallel program with n processors with a parallel execution time $T_p(n)$ is defined as

$$S_p(n) = \frac{T_p(1)}{T_p(n)} \tag{2.12}$$

with $T_p(1)$ being the execution time to solve the same problem using the sequential version of the parallel implementation.

The scalability of a parallel program expresses the efficiency of the program while increasing the problem size with a fixed number of n processors. The scalability $S_s(m)$ is defined here as a proportion of the execution time $T_s(m)$ of a problem with a size m to the execution time of a problem with an appropriate selected reference problem size $T_s(m_0)$

$$S_s(n) = \frac{T_s(m)}{T_s(m_0)}. \tag{2.13}$$

In the present paper, a simulation case with a computational domain of 640×32×32 grid nodes was used to measure the speedup and scalability of the program using Sun X2100, dual core Opteron CPUs with Gigabit Ethernet. The settings are similar to the case 0 in the previous section, except that the bubbles are homogeneously generated throughout the computational domain to equally distribute the computational load at every processor. The studies were carried out for 1 s, i.e., 10,000 time steps.

Figure 2.15(a) shows the speedup obtained with 1, 2, 4, 8, 16 and 32 processors. The simulation cases contain 64,000 bubbles in total at every instance. The measurement of the execution time for the dispersed gas phase and the continuous liquid phase are performed separately. The total speedup is the weighted average of the underlying dispersed and continuous phase calculation. It should be noted that in our cases, the computational time of the dispersed phase is approximately 85% of the total computational time. As can be seen, excellent

overall and dispersed-phase speedups are obtained, while the speedup of the liquid phase decreases with an increasing number of processors. The reason for the deterioration of the speedup of the continuous phase part (i.e., the LB scheme calculation) in our test case is that, the layers being calculated on each processors are the summation of the real domain layers and the ghost layers (including the communication of these layer), therefore the computational resources being used for the ghost layer becomes significant when the number of processors increases. For instance, based on our test case, with 16 processors, each processor performs a calculation of 40 real domain layers and 6 ghost layers, i.e., the ratio is being 40:6, while the ratio is equal to 20:6 with 32 processors. Thus, the calculation of the ghost layers is increased from 15% to 30% of the total LB scheme calculation. An alternative to improve the speedup might be to perform two-dimensional parallelization. It is worth to repeat that, the overall performance is characterized by the Lagrangian particle tracking part which takes approximately 85% of the calculation time. Therefore, the main benefit from the presented modeling technique being the high parallel efficiency of the stochastic-based Lagrangian particle tracking, the well-known flexibility of complex geometry handling provided by LB scheme, and the parallel performance of the LB scheme (when an appropriate ratio between the real domain layers and the ghost layers is used). These provide us an alternative for simulations of multiphase dispersed flow within a complex geometry, e.g., flow in a multiphase stirred vessel. It is also important to note that, albeit an excellent overall speedup, the time step used in this study is approximately two orders of magnitude smaller than the conventional CFD calculation, e.g., in the work of Zhang et al. (2006). Therefore, the maximum benefit of using a LB-based simulation can be explored when solving a large-scale problem where a massive parallelization can be utilized.

The scalability of the program is shown in Figure 2.15(b). In this comparison, the base case has a total number of 40,000 bubbles, while the number of bubbles is equal to 4,000,000 in the largest case. The computational domain is kept constant in every case. The execution time used in this analysis is only the execution time of the dispersed gas phase. An excellent scalability of the program is obtained. Figure 2.15 (b) shows that an increase of the problem size does not lead to an increase of the simulation time. For example, a 100-fold increase of the problem size leads to a 90-fold increase of the simulation time. This might be attributed to the fact that the Eulerian part of the dispersed phase calculation is kept constant, independent to the number of bubbles, while the scalability of the Lagrangian part is linear.
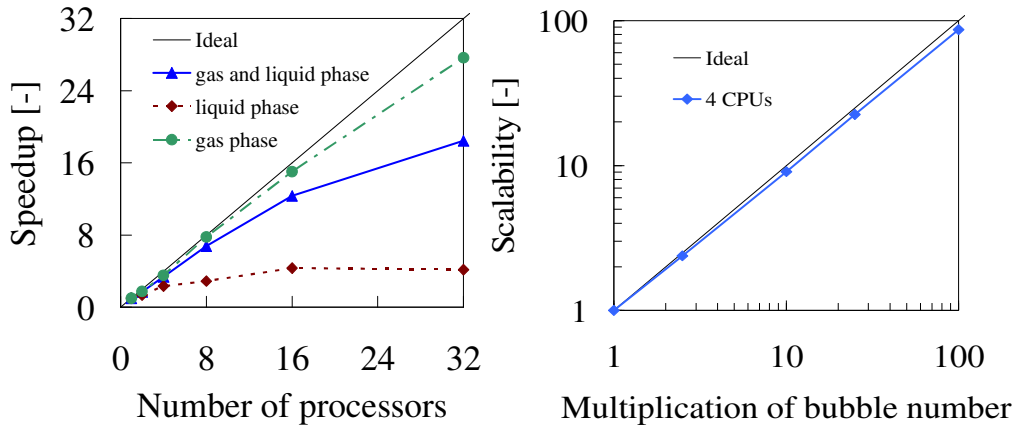
Figure 2.15. Speedup and scalability of the present modeling technique. The simulations were performed for 640×32×32 grid nodes and 64,000 bubbles. The simulations in the scalability study were performed using 4 processors and contain 640×64×64 grid nodes with 40,000 bubbles in the base case (with a multiplication factor of 1) and 4,000,000 bubbles in the largest case (with a multiplication factor of 100).

2.4   Conclusions

A novel modeling technique for the simulation of turbulent gas-liquid bubbly flows according to the Eulerian-Lagrangian (EL) approach has been presented. Each individual bubble was treated as a single, point-volume particle and was tracked in a turbulent liquid flow field. The turbulence in the liquid phase was represented by filtered conservation equations. The impact of the residual (sub-filter) fluctuation components on the motion at the grid scales was modeled using the Smagorinsky model. It was shown that the choice of the Smagorinsky constant C_S slightly affects the predicted flow field with the best result obtained using $C_S = 0.10 - 0.12$. It is important to note that the filtering process employed here should be viewed as an engineering model, rather than a large eddy simulation (LES). This is due to the restriction of our EL approach that requires the grid size should be larger than the bubble size. Consequently, the grid space is too coarse to sufficiently resolve the flow field required for a regular LES. The motion of bubbles was computed considering gravity/buoyancy, fluid stresses, drag, lift and added mass forces. The Basset history force was neglected for physical (and computational) reasons. It is well known that as of yet there is no universal inter-phase closure model available for the simulation of bubbly flow. Thus, a set of appropriate empirical correlations for the inter-phase closures was carefully chosen from the literature.

Specifically the main results of this work are:

- It has been demonstrated that due to the coarse grid space used in the simulations, the residual fluctuating velocity components of the liquid phase have a significant effect on the bubbles motion which is represented by the predicted mean and fluctuating flow fields. In our work, the residual fluctuations were considered by means of a Langevin equation model.

- Collisions between bubbles were considered using a stochastic inter-particle collision model. The model is based on the generation of a fictitious collision partner and a collision probability according to the kinetic theory. The collision model dramatically decreases computing time compared to the direct collision method and provides excellent computational efficiency on parallel platforms.

- The predicted results were compared with experiments of Deen et al. (2001). Both mean and fluctuating velocities are in excellent quantitative and qualitative agreement with the measured data. Furthermore, the sub-grid model used (i.e., the Smagorinski model) provides an excellent agreement between experimental and simulation data. Thus, the simulation can be used to obtain detailed, quantitative insight into the dynamics of the dispersed and the continuous phase in the bubble column.

- The speedup and the scalability of the presented modeling technique on parallel platforms have been analysed. Excellent overall parallelization performance and scalability of the program were demonstrated. The maximum benefit of the presented modeling technique can be obtained when a large-scale simulation, in which the ratio between the characteristic length and the bubble diameter is several order higher, and a massively parallelization are realized.

While the study presented here has been carried out for a bubble column with a relatively low global gas holdup (approximately 1%), the modeling techniques can be applied to a wide range of problems, involving turbulent gas-liquid bubbly flow in stirred systems. Nevertheless, in order to deal with real industrial problems, which often involve a high global gas holdup, further work will address for the inclusion of the gas void fraction in the conservation equations, the void fraction dependence of drag force, as well as models for bubble coalescence and breakup.

2.5   References

1   Bernaschi M, Fatica M, Melchionna S, Succi S, Kaxiras E. A flexible high-performance lattice Boltzmann GPU code for the simulations of fluid flows in complex geometries. *Concurrency and Computation: Practice & Experience*. 2010;22l:1-14.

2   Deen NG. An experimental and computational study of fluid dynamics in gas-liquid chemical reactors. PhD Thesis. 2001. Aalborg University Esbjerg, Denmark.

3   Deen NG, Solberg T, Hjertager BH. Large eddy simulation of the gas-liquid flow in a square cross-sectioned bubble column. *Chemical Engineering Science*. 2001;56:6341-6349.

4   Deen NG, Van Sint Annaland M, Kuipers JAM. Multi-scale modeling of dispersed gas-liquid two-phase flow. *Chemical Engineering Science*. 2004;59:1853-1861.

5   Delnoij E. Fluid dynamics of gas-liquid bubble columns: A theoretical and experimental study. PhD Thesis. 2001. Twente University, the Netherlands.

6   Derksen JJ. Numerical simulation of solids suspension in a stirred tank. *AIChE Journal*. 2003;49:2700-2714.

7   Derksen JJ. Simulations of lateral mixing in cross-channel flow. *Computers & Fluids*. 2010;39:1058-1069.

8   Derksen JJ, Van den Akker HEA. Large eddy simulations on the flow driven by a Rushton turbine. *AIChE Journal*. 1999;45:209-221.

9   Derksen JJ, Van den Akker HEA, Sundaresan S. Two-way coupled large-eddy simulations of the gas-solid flow in cyclone separators. *AIChE Journal*. 2008;54:872-885.

10 Eggels JGM, Somers JA. Numerical simulation of free convective flow using the lattice-Boltzmann scheme. *International Journal of Heat and Fluid Flow*. 1995;16:357-364.

11 Hirt CW, Nichols BD. Volume of fluid (VOF) method for the dynamics of free boundaries. *Journal of Computational Physics*. 1981;39:201.

12 Ho CA. Modellierung der Partikelagglomeration im Rahmen des Euler/Lagrange-Verfahrens und Anwendung zur Berechnung der Staubabscheidung im Zyklon. PhD Thesis. 2004. Martin-Luther-Universität Halle-Wittenberg. Germany.

13 Hu G. Towards large eddy simulation of dispersed gas-liquid two-phase turbulent flows. PhD Thesis. 2005. West Virginia University. United States.

14 Hu G, Celik I. Eulerian-Lagrangian based large-eddy simulation of a partially aerated flat bubble column. *Chemical Engineering Science*. 2008;63:253-271.

15 Joshi JB. Computational flow modeling and design of bubble column reactors. *Chemical Engineering Science*. 2001;56:5893-5933.

16 Loth E. Numerical approaches for motion of dispersed particles, droplets and bubbles. *Progress in Energy and Combustion Science*. 2000;26:161-223.

17 Milelli M, Smith BL, Lakehal D. Large-eddy simulation of turbulent shear flows laden with bubbles. In Direct and Large-Eddy Simulation-IV, Geurts, B.J., Friedrich, R., Metais, O. (Eds.), Vol 8 of ERCOFTAC Series. 2001. Kluwer Academic Publishers, Dordrecht, The Netherlands, pp. 46-470.

18 Nicěno B, Boucker M, Smith BL. Euler-Euler large eddy simulation of a square cross-sectional bubble column using the Neptune CFD code. *Science and Technology of Nuclear Installations*. 2009;Article 410272.

19 Pozorski J, Apte SV. Filtered particle tracking in isotropic turbulence and stochastic modeling of subgrid-scale dispersion. *International Journal of Multiphase Flow*. 2009;35:118-128.

20 Ranade VV. Computational Flow Modeling for Chemical Reactor Engineering. Academic Press. 2002.

21 Rauber T, Rünger G. Parallel programming for multicore and cluster systems. Springer. 2009.

22 Smagorinsky J. General circulation experiments with the primitive equations: 1. The basic experiment. *Monthly Weather Review*. 1963;91:99.

23 Somers JA. Direct simulation of fluid flow with cellular automata and the lattice-Boltzmann equation. *Journal of Applied Sciences Research*. 1993;51:127-133.

24 Sommerfeld M. Validation of a stochastic Lagrangian modeling approach for inter-particle collisions in homogeneous isotropic turbulence. *International Journal of Multiphase Flow*. 2001;27:1829-1858.

25 Sommerfeld M, Bourloutski E, Broeder D. Euler/Lagrange calculations of bubbly flows with consideration of bubble coalescence. *The Canadian Journal of Chemical Engineering*. 2003;81:508-518.

26 Sommerfeld M, Kohnen G, Rueger M. Some open questions and inconsistencies of Lagrangian particle dispersion models. In: Proceedings of the Ninth Symposium on Turbulent Shear Flows. Kyoto Japan. 1993;Paper No. 15-1.

27 Unverdi SO, Tryggvason G. A front-tracking method for viscous, incompressible multi-fluid flow. *Journal of Computational Physics*. 1992;100:25-37.

28 Van den Hengel EIV, Deen NG, Kuipers JAM. Application of coalescence and breakup models in a discrete bubble model for bubble columns. *Industrial and Engineering Chemistry Research*. 2005;44:5233-5245.

29 Zhang D, Deen NG, Kuipers JAM. Numerical simulation of the dynamic flow behavior in a bubble column: A study of closures for turbulence and interface forces. *Chemical Engineering Science*. 2006;61:7593-7608.

2.6 Appendix

Correlation function in Langevin equation model

$$R_p(\Delta t, \Delta r) = R_L(\Delta t) \times R_E(\Delta r).$$
(A 2.1)

The Lagrangian velocity auto-correlation function

$$R_L(\Delta t) = \exp\left(-\frac{\Delta t}{T_L}\right).$$
(A 2.2)

The Lagrangian integral time scale

$$T_L = c_T \frac{\sigma_{SGS}^2}{\varepsilon} \text{ with } c_T = 0.4.$$
(A 2.3)

The Eulerian correlation tensor

$$R_{E,ij}(\Delta r) = \{f(\Delta r) - g(\Delta r)\}\frac{r_i r_j}{r^2} + g(\Delta r)\delta_{ij},$$
(A 2.4)

with

$$f(\Delta r)_i = \exp\left(-\frac{\Delta r}{L_{E,i}}\right), \ g(\Delta r)_i = \left(1 - \frac{\Delta r}{2L_{E,i}}\right)\exp\left(-\frac{\Delta r}{L_{E,i}}\right).$$
(A 2.5)

The integral length scale

$$L_{E,x} = 1.1 T_L \sigma_{SGS}, \ L_{E,y} = L_{E,z} = 0.5 L_{E,x}.$$
(A 2.6)

The particle response time

$$\tau_p = \frac{4}{3} \frac{d_p^2}{C_D |\mathbf{u} - \mathbf{u}_p|} \text{ where } Re > 1.$$
(A 2.7)

3

MODELING OF A GAS-LIQUID STIRRED REACTOR WITH NEWTONIAN LIQUID[1]

Simulations of a gas-liquid stirred reactor including bubble breakage and coalescence were performed. The filtered conservation equations for the liquid phase were discretized using a lattice Boltzmann scheme. A Lagrangian approach with a bubble parcel concept was used for the dispersed gas phase. Bubble breakage and coalescence were modeled as stochastic events. Additional assumptions for bubble breakup modeling in an Euler-Lagrange framework were proposed. The action of the reactor components on the liquid flow field was described using an immersed boundary condition. The simulation results were compared to experimental data for a laboratory-scale gas-liquid stirred reactor with dilute dispersion. The predicted number-based mean diameter agrees qualitatively and quantitatively well with the measured data. Despite a relatively coarse grid resolution employed in the simulations, a good agreement with measured data for the long-term averaged liquid velocity components was achieved. Effects of the presence of bubbles, as well as the increase of the gas flow rate, on the hydrodynamics were numerically studied. The modeling technique offers an alternative engineering tool to gain detailed insights into complex industrial-scale gas-liquid stirred reactors.

---

[1] This chapter is based on Sungkorn R, Derksen JJ, Khinast JG. Euler-Lagrange modeling of gas-liquid stirred reactor with consideration of bubble breakage and coalescence. Submitted to *AIChE Journal* (2011).

3.1   Introduction

Stirred tank reactors are among the most widely used reactor types in a large variety of industrial processes involving multiphase flows. Typical examples include industrial hydrogenations or oxidations, as well as aerobic fermentation processes in which gas bubbles are dispersed in turbulent fluid flow induced by one or more impellers. In biotechnological processes, the activity and the growth of microorganisms (e.g., bacterial or fungal systems) or cells are sensitive to a number of parameters, such as dissolved oxygen content, substrate concentration and pH-level. A major challenge in these processes is to provide adequate liquid mixing and to generate a large interfacial contact area, while avoiding shear damage of microorganisms and cells caused by hydrodynamic effects (Gogate et al., 2000; Arlov et al., 2008).

The flow structures in a single liquid-phase stirred reactor are known to be highly complex associated with time-dependent, three-dimensional phenomena covering a wide range of spatial and temporal scales (Derksen & Van den Akker, 1999). The complexity increases drastically when a gas phase is introduced. Additional effects include the interaction between phases in terms of mass, energy and momentum exchange, the interaction between the second phase and the impeller, and bubble breakage and coalescence. Since the reactor performance is a complex function of the underlying phenomena, a detailed knowledge regarding the hydrodynamics and the evolution of the dispersed phase are essential for the engineering of a high performance reactor.

Traditionally, engineering of gas-liquid stirred reactors is based on empirical correlations derived from experiments. The information obtained from this approach is usually described in global parametric form and applicable within a narrow window of geometry configurations and operating conditions. Recently, the use of computational fluid dynamics (CFD) has gained some popularity among researchers and practitioners for the engineering of stirred reactors. Significant progress has been made over the last decades in the fields of turbulence and multiphase-flow modeling, numerical methods as well as computer hardware. Consequently, time-dependent, three-dimensional simulations of gas-liquid stirred reactors with a sophisticated level of detail and accuracy are feasible today.

Various CFD modeling techniques for gas-liquid flows, where the gas phase is dispersed in the liquid phase, have been reported in the literature. These techniques can be grossly categorized based on their treatment of the dispersed phase into Euler-Euler (EE) and Euler-Lagrange (EL) approaches (Crowe et al., 1998; Loth, 2000). In the EE approach, both phases are treated as interpenetrating continua. The interactions between phases are modeled via

the phase interaction terms that appear in the conservation equations describing the dynamics of the system. The EE approach assuming mono-disperse spheres has been used in the work of Deen et al. (2002), Khopkar et al. (2005) and Zhang et al. (2008) for simulations of gas-liquid stirred reactors. A more sophisticated EE approach, where the local bubble size distribution (BSD) is computed by solving population balance equations (PBEs), has been reported by Venneker et al. (2002), Laakkonen et al. (2007) and Montante et al. (2008). In the EL approach, each individual bubble or a parcel of bubbles is represented by a single point. The linear motion of the bubbles is governed by Newton's law of motion. Rotational momentum balances are typically not considered. The EL approach requires closure relations to account for the inter-phase forces, which can be obtained from empirical relations or from simulations with higher level of detail, e.g., a front tracking (FT) approach (Unverdi & Tryggvason, 1992) or volume of fluid (VOF) methods. Closures for gas-liquid systems which take into account the effect of high gas-phase loadings are still an area of ongoing research (e.g., Behzadi et al., 2004). The EL approach is computationally expensive. However, its advantages are the high flexibility with respect to incorporating microscopic and bubble-level phenomena, such as bubble-bubble interactions, bubble-wall interactions, breakup and coalescence of bubbles. Simulations of gas-liquid stirred reactors using the EL approach are relatively rare in the literature. Some examples include the work of Wu et al. (2001) and Arlov et al. (2008) for simulations of reactors with mono-disperse spheres and the work of Nemoda & Zivkovic (2004) for the simulation of a reactor with bubble breakage.

The goal of this work is to assess the detailed modeling of a gas-liquid stirred reactor by an EL approach. The simulations are restricted to laboratory-scale reactors (with a volume in the order of 10 liters) with dilute dispersion (i.e., a global gas phase of up to 2% volume fraction). The reason for simulating these systems is that, in this work, we mainly focus on the validation of the modeling technique presented in the next section. Detailed validation requires highly resolved experimental information concerning liquid flow field and local bubble size distributions (BSD) which hard (if not impossible) to obtain in dense systems. Dispersed-phase volume fraction effects in the conservation equations of the continuous phase, and high-frequency collisions drastically increase the complexity in denser systems, also from a computational point of view. Being able to numerically deal with denser systems is the subject of (our) current research. In engineering practice, the gas phase fraction and the size of the reactor are typically much larger. However, since the presented modeling technique is based on elementary physical principles which also play a role at the full-scale, the understanding of the

underlying phenomena obtained in this work makes it worthwhile for researchers and practitioners. The main elements of the modeling technique used in our study are:

- The continuous liquid phase is modeled using a variation of the lattice-Boltzmann (LB) scheme due to Somers (1993). The LB scheme is used to solve the large-scale motions of the turbulent flow using the filtered conservation equations. The Smagorinsky subgrid-scale model is applied to model the effects of the sub-filter scales (Smagorinsky, 1963). It has been demonstrated that the scheme can accurately predict turbulent hydrodynamics in single phase system (Derksen & Van den Akker, 1999) as well as in multiphase systems (Derksen, 2003; Derksen et al., 2008; Sungkorn et al., 2011).

- An adaptive force-field procedure (Derksen et al., 1997), also known as an immersed boundary method, is used for describing the action of the reactor components (i.e., the impeller, tank wall, baffles and internals) on the liquid flow field.

- The motion of the individual bubbles are computed by Lagrangian tracking taking into account the sum of forces due to stress gradients, net gravity, drag , lift and added mass. The momentum transfer between phases, i.e., the two-way coupling, is achieved by the mapping function with the virtual diameter concept introduced by Deen et al. (2004). The impact of turbulence on the motion of the bubbles, i.e., the fluctuations of the sub-filter or residual fluid velocity along the bubble trajectory, is computed using the Langevin equation model introduced by Sommerfeld et al. (1993).

- Collisions of bubbles are governed by the so-called stochastic inter-particle collision (Sommerfeld, 2001). Based on the stochastic model, coalescence of bubbles is determined by comparing the film drainage time with the bubble contact time (Sommerfeld et al., 2003). Breakup of bubbles is accounted for using a theoretical model derived from the theory of isotropic turbulence (Luo & Svendsen, 1996). It is assumed that breakup is caused mainly by the interaction of bubbles with turbulent eddies.

Although various elements of our approach have been reported in literature, the present modeling technique, for the first time, assesses the feasibility of using the LB scheme with the Lagrangian particle tracking (LPT) model with consideration of bubble breakage and coalescence for simulations of gas-liquid stirred reactors. The simulations provide a detailed insight into gas-liquid stirred reactors with a high level of accuracy along with reasonable computational requirement.

In the next section, the modeling technique for turbulent bubbly flows in the EL framework will be briefly introduced. A detailed discussion of this approach can be found in our previous work (Sungkorn et al., 2011). Additional models for the simulation of gas-liquid

stirred reactors, e.g., the treatment of reactor components, bubble breakup and coalescence, will be discussed in detail. In the subsequent section, the model validation, ranging from a bubble column to a gas-liquid stirred reactor, will be presented and discussed in detail. The conclusion will be summarized in the final section.

3.2   Numerical Modeling Aspects

3.2.1   Liquid phase hydrodynamics

In this work, the lattice-Boltzmann (LB) scheme is used to model the turbulent liquid flow. The LB scheme is based on a simple form of the Boltzmann kinetic equation, which can be used to recover the macroscopic hydrodynamic behavior of fluids (Succi, 2001). The basic idea is that fluid flow, which is governed by conservation laws, can be simulated by a many-particles system obeying the same laws. A set of (fictitious) particles residing on a lattice moves to neighbor sites and exchanges momentum (i.e., collide) with particles coming from other directions. The collision rules and the topology of the lattice are defined such that the Navier-Stokes equations are recovered (Chen & Doolen, 1998).

The specific LB scheme employed here is due to Somers (1993) (see Eggels & Somers, 1995; Derksen & Van den Akker, 1999) with a cubic and uniform lattice. The scheme was chosen because of its robustness for turbulence simulations. This is due to the explicit treatment of the high-order terms which results in enhanced stability at low viscosities and, thus, allows simulations of high Reynolds numbers. In the LB scheme, the arithmetic operations are local, i.e., data required for updating the flow in a grid point are obtained from its next neighbors and, specifically, the stress tensor is explicitly obtained from the data stored in a single node. Therefore, parallelization through domain decomposition requires only communication of subdomain boundary values, resulting in efficient parallel algorithms.

Gas-liquid flows in a bubble column or in a stirred reactor, are normally turbulent, even at lab scale and with gas volume fraction as low as 1%. Considering the liquid motions induced by dispersed gas bubbles, the turbulent stress can be divided into two components; one due to bubble buoyancy leading to liquid velocities above the turbulence onset and one part due to the so-called pseudo-turbulence caused by the fluctuation of the bubbles, i.e., the zig-zagging motion of bubbles relative to the fluid, resulting in turbulent-like flows due to vortex shedding and interaction phenomena. Direct numerical simulation (DNS) of these flows is not feasible due to limitation in computational resources, as the resolution of all length and time scales requires enormous amounts of grid cells and time steps. In order to overcome this limitation, only the evolution of the large-scale motions is resolved by applying a filtering process to the

conservation equations of the liquid phase. The resolved flow can be interpreted as a low-pass filtered representation of the real flow. The impact of the residual motion that resides at scales smaller than the filter width is modeled using the sub-grid scale (SGS) model due to Smagorinsky (1963). In this model, the SGS motion is considered to be purely diffusive and the model only drains energy from the resolved motions without feed-back. A larger fraction of the eddies and more of the energy residing in the flow are resolved with a finer grid spacing, i.e., a higher resolution. However, the choice of grid spacing in the EL approach is also restricted by the size of the bubbles, as will be discussed in detail in the next section. Furthermore, Hu & Celik (2008) pointed out that the residual motion of the pseudo-turbulence, which posses a universal energy spectrum different from the classical -5/3 decay in single phase turbulence, could (in principle) be captured using a dedicated SGS model. Such a reliable and accurate SGS model for multiphase flows is not available. Therefore, the SGS model used in this work is adopted directly from the single-phase SGS model. This is justified by our favorable results in relation to experimental data as will be shown later in this work. The eddy viscosity ν_t concept is used to represent the impact of the SGS motion as:

$$\nu_t = \left(C_S \Delta\right)^2 \sqrt{S^2} \; , \tag{3.1}$$

with the Smagorinsky constant C_S, the filter width Δ (equal to the cubic grid cell size h) and the resolved deformation rate $\sqrt{S^2}$. The value of C_S is kept constant at 0.10 throughout this work. It has been demonstrated that the variation of C_S has only marginal effect on the predicted flow field (Derksen, 2001; Sungkorn et al., 2011).

Since the simulations discussed here are restricted to dilute dispersions, i.e., global gas volume fractions of up to 2%, it can be assumed that the void fraction term in the momentum conservation equations for the liquid phase has a relatively small effect on the flow. The filtered conservation equations (with source terms representing forces exert by the bubbles and the reactor components) for single phase flow are approximately valid. The formulation and detailed discussion for the conservations equations employed in this work can be found in Eggels & Somers (1995) and Derksen & Van den Akker (1999). This assumption has been successfully used for simulations of multiphase flows within the dilute dispersion limit by several researchers (e.g. Derksen, 2003; Hu & Celik, 2008; Sungkorn et al., 2011).

3.2.2 *Impeller and tank wall treatment*

Stirred tanks typically consist of a cylindrical vessel equipped with one or more impellers, baffles, and, optionally, other internals. They can be divided, into static (i.e., tank wall, baffles,

and internals) and moving components (i.e., impellers and shaft). In this work, an adaptive force-field technique, also known as an immersed boundary method, (Goldstein et al., 1993; Derksen et al., 1997) is employed to describe the action of the reactor components on the liquid flow field. The method mimics these components by a set of control points on their surface. It computes forces on the flow such that the flow field has a prescribed velocities at the control points within the domain, i.e., equal to zero at static components and equal to the surface velocity for the moving components. The deviation from the prescribed velocities is estimated by a second-order interpolation and imposed back on the lattice sites during the collision step (Derksen & Van den Akker, 1999).

In the vicinity of walls, the turbulence becomes anisotropic, i.e., fluctuations in the wall-normal direction are suppressed. Consequently, the SGS Reynolds stresses should become zero. These effects are accounted for by employing the Van Driest wall damping function (Van Driest, 1956) with the universal velocity profiles (Spalding, 1961).

3.2.3 Bubble dynamics

The dispersed phase (i.e., the bubble phase) is tracked in a Lagrangian manner. A point-volume (also known as point-force) assumption is employed. In this assumption, the bubble is assumed to have a spherical shape and the bubble surface effect on the continuous fluid is neglected (Loth, 2000). Each point representing a parcel of bubbles with identical properties (i.e., position, velocity and diameter) is tracked simultaneously in the time-dependent, three-dimensional flow field. It is noted that the number of bubbles in a parcel is a real number $\{\Re\}$. Its trajectory is computed based on Newton's law of motion. All relevant forces, such as net gravity force, forces due to stress gradients, drag, net transverse lift, and added mass force are considered. Thus, the following set of equations will be solved for the motion of bubbles in a parcel:

$$d_t \mathbf{x}_p = \mathbf{u}_p, \tag{3.2}$$

$$\begin{aligned} \rho_p V_p d_t \mathbf{u}_p = (\rho_p - \rho_l) V_p \mathbf{g} + \rho_l V_p D_t \mathbf{u} - \frac{1}{8} C_D \rho_l \pi d_p^2 |\mathbf{u}_p - \mathbf{u}| (\mathbf{u}_p - \mathbf{u}) \\ - C_L \rho_l V_p (\mathbf{u}_p - \mathbf{u}) \times \nabla \times \mathbf{u} - C_A \rho_l V_p (D_t \mathbf{u}_p - D_t \mathbf{u}) \end{aligned}, \tag{3.3}$$

with $\mathbf{x}_p$ being the centroid position of the parcel, $\mathbf{u}_p$ the velocity, ρ_p the bubble density, V_p the bubble volume with the diameter d_p, $\mathbf{g}$ the gravitational acceleration, ρ_l the liquid density, and $\mathbf{u}$ the liquid velocity at $\mathbf{x}_p$. The drag C_D and lift C_L coefficients depend on the bubble Reynolds number $Re_p = |\mathbf{u}_p - \mathbf{u}| d_p / \nu_l$ and the Eötvös number $\mathbf{Eo} = (\rho_l - \rho_p) |\mathbf{g}| d_p^2 / \sigma$. The

added mass force coefficient C_A is assumed to be constant at 0.5. Expressions for the forces acting on a bubble and its coefficients are summarized in the Appendix. The liquid velocity $\mathbf{u}$ at the centroid of the parcel in Eq. (3.3) consists of the resolved liquid velocity $\tilde{\mathbf{u}}$ and a (residual) liquid fluctuating component $\mathbf{u}'$. The latter component is used to mimic the impact of turbulence on the motion of the bubble, i.e., the fluctuations of the sub-filter (residual) liquid velocity along the bubble trajectory.

The interpolation of the liquid properties on the Eulerian grid nodes to the centroid of the parcel on the Lagrangian reference frame (and vice versa) is achieved using a "cheap clipped fourth-order polynomial" mapping technique proposed by Deen et al. (2004) (see Appendix for the formulation). In principal, the mapping function ς evaluates a property, such as the liquid velocity at the parcel centroid, by the integration of the liquid velocity at the Eulerian grid nodes that is located inside a predefined influence diameter (set to $2d_p$ in this work). Forces exerted by a parcel on the Eulerian grid nodes are accounted for via the inter-phase force terms in the conservation equations $\mathbf{F}_{p \rightarrow l}$, i.e., the back coupling. The force terms consist of the drag $\mathbf{F}_D$, lift $\mathbf{F}_L$, and added mass forces $\mathbf{F}_A$ as a function of the mapping function ς and the number of bubbles in the parcel n_p. At a grid node j with volume $V_{cell,j}$, the forces exerted by a parcel i can be expressed as:

$$\mathbf{F}_{p,i \rightarrow l,j} = -\frac{\varsigma_j \, n_p}{V_{cell,j}} \left(\mathbf{F}_D + \mathbf{F}_L + \mathbf{F}_A \right). \tag{3.4}$$

As mentioned earlier, a larger fraction of the eddies (and more of the energy residing in the flow) can be resolved using a higher grid resolution. Thus, a more accurate prediction of turbulent flow hydrodynamics requires finer grid spacing. In the framework of the EL approach, it is, however, suggested that the grid spacing ratio to the bubble diameter h/d_p should be greater than unity to maintain the validity of the point-volume approach. Therefore, the h/d_p value employed here should compromise between a sufficiently fine grid resolution to capture the most energetic eddies and a sufficiently coarse grid resolution to keep the point-volume assumption valid. However, we relax this restriction by allowing the h/d_p value to be lower than unity but greater than 0.5. This allows us to include large bubbles (with a diameter greater than the grid spacing) which are present mostly at the sparger and close to the impeller shaft. Note that the volume of parcels with large bubble is lower than 10% of the total bubble volume (and the number of large-bubble parcels is less than 1% of the total number of bubbles) having

only a minor effect on the resolved flow field. The applicability of a h/d_p value less than unity has been demonstrated by Darmana et al. (2009), and is justified by favorable results obtained in this work.

3.2.4 *Collisions*

Collisions between bubbles can be analyzed using direct collision models, e.g., soft sphere (Tsuji et a., 1992) and hard sphere collision model (Hoomans et al., 1996), or statistics-based collision models, e.g. the stochastic inter-particle collision model (Sommerfeld, 2001). In this stochastic model, no direct collisions, where a large amount of information from surrounding bubbles is required, are considered. Instead, only a fictitious collision partner (i.e., parcel) is assumed and a collision probability according to kinetic theory is established for each parcel at each time step of the trajectory calculation. The fictitious parcel is statistically generated based on information regarding bubble size distribution and velocity collected at Eulerian grid nodes. The fictitious parcel consists of bubbles with identical properties and similar number as in the considering parcel. Hence, the bubbles in the fictitious parcel can be considered as a representative for the surrounding bubbles. The collision probability P_{coll} is calculated based on the properties of the parcel (and its collision partner) and the local fluid properties as:

$$P_{coll} = \frac{\pi}{4}(d_p - d_{fict})^2 \left| \mathbf{u}_p - \mathbf{u}_{fict} \right| n_p \Delta t , \tag{3.5}$$

where the subscript *fict* represents properties of the bubbles in the fictitious parcel. The occurrence of a collision between a parcel and a fictitious parcel is determined by a comparison between the probability with a uniform random number in the interval [0,1]. The collision can result in momentum exchange (bouncing) or coalescence between the bubbles in the parcels. In case of a bouncing collision, the impact point is statistically determined on a collision cylinder where the fictitious parcel is stationary. A detailed description of the stochastic inter-particle collision procedure can be found in the work of Sommerfeld (2001). The procedure to determine coalescence of bubbles will be described in the next section.

Collisions between a parcel and the surfaces (tank, baffles and impeller) are considered to be elastic and frictionless. Since the motion of the moving components (e.g., impeller shaft, blades, and disc) is rotational, a collision with these components adds momentum to the bubble resulting in a change of the bubble tangential velocity (Derksen, 2003):

$$u_{p,\theta,out} = -u_{p,\theta,in} + 2r_p\Omega , \tag{3.6}$$

where $u_{p,\theta,out}$ and $u_{p,\theta,in}$ represent the tangential velocity after and before the collision, respectively. The local velocity at the impact point $r_p\Omega$ is the product of the angular velocity $\Omega = 2\pi N$ (with N being the impeller rotational speed) and the distance from the center axis r_p. At impact the distance between a parcel and a solid component is calculated based on the effective radius r_{eff} of a parcel-bubble as

$$r_{eff} = \left(\frac{3n_p V_p}{4\pi}\right)^{1/3} ,$$ (3.7)

with n_p being the number of bubbles in the parcel and V_p being the bubble volume.

3.2.5   *Coalescence model*

Following a collision between a parcel and a fictitious parcel described in the previous section, coalescence between the bubbles in parcel and the bubbles in the fictitious parcel is determined using the approach due to Prince & Blanch (1990). In this approach, coalescence will take place when the bubble contact time τ_{ij} is greater than the film drainage time t_{ij}. Otherwise, a rebound occurs. It is assumed that, in the frame of the considered Lagrangian collision model, the contact time can be expressed by:

$$\tau_{ij} = \frac{C_C R_{ij}}{u_n} ,$$ (3.8)

with the equivalent bubble radius R_{ij}

$$R_{ij} = 2.0\left(\frac{2}{d_p} + \frac{2}{d_{fict}}\right)^{-1} ,$$ (3.9)

where u_n is the relative approaching velocity in normal direction, C_C is the deformation distance as a fraction of the effective bubble radius; its value of 0.25 gives the best agreement with the experimental data (Sommerfeld et al., 2003) and is used throughout this work. Neglecting the effects due to surfactants and Hamaker forces, the film drainage time can be expressed as:

$$t_{ij} = \sqrt{\frac{R_{ij}^3 \rho}{16\sigma}} \ \ln\left(\frac{h_0}{h_f}\right),$$ (3.10)

with the initial film thickness h_0 for air-water set to 0.1 [mm], the final film thickness before rupture h_f set to 0.01[μm] (Prince & Blanch, 1990), and the surface tension σ. The properties

of the new bubble after coalescence are calculated from a mass and momentum balance. The new bubble diameter after coalescence is calculated as

$$d_{p,new} = \left(d_{p,old}^3 + d_{fict}^3\right)^{1/3}. \tag{3.11}$$

Since the total volume of the parcel must be conserved, the number of bubbles in a parcel after coalescence is expressed as

$$n_{p,new} = n_{p,old}\left(\frac{d_{p,old}}{d_{p,new}}\right)^3. \tag{3.12}$$

Based on the collision cylinder where the fictitious parcel is stationary, only the bubble normal velocity to the bubble in the fictitious parcel is changed, while the other velocity components remain unchanged. Thus, the normal velocity after coalescence $u_{p,n,new}$ can be expressed as

$$u_{p,n,new} = u_{p,n,old}\left(\frac{d_{p,old}^3}{d_{p,old}^3 + d_{fict}^3}\right). \tag{3.13}$$

It is important to emphasize here that a coalescence of bubbles takes place between a (real) parcel and a fictitious parcel, not between two real parcels. In the case of bouncing collisions (the contact time less than the drainage time), the normal velocity after collision is a function of the coefficient of restitution α (set to 0.90 in this work) and can be described by:

$$\tag{3.14}$$
$$u_{p,n,new} = u_{p,n,old}\left(\frac{d_p^3 - \alpha d_{fict}^3}{d_p^3 + d_{fict}^3}\right).$$

3.2.6 Breakup model

A breakup model due to Luo & Svendsen (1996) is employed in our work. The model was derived from the theories of isotropic turbulence and contains no adjustable parameters. The bubble interaction with turbulent eddies is assumed to be the dominant breakup mechanism. It is further assumed that only the eddies of length scale smaller than or equal to the bubble diameter participate in the breakup mechanism. Larger eddies simply transport the bubble without causing breakup. The breakup rate of bubbles with volume V_p into volumes of $V_p f_{BV}$ and $V_p\left(1 - f_{BV}\right)$ when being in contact with turbulent eddies in the size range of λ_{min} to d_p can be expressed as:

$$\frac{\Omega_B\left(V_p:V_pf_{BV}\right)}{\left(1-\alpha_g\right)n_p}=0.923\left(\frac{\varepsilon}{d_p^2}\right)^{1/3}\int_{\xi_{min}}^{1}\frac{\left(1+\xi\right)^2}{\xi^{11/3}}\exp\left(-\frac{2c_f\sigma}{\rho\,\varepsilon^{2/3}\,d_p^{5/3}\,\xi^{11/3}}\right)d\xi\,, \tag{3.15}$$

where α_g is the gas phase volume fraction, ε the energy dissipation at the centroid of the parcel, and $\xi_{min}=\lambda_{min}/d_p$. The breakage volume fraction f_{BV} is calculated from:

$$f_{BV}=0.5+0.5\tanh\left(10\frac{\left(RN-0.5\right)}{\pi}\right), \tag{3.16}$$

where RN is an uniform random number with the interval [0,1]. The resulting volume fraction of the daughter bubbles has a U-shaped distribution, i.e., the breakup into equal size has the lowest probability, while the breakup into infinitesimal volumes has the highest probability. In this work, we limit the range of breakage volume fraction in the interval [0.2,0.8]. Accordingly, the increase coefficient of surface area c_f is expressed as:

$$c_f=f_{BV}^{2/3}+\left(1-f_{Bv}\right)^{2/3}-1. \tag{3.17}$$

The minimum size of eddies in the inertial subrange of isotropic turbulence λ_{min} is assumed to be proportional to the length of the Kolmogorov-scale eddies λ_{ms}:

$$\lambda_{min}=11.4\lambda_{ms}\,, \tag{3.18}$$

with

$$\lambda_{ms}=\left(\frac{\nu^3}{\varepsilon}\right)^{1/4}, \tag{3.19}$$

where ν is the liquid phase kinematic viscosity.

In this work, the breakup rate is considered to be a stochastic value determined from a randomly generated breakage volume fraction Eq. (3.16). Thus, the breakup of a parcel within a certain interval is decided in the similar manner as for the collision of bubbles, i.e., by comparison with a uniform random number in the interval [0,1]. Furthermore, it is assumed that the breakup only takes place within the parcel and will not result in a new parcel. Instead, it will result in a parcel with a new bubble diameter calculated according to the breakage volume fraction. The number of bubbles in a parcel after breakup is calculated using the Eq. (3.12). Regardless of the success of the breakup, the parcel is assumed to interact with certain eddies in a certain interval characterized by the particle-eddy interaction time t_e. The next estimation of the breakup rate will be carried out after t_e [s], see Appendix for the formulations. This assumption is very important for a system where a high level of turbulence is present, e.g., in a

stirred reactor. It prevents unphysical consecutive breakups of bubbles and provides a time step resolution-independent solution.

3.3 Results and Discussion

3.3.1 *Bubble column with mono-disperse bubbles*

Dispersed gas-liquid flows in three-dimensional (non-stirred) bubble columns have been studied experimentally by several groups, including Deen et al. (2001) and Van den Hengel et al. (2005). Coalescence of bubbles was inhibited by adding salt solution resulting in a bubble column with (approximately) uniform bubble size. As their data are used to validate our model, we neglected breakup and coalescence of bubbles in this part of the study. Fluid flow was induced mainly by bubbles where the motion of bubbles relative to the liquid resulted in turbulent-like flow. The bubble plume fluctuated only weakly at the lower part of the column and was meandering around the column at the upper part. This fluctuation was caused by various mechanisms including, most importantly, bubble-bubble collisions and turbulence.

Modeling of these bubble columns was reported by Sungkorn et al. (2011). Their predicted mean and fluctuating liquid velocity components were in good agreement with the experimental data of Deen et al. (2001) cited above. Sensitivity to grid size over bubble diameter ratio h/d_p was also studied by performing simulations with a h/d_p-value of 1.10, 1.25, and 1.50. The study concluded that a finer grid (i.e., a lower h/d_p value) provides a better agreement with the experiment, while the coarsest grid was not sufficient to correctly capture the features of the flow field.

In the present work, we study the sensitivity of the predictions when a h/d_p-value lower than unity is used. It is worth to emphasize that in the EL approach considered here, a point-volume assumption is used and that the bubbles' surface effect on the continuous fluid flow is neglected. We relax the assumption by further assuming that a h/d_p-value less than unity (but greater than 0.5) can be used and will not drastically violate the point-volume assumption. This additional assumption will be justified by the favorable results obtained here.

The bubble column considered has a square cross-section with a width, depth and height of 0.15, 0.15 and 0.45 [m], respectively. Air bubbles are introduced at the bottom-center plane with an area of 0.03×0.03 [m^2] with a superficial gas velocity of 4.6 [mm/s]. A bubble mean diameter of the order of 4 [mm] was observed in the experiments (Deen et al., 2001). Bubbles were assumed to have uniform size in this work. In order to verify the validity of a model with a

h/d_p-value less than unity, a simulation with a h/d_p value of 0.75 was carried out and compared with the simulation results reported in Sungkorn et al. (2011) for a h/d_p value greater than unity.

The domain was discretized by a uniform cubic grid of 50×50×150 lattices in width, depth, and height, respectively. This resulted in a bubble size of 1.5 times the lattice distance. A no-slip boundary condition was applied at the walls, except for the top where a free-slip boundary condition was applied. Bubble parcels were injected at the bottom of the column and left the simulation domain once they touched the top surface. In this case, due to the low gas phase fraction, one parcel contained only one bubble. The calculation started with a quiescent liquid and proceeded for 150 [s] with a time step for the liquid phase of 10 [μs]. A sub-time step of 1 [μs] was used for the calculation of the bubble motion. In order to obtain statistically meaningful data, the averaged quantities were computed from 20 to 150 [s].

A comparison between the simulations with various h/d_p values and measured data is shown in Figure 3.1. As can be seen from the top figure, the averaged vertical velocity profile is accurately reproduced in all cases except for a h/d_p value of 1.50. Similarly, the fluctuating components of the resolved flow field were correctly captured by all simulations except, again, for a h/d_p value of 1.50. This might be attributed to an insufficient resolution when a grid too coarse is employed. As can be seen, the use of a h/d_p value of 0.75 improves the predictions, especially at the region near the wall. This is because, with a finer grid resolution, a larger fraction of the eddies and, consequently, more of the energy residing in the flow are resolved. These favorable results show that the use of a h/d_p value lower than unity in this case will not deteriorate the simulation, at least in the prediction of the flow field. However, it is important to note that the refinement of the grid also results in an increase of computational cost: reducing the (uniform) grid spacing by a factor q increases the grid size with a factor q^3 and (due to explicit time stepping) the computational effort by q^4.
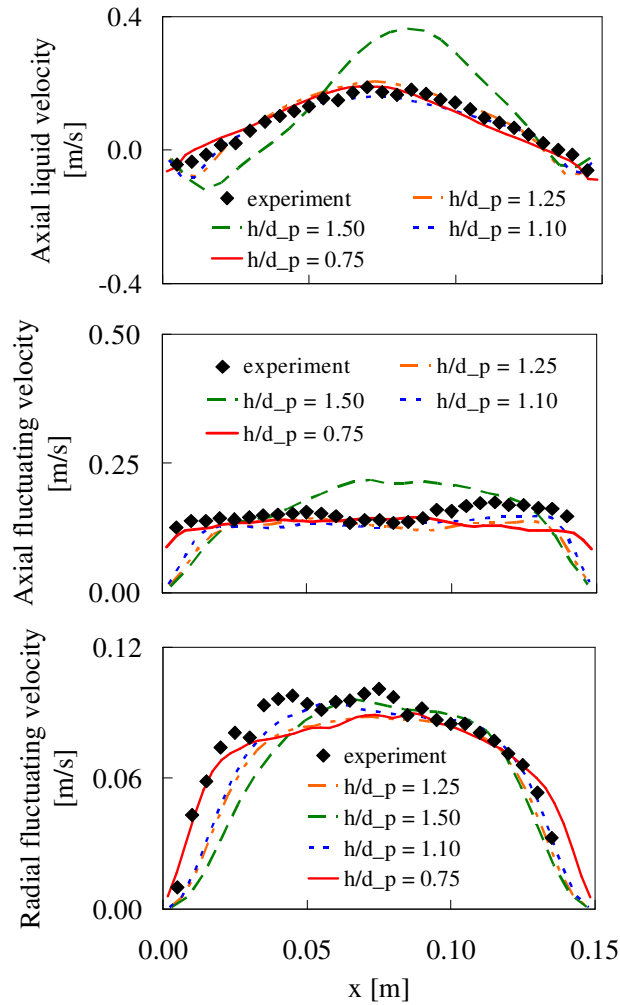
Figure 3.1. Comparison of the predicted and experimental long-term averaged liquid velocity and fluctuating velocity components with various grid size to bubble diameter ratios h/d_p at a height of 0.28 [m] and a depth of 0.075 [m].

3.3.2   *Bubble column with inclusion of breakage and coalescence*

A pseudo-two-dimensional bubble column has been used to study the effect of superficial gas velocity on the bubble size distribution (BSD) by Van den Hengel et al. (2005). The underlying phenomena are similar to the bubble column discussed earlier with the additional complexity due to bubble coalescence. The dimensions of the bubble column are 0.20, 0.03 and 1.40 [m], in width, depth, and height, respectively. Air bubbles were injected at the mid-bottom from a nozzle with a diameter of 0.02 [m] with a gas superficial velocity of 1.39×10^{-3}, 2.78×10^{-3}, and 4.17×10^{-3} [m/s]. It was reported in their work that the bubbles at the nozzle had a size distribution around 3 [mm].

In our study, the fluid domain was discretized on a uniform cubic grid of 40×6×280 lattices in width, depth, and height, respectively. The other simulation settings were similar to the previous simulation case. Gaussian-shape BSDs with a mean diameter of 2.5 and 3 [mm] (corresponding to a bubble size of 0.5 and 0.6 times the lattice distance, respectively) and a variance of 0.25 [mm] were generated at the nozzle. Breakup and coalescence of bubbles were taken into account. Due to the restriction of the h/d_p value discussed earlier, coalescence will only take place with a bubble smaller than 2.0 times the lattice spacing and, similarly, breakup will only take place with a bubble larger than 0.1 times the lattice spacing. The long-term averaged results were based on results between 20 and 150 [s].
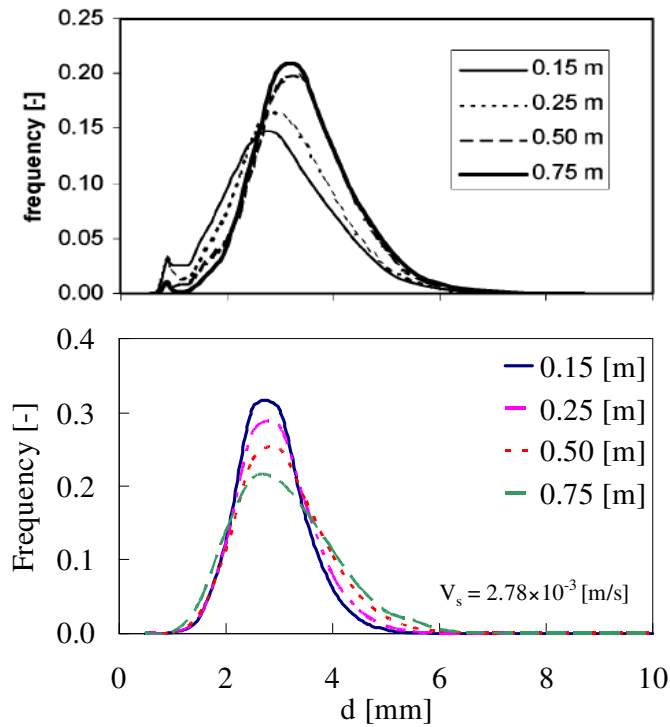
Figure 3.2. Comparison of the experimental (top) and the predicted (bottom) bubble size distribution at various heights with the superficial gas velocity of 2.78×10^{-3} [m/s]. The simulation was performed with a BSD with a mean diameter of 2.5 [mm] at the nozzle.

Figure 3.2 shows the measured and predicted long-term averaged BSD at various heights. It can be observed from the experimental data that the mean bubble diameter and the BSD slightly shifted to the right side, i.e., to bigger diameters, caused by bubble coalescences. A similar behavior is obtained in the simulations. Although the agreement is quite good, there exist, however, some deviations in the BSD profiles. Similar deviations were also obtained in

the simulations of Van den Hengel et al. (2005). One reason for this observation may be the resolution of the measurement and/or the lack of accurate BSD data at the nozzle (i.e., at the air inlet). The latter explanation is also supported by the fact that in the experiment a bi-modal BSD is observed.
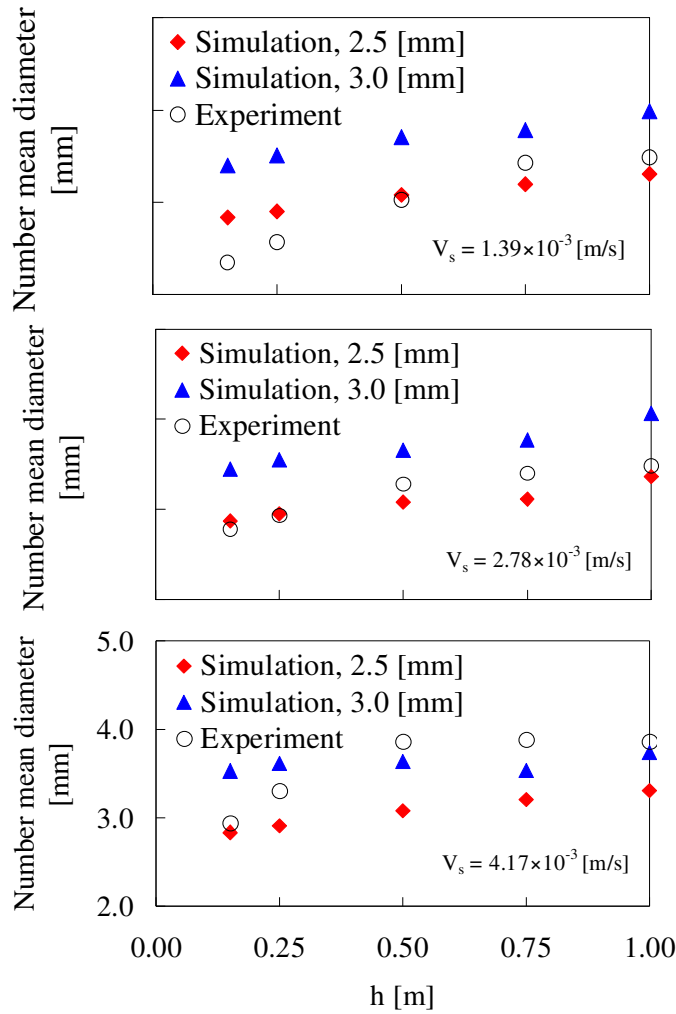
Figure 3.3. Comparison of predicted and experimental number-mean diameters at various heights using different initial bubble diameters and gas superficial velocities. (All diagrams have the same y-axis scale)

Figure 3.3 shows the number mean diameter at various heights with different superficial gas velocities. The sensitivity of the BSD with respect to the sparger (initial) BSD was studied by using initial BSDs with a mean diameter of 2.5 and 3 [mm]. At low superficial gas velocities (i.e., 1.39×10^{-3} and 2.78×10^{-3} [m/s]), good agreements for the number mean diameter d_{10} along the axial direction were obtained with the initial BSD of 2.5 [mm]. However, the simulation

with the initial BSD of 3.0 [mm] provides a good agreement with the experiment at a higher superficial gas velocity (i.e. 4.17×10^{-3} [m/s]). This behavior may be explained by the well-known fact that the initial bubble size at the sparger increases with increasing superficial velocity (Laakkonen et al., 2007). Furthermore, also immediate coalescence at the sparger occurs. This, again, highlights the importance of knowing the initial BSD at the sparger for an accurate prediction. Although the initial bubble size can be roughly estimated using, for example, the model proposed by Geary & Rice (1991), detailed information concerning the sparger is essential, yet rarely available in literature.

3.3.3 *Gas-liquid stirred reactor*

Detailed experimental investigations of a gas-liquid stirred reactor were reported by Montante et al. (2007) and Montante et al. (2008) and were used for validation of our method. In their work image analysis was employed to collect data concerning liquid flow field and the BSD at the mid-plane between the baffles. The reactor had a standard configuration consisting of a cylindrical, flat-bottomed, baffled tank with diameter T = 23.6 [cm] and the liquid filled-level $H = T$. The reactor was equipped with a Rushton turbine with a diameter $D = T/3$, at the center of the reactor $C = T/2$. The geometry of the reactor is depicted in Figure 3.4. The working fluid was water with a viscosity ν of 1.0×10^{-6} [m²/s] and density ρ of 1.0×10^{3} [kg/m³]. The impeller rotational speed N was fixed at 450 [rpm] throughout the study, corresponding to a blade tip speed of 1.85 [m/s] and a Reynolds number, defined as $\mathrm{Re} = ND^{2}/\nu$, of approximately 46,000. Air bubbles were injected into the system via a sparger made of a tube of 3.3 [mm] diameter with a porous membrane on top. The sparger had a distance of $T/4$ from the bottom. The gas flow rate was varied from 0.02, 0.05, to 0.07 [vvm]. The reactor operated in the complete dispersion regime (Montante et al., 2007).
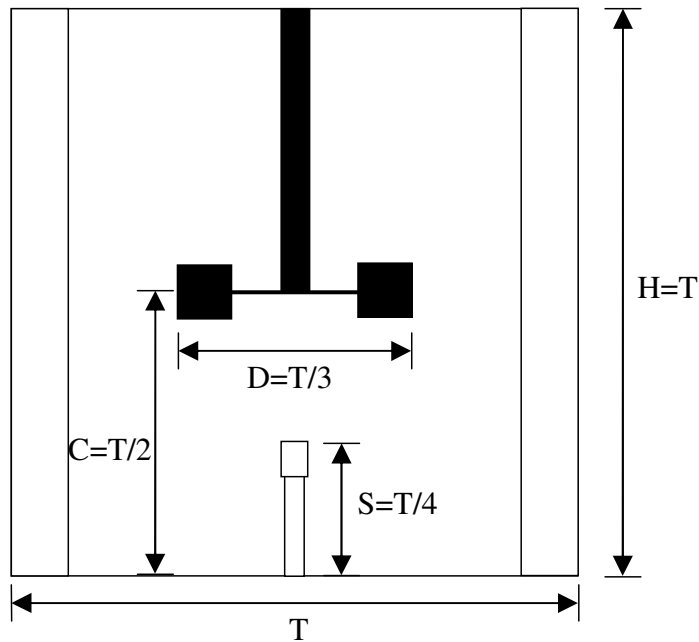
Figure 3.4. Geometry of the stirred reactor with a Rushton turbine and a tube sparger.

For the simulations a cubic computational grid of 85^3 lattice cells was defined. A no-slip boundary condition was employed at all faces except for the top surface, where a free-slip boundary condition was defined to represent the free surface. Sets of control points, representing the cylindrical wall, the baffles, the impeller, the impeller shaft, and the sparger tube, were generated inside the computational domain according to the forcing algorithm introduced earlier. In the simulations, a grid spacing h equal to 2.9×10^{-3} [m] was employed. The diameter of the impeller had a size of 27 times the grid spacing. The distance between two control points at the impeller surface was $0.7h$. Similar strategy was used to represent the other parts. The total number of control points in the domain was 33,000. The simulations started with the reactor at rest and proceeded with a time step for the liquid phase of 20 [μs] and a sub-time step of 4 [μs] for the calculation of the bubble motion. Thus, the impeller completes a full revolution in 6667 time steps. At any given moment, for example, in case 5, the simulation has approximately 1,300 parcels, corresponds to 90,000 bubbles and global gas holdup of 0.4 % (also Montante et al. (2008) report gas holdups below 1%). After 30 impeller revolutions, the data of the liquid flow field and the BSD were collected for the following 60 revolutions and statistically analyzed. The wall-clock time for one impeller revolution was approximately 1.5 hours when 4 Intel® Xeon® E5540 (at 2.53 GHz) processors were used. This averaging period was shown to be sufficiently long for generating statistically meaningful results. An overview of the simulation cases is shown in Table 3.1. Note that the initial bubble diameter used in the

simulations was greater than the grid spacing, i.e., a h/d_p value less than unity. For example, an initial diameter of 4 [mm] results in a h/d_p value of 0.74. As will be shown later, the significant bubble breakup occurs in the impeller region, resulting in much smaller bubbles. Hence, only 1% of the bubbles or less in the reactor have a diameter greater than the grid spacing.

Case	N [rpm]	Q_g [vvm]	Initial d_p [mm]
1	450	0.02	4.0
2	450	0.02	mean = 3.5 / variance = 0.5
3	450	0.0	-
4	450	0.05	4.0
5	450	0.07	4.0

Table 3.1. Overview of the stirred tank simulation cases.

First, the influence of the initial bubble diameter on the simulation results was studied. Two simulations were carried out: one with an initial bubble diameter of 4 [mm] (case 1) and another one with a Gaussian BSD distribution with a mean diameter of 3.5 [mm] and variance of 0.5 [mm] (case 2). The gas flow rate was set to 0.02 [vvm] in both cases. Figure 3.5 shows the measured and predicted long-term averaged local number-mean diameter d_{10} in the reactor. Note that the predicted d_{10} shown here is a angle-averaged value. The trend and magnitude of the predicted d_{10} in both cases agrees fairly well with the measured data. In case 1, the simulations slightly over-predicted d_{10} in the impeller regime and slightly under-predicted the diameter in the rest of the reactor. In contrast, the predicted d_{10} in case 2 agrees well with the measured data in most parts, except in the impeller regime where the d_{10} is over-predicted. This, again, highlights the importance of initial bubble size accuracy of the simulation. In order

to reduce the parameters that will influence the prediction and for the simplicity of the study, a uniform initial bubble size of 4 [mm] was used for the rest of the study.

<u>1.091</u> 0.832 0.982	<u>1.038</u> 0.838 0.996	<u>0.828</u> 0.670 0.968
<u>1.013</u> 0.862 1.025	<u>1.041</u> 0.847 0.987	<u>0.818</u> 0.804 0.970
	<u>0.754</u> / 0.850 / 1.013	
<u>0.929</u> 0.774 1.163	<u>0.992</u> 0.876 0.993	<u>0.970</u> 0.926 1.026
<u>0.924</u> 0.659 0.867	<u>1.030</u> 0.830 0.940	<u>0.944</u> 0.928 1.063

Figure 3.5. Local number mean diameter [mm] in the reactor with N = 450 [rpm] and Q = 0.02 [vvm]. Measured data are underlined following with the predicted values from the case 1 and 2, respectively.

A comparison between the predicted (case 1) and the measured cumulative size distribution (CSD) of bubble at the lower and upper part is shown in Figure 3.6. The predicted CSD was calculated by dividing the diameter between 0.0 and 4.5 [mm] into 15 classes and counting the frequency of bubbles in each class. As can be seen, the predicted CSD distribution agrees very well with the measured data. Deviation can be observed in the regime of small bubbles. This could be due to many reasons, for example, in the break up model, where the daughter size distribution is governed by the U-shape distribution Eq. (3.16) in which the

probability of very small and very large daughter sizes is the highest. Thus, other daughter size distributions, such as an M-shape distribution (Lehr & Mewes, 1999), may be used to improve the prediction. It is also important to note that the smallest detectable bubble in the experiment of Montante et al. (2008) was 0.3 [mm] whereas, in the simulation, the smallest allowable bubble was approximately 0.25 [mm] and was included in the first cumulative class.
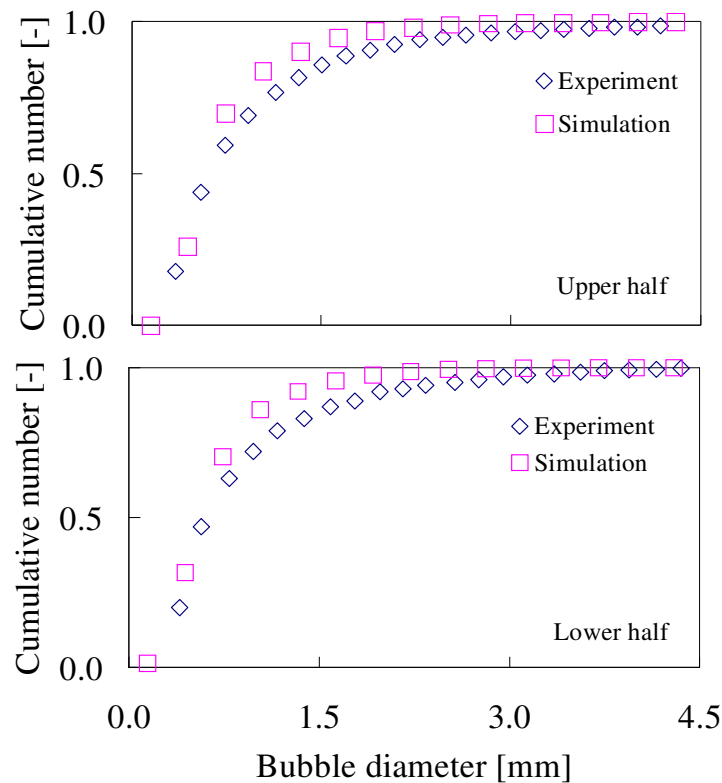
Figure 3.6. Cumulative distribution of bubble equivalent diameter in the upper half and lower half of the reactor with N = 450 [rpm] and Q = 0.02 [vvm]. The prediction from the simulation case 1 is shown.

Based on the good agreement between experiment and simulation for the dispersed phase, we further examined the quality of the prediction of the liquid flow field. Predicted and experimental axial and radial long-term averaged liquid velocity components along the radial direction at various heights are shown in Figure 3.7. As can be seen, a quite good agreement between the predicted and measured data is achieved at all considered heights. The radial velocity profiles changes only slightly along the radial direction. A significant change in magnitude can be seen at the height of the impeller where a strong outflow exists (z/T = 0.49) as the configuration corresponds to a radially discharging impeller. In contrast, the axial velocity profiles change in magnitude and sign along the radial direction at all elevations. Also, a very

good agreement is achieved for the long-term averaged velocity components along the axial direction at various radial positions, see Figure 3.8. A jet-like radial outflow has the highest magnitude close to the impeller and decreases with further distance from the impeller. The axial velocity component changes its magnitude along the axial direction and radial position according to flow recirculation generated by the Rushton turbine. Slight deviations can be noticed for the radial velocity component at the peak of the impeller jet.
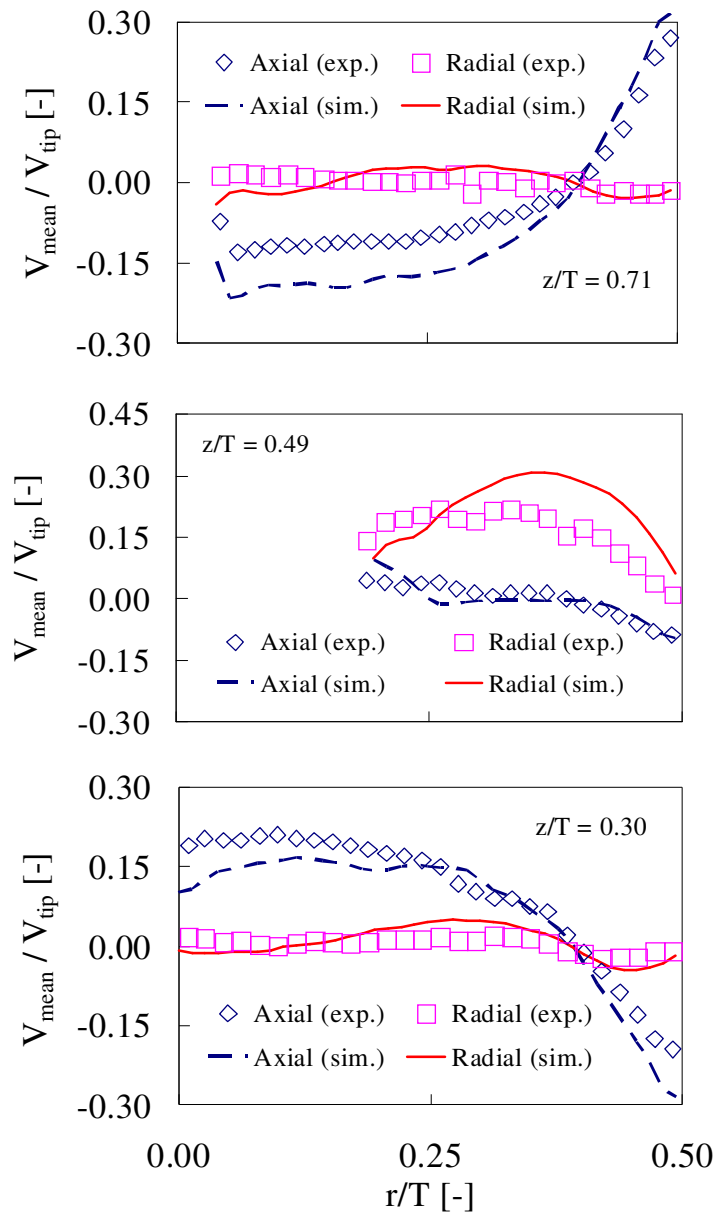
Figure 3.7. Experimental and predicted (case 1) long-term averaged axial and radial liquid velocity components at three heights.
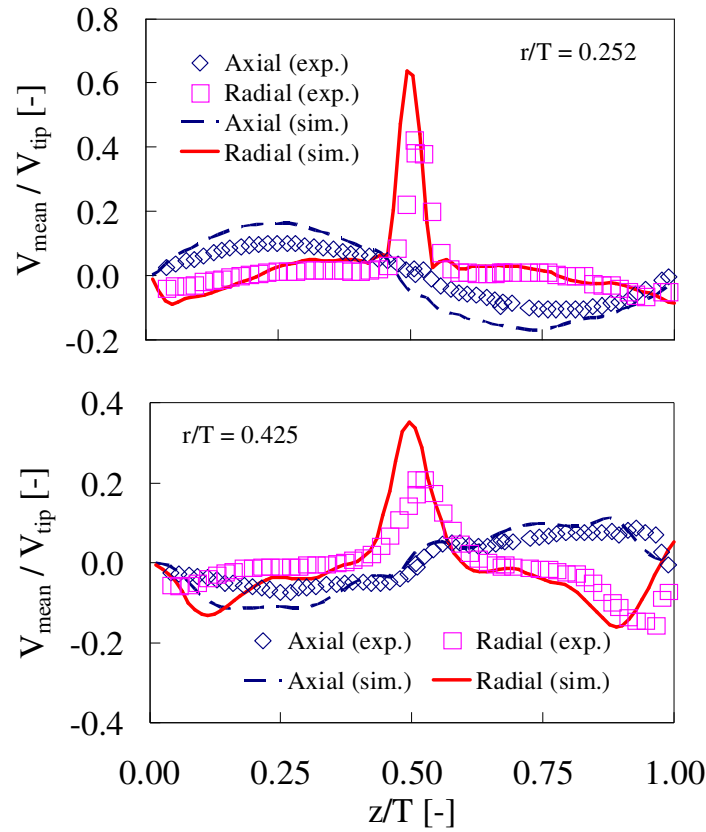
Figure 3.8. Experimental and predicted (case 1) long-term averaged axial and radial liquid velocity components at two radial distances.

In Figure 3.9, the long-term averaged root mean square (RMS) radial and axial velocity components at various elevations are shown. The simulation and the experiment have the maximum magnitude of the RMS values at the height of the impeller ($z/T = 0.49$). While the agreement between experiments and simulations is not as good as for the averaged velocities, the predicted RMS values have similar order of magnitude as in the experiment. However, deviations can be observed, especially near the impeller. Clearly, these deviations were due to an insufficient grid resolution used in this work. However, it is worth to repeat here that the grid resolution is restricted by the size of bubbles present in the system. That is, the h/d_p value has to be a compromise between a sufficiently fine grid resolution to capture the most energetic eddies and a sufficiently coarse grid resolution to keep the point-volume assumption valid.
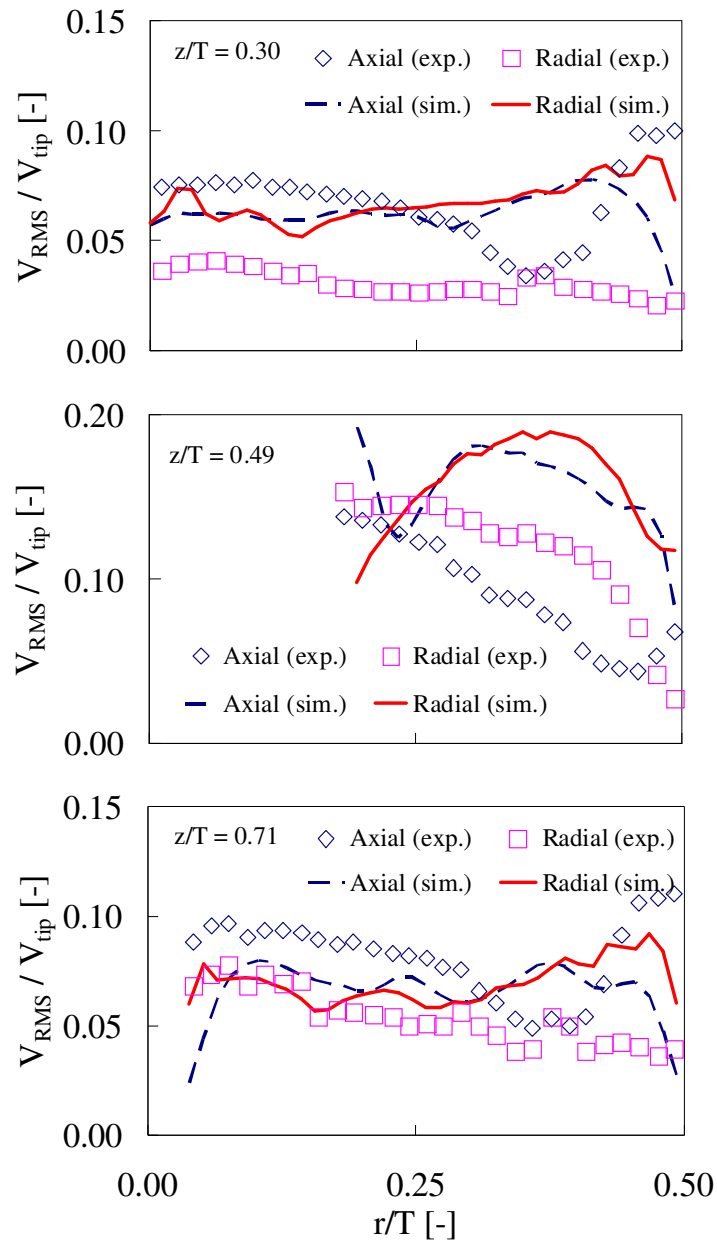
Figure 3.9. Experimental and predicted (case 1) long-term averaged axial and radial fluctuating components at three heights.

The predicted instantaneous and long-term averaged velocity vector fields are shown in Figure 3.10. Several small and large vortices induced by a jet-like outflow from the Rushton impeller can be observed in the plot of the instantaneous flow field. These vortices interact with each other and change their size, shape and position randomly with time. The long-term averaged velocity vector field reveals two primary liquid recirculation zones at the upper and

lower part of the reactor. Two small recirculations at the upper and lower corners can be also noticed. Snapshots of the predicted bubble dispersion pattern from the front and top view are shown in Figure 3.11 and Figure 3.12, respectively. As can be seen, the bubbles introduced at the sparger fluctuate within a small range before they are drawn into the impeller regime. Consequently, the bubbles collide with the impeller, exchange their momentum and velocity direction and are drawn into the vortex behind the impeller blades. Most of bubble breakup takes place in this region due to the presence of high turbulence activity. The bubbles are then dispersed following the jet-like outflow. Small bubbles tend to follow the recirculations resulting in a long residence time, while large bubbles tend to rise near the wall or move into a region with low turbulence activity, i.e., near the impeller shaft. These underlying phenomena and much more, such as bubble trailing and rolling of bubble swarm, can be observed in three-dimensional and anaglyphical animated results made available in the journal's website.
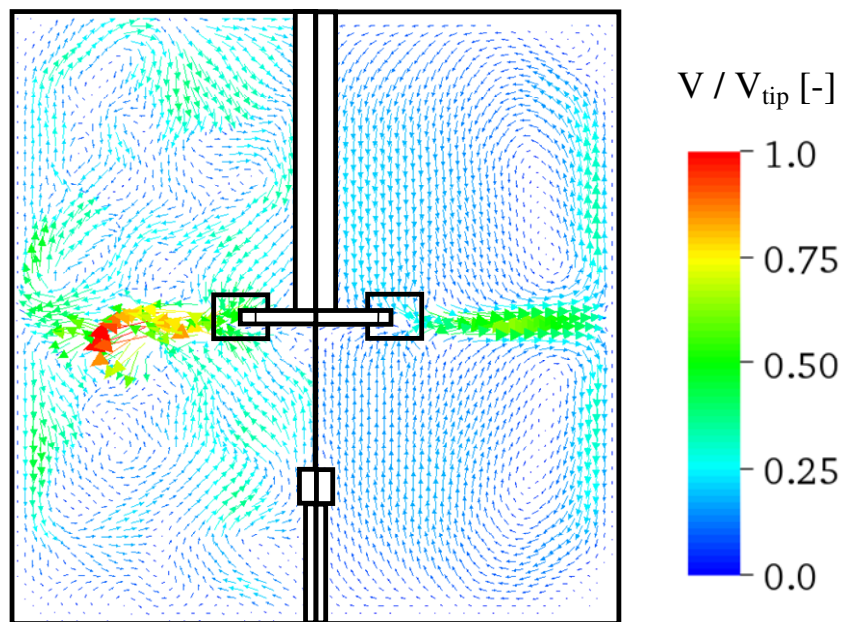
Figure 3.10. Predicted instantaneous (left) and long-term averaged (right) liquid velocity vector field at the mid-plane between baffles obtained from case 1.
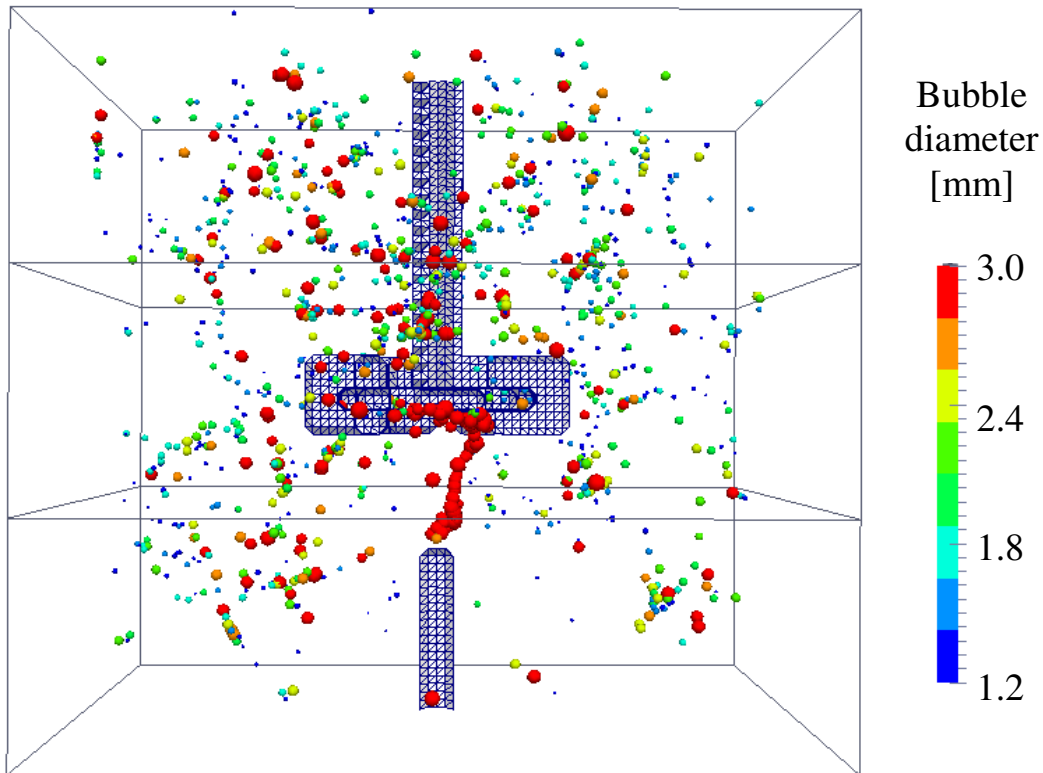
Figure 3.11. Snapshot of bubble dispersion pattern. The reactor operates at N = 450 [rpm] and Q = 0.02 [vvm]. Note that the impeller and the sparger geometry are only an interpolated contour plot. The baffles and tank wall are excluded for visualization purpose.

A contour plot of the long-term averaged resolved liquid phase turbulent kinetic energy (TKE) at the mid-plane between baffles is shown in Figure 3.13. A region of high turbulent activity, i.e., high TKE, is found to emanate from the blades region and has a maximum of TKE at the midway between the impeller and the tank wall. The TKE profile is qualitatively similar to that for single phase flows - see for example Derksen & Van den Akker (1999). It can be concluded that the TKE is only weakly modified by the presence of bubbles due to the relatively low gas flow rate investigated here.

A simulation of a single-phase stirred tank (case 3) was carried out to study the effect of bubbles on the liquid flow field. The predicted single-phase long-term averaged velocity vector field is shown on the left side of Figure 3.14. For the investigated range of the gas flow rate, no significant changes in liquid flow field are observed. More details can, however, be deduced by subtracting the averaged vector field obtained from the simulation with gassing (case 1) from the field without gassing (case 3). The result is shown on the right side of Figure 3.14. As can

be seen, most of the differences take place in the outflow of the impeller region, where the liquid motion is modified by the bubbles. Our observation agrees qualitatively well with the result obtained from the experiment of Montante et al. (2007). It should be noted however, that the magnitude of the difference is approximately one order of magnitude lower than the averaged flow field.
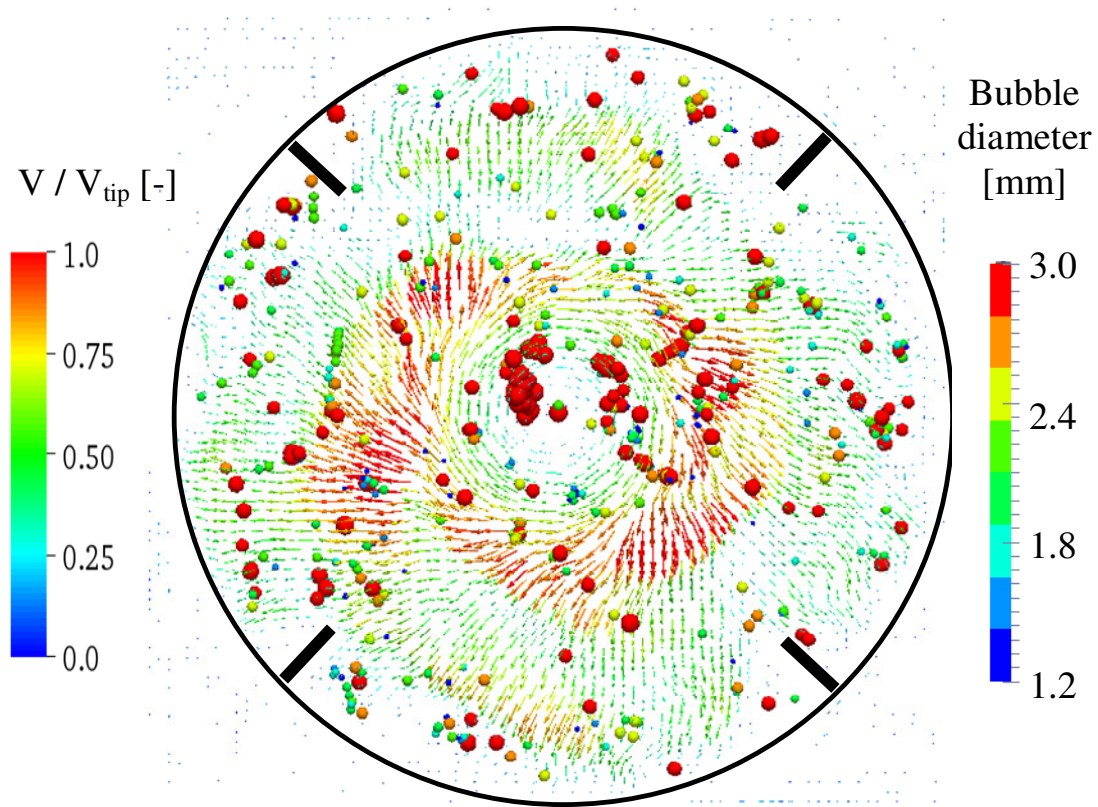
Figure 3.12. Snapshot of bubble dispersion pattern and the liquid velocity vector field at cross section below the impeller. The reactor operates at N = 450 [rpm] and Q = 0.02 [vvm]. (Only bubbles below the impeller are shown)
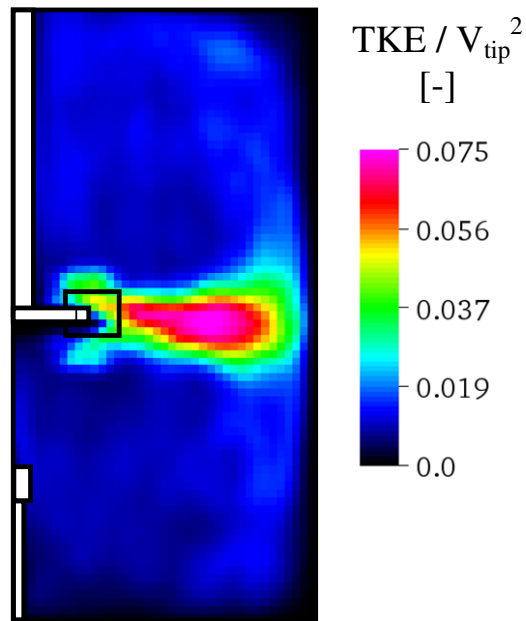
Figure 3.13. Contour plot of the predicted long-term averaged turbulent kinetic energy TKE for case 1.
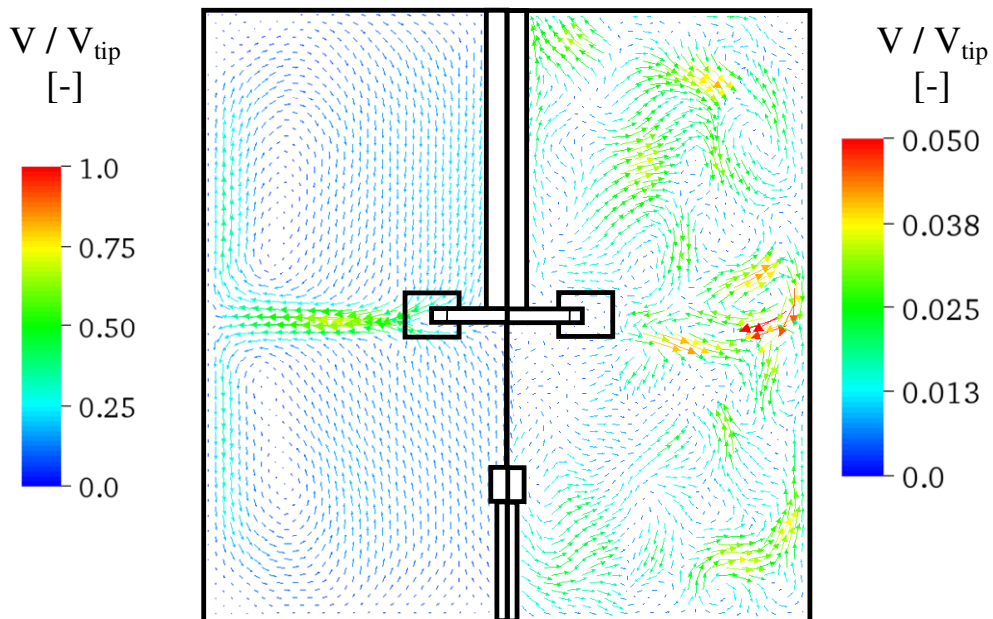
Figure 3.14. Vector plot of long-term averaged velocity field for ungassed conditions (case 3) (left) and the difference between the liquid velocity for gassed (case 1) and ungassed conditions (case 3) (right).

0.833 0.819 0.814	0.839 0.810 0.803	0.670 0.793 0.819
0.862 0.839 0.828	0.847 0.823 0.802	0.803 0.800 0.784
	0.850 / 0.823 / 0.809	
0.774 0.743 0.746	0.876 0.834 0.817	0.926 0.881 0.874
0.659 0.607 0.618	0.830 0.784 0.783	0.928 0.883 0.870
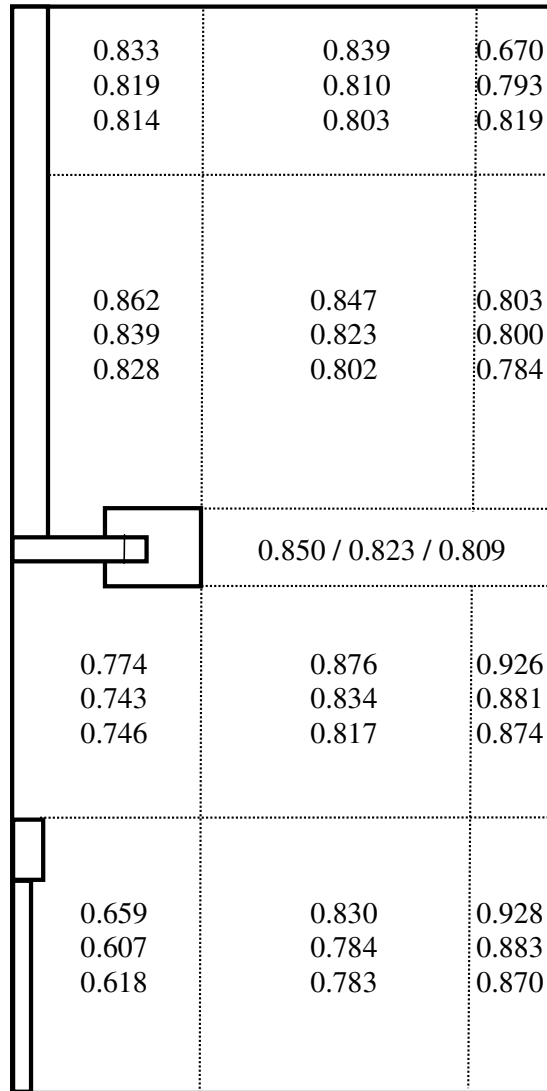
Figure 3.15. Local number-mean diameter [mm] in the reactor at the gas flow rate of (from top to bottom) 0.02, 0.05, and 0.07 [vvm], respectively. The impeller rotational speed was fixed at 450 [rpm].

In another set of simulations the gas flow rate was increased from 0.02 to 0.05 and 0.07 [vvm] in case 4 and 5, respectively, to investigate the effect of gassing on the gas-liquid hydrodynamics. The initial bubble diameter was assumed to 4 [mm] in all cases. Figure 3.15 shows the predicted local number mean diameter obtained from the simulations with various gas flow rates. At all gas flow rates, the evolution of the bubble size follows a similar trend as discussed in the previous section. However, it can be noticed that the increase of the gas flow rate results in a smaller mean bubble diameter in most parts of the reactor. Significant changes occured when the gas flow rate was increased from 0.02 to 0.05 [vvm]. The difference between

the flow rate of 0.05 and 0.07 [vvm] was minor. An explanation can be provided by the help of the contour plot of the phase-averaged gas volume fraction shown in Figure 3.16. (It should be noted that the plot of the gas fraction was made by mapping the bubble's volume based on its position on the Lagrangian frame of reference to its nearest Eulerian grid node). A significant increase in the concentration and the dispersion area of the gas phase can be observed by raising the flow rate from 0.02 to 0.05 [vvm]. In the first case, the dispersion pattern, i.e., the gas volume fraction contour, is divided into three regimes: impeller outflow, upper, and lower recirculation zones. This is because the bubbles are only dispersed from the impeller but the recirculations are not strong enough to draw the bubbles back in the impeller regime. In contrast, the dispersion pattern for 0.05 [vvm] are completely connected. Thus, the bubbles are recirculating into the impeller outflow region. Consequently, more breakup takes place, resulting in smaller bubble diameters. An increase of the flow rate from 0.05 to 0.07 [vvm] does not qualitatively change the picture and results mainly in an increase of the concentration of the gas phase, especially in the regime near the impeller. The mean diameter of bubble changes only significantly in the regimes near the impeller shaft, where a higher rate of bubble coalescence occurs. Note, that a different trend of the the mean diameter will be obtained in experiments. This is because, as discussed in the previous section, the BSD at the sparger increases significantly with the gas flow rate and, consequently, the BSD in the reactor.
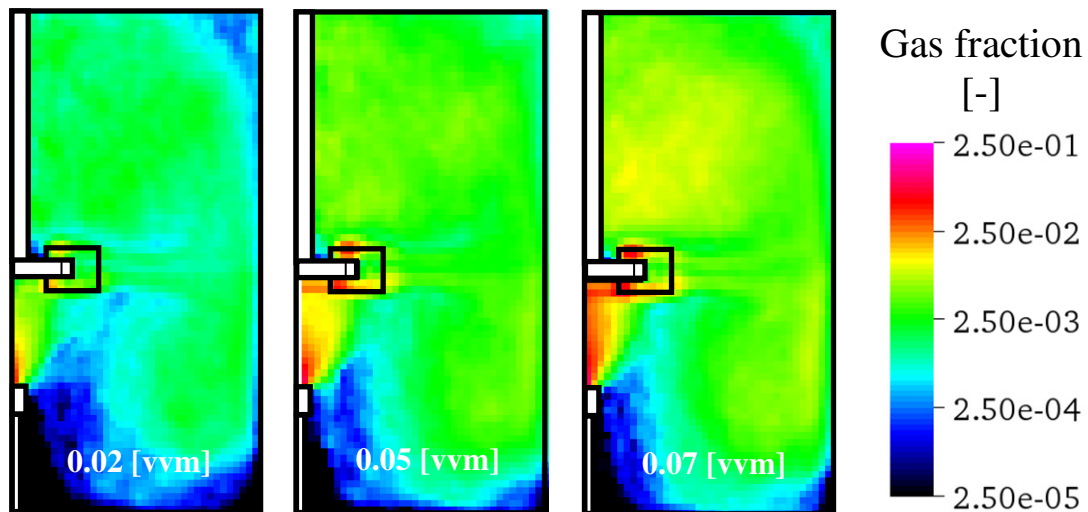
Figure 3.16. Long-term averaged gas volume fraction at the mid plane between baffles at gas flow rate of 0.02, 0.05, and 0.07 [vvm], i.e. case 1, 4, and 5, respectively.

3.4 Conclusions

A modeling technique for the simulations of gas-liquid stirred tank reactors based to an EL approach has been presented. The turbulent flow field was established using the filtered conservation equations. A variation of the LB scheme proposed by Somers (1993) was used to discretize the equations. The bubble parcel concept was used to represent a group of bubbles with identical properties. A point-volume concept was used to track the trajectory of the bubble, i.e., the parcel. A set of appropriate correlations for the inter-phase closure was carefully chosen from the literature. The immersed boundary condition method (Derksen, 1997) was employed to describe the action of the moving components and the tank walls.

The restriction regarding the grid size over bubble diameter ratio, h/d_p, was relaxed. It was demonstrated that the use of a h/d_p value less than unity (but greater than 0.5) can be employed in EL simulations. This approach can be envisioned as a "distributed" bubble approach where bubbles are allowed to be slightly bigger than the grid size and represented with a more spatially distributed forces. However, the h/d_p value employed in a simulation should be a compromise between a sufficiently fine grid resolution to capture the most energetic eddies and a sufficiently coarse grid to keep the point-volume assumption valid. It should be noted that, this resolution limitation will largely disappear when a simulation of an industrial-scale reactor is considered. Since an increase of the reactor size will typically result in only slightly larger bubbles, finer grids (relative to the reactor size) will have h/d_p ratios greater than one.

Collisions and coalescence of bubbles was modeled based on the stochastic inter-particle collision model as used by Sommerfeld et al. (2003). Using the coalescence model, a good agreement between the predicted and measured BSD in a bubble column has been obtained. Simulations with various initial bubble sizes and gas flow rates showed that the accuracy of the prediction is highly sensitive to the initial bubble size at the sparger. Therefore, detailed information concerning bubble size (or air inlet/sparger) is essential for an accurate prediction.

The breakup model of Luo & Svendsen (1996) was employed. In this work, breakup of bubble was treated as a stochastic event. A daughter size was randomly selected from a U-shape distribution. Accordingly, breakup of bubbles was decided by comparing a breakup frequency with a uniform random number. Additionally, in this work we proposed that this event should be bounded by an involved time scale which is a function of the flow field, i.e., the particle-eddy interaction time, to obtain time resolution-independent solution and to avoid unphysical consecutive breakups.

Our modeling technique was then used to simulate gas-liquid flow in a stirred tank reactor following the experiments of Montante et al. (2007; 2008). The simulations were able to reproduce the trends and the magnitude of the local BSD from the experiment. Small bubbles were over-predicted. This could be improved by employing alternative daughter bubble-size distributions. Also, despite a coarse grid spacing used in this work, the simulations provided a good agreement with measured data for the long-term averaged velocity components. This is because the scale of large energy-containing eddies in a stirred reactor is of similar size as the impeller diameter. Therefore, the largest part of the energy in the liquid flow field was resolved. However, due to the restriction of the choice of the grid spacing, the predicted second-order statistics (RMS of velocity components) agree only by order of magnitude with the measured data. In order to improve the prediction of the second-order statistics, an alternative approach, such as very-large-eddy simulations (VLES), may be employed. The VLES approach uses a spatial-filtering process with a turbulence model (similar to that for unsteady Reynolds-averaged Navier-Stokes (URANS) approach) on a coarse grid to resolve a minor part of the turbulence spectrum and to model the rest (Ruprecht et al., 2003; Fares, 2006).

Bearing in mind the capabilities and limitations of the presented modeling technique, the effects of the bubble phase and the gas flow on the gas-liquid were studied numerically. It can be concluded that the presence of bubbles, in the investigated range of operating conditions, slightly modifies the flow at the impeller outflow region. Furthermore, it has been found that the increase of the gas flow rates triggers a change in the dispersion pattern and, consequently, the BSD.

While the study presented here has been carried out for laboratory scale reactors with dilute dispersions, the present modeling technique consists mainly of models based on elementary physical principles which are also valid for a larger scale. The models contain not many adjustable parameters; only some rooms exists for adopting different closures and for using different theoretical constants. It should be also stressed, that all elements of the present modeling technique provide high efficiency for parallel computing, as has been demonstrated by Derksen & Van den Akker (1999) and Sungkorn et al. (2011). The maximum benefit of the present modeling technique can be achieved when industrial large-scale simulations are realized.

3.5   References

1   Arlov D, Revstedt J, Fuchs L. Numerical simulation of gas-liquid Rushton stirred reactor – LES and LPT. *Computers & Fluids*. 2008;37:793-801.

2   Behzadi A, Issa RI, Rusche H. Modelling of dispersed bubble and droplet flow at high phase fractions. *Chem Eng Sci*. 2004;59:759-770.

3   Bernaschi M, Fatica M, Melchionna S, Succi S, Kaxiras E. A flexible high-performance lattice Boltzmann GPU code for the simulations of fluid flows in complex geometries. *Concurrency and Computation: Practice & Experience*. 2010;221:1-14.

4   Chen S, Doolen GD. Lattice Boltzmann method for fluid flows. *Annu Rev Fluid Mech*. 1998;30:329.

5   Crowe C, Sommerfeld M, Tsuji Y. Multiphase flows with droplets and particles. Boca Raton: CRC Press; 1998.

6   Darmana D, Deen NG, Kuipers JAM. Numerical study of homogeneous bubbly flow: Influence of the inlet conditions to the hydrodynamic behavior. *Int J Multiphas Flow*. 2009;35:1077-1099.

7   Deen N, Van Sint Annaland M, Kuipers JAM. Multi-scale modeling of dispersed gas-liquid two-phase flow. *Chem Eng Sci*. 2004;59:1853-1861.

8   Deen NG, Solberg T, Hjertager BH. Flow generated by an aerated Rushton impeller: Two-phase PIV experiments and numerical simulations. *Can J Chem Eng*. 2002;80:1-15.

9   Deen NG, Solberg T, Hjertager BH. Large eddy simulation of the gas-liquid flow in a square cross-sectioned bubble column. *Chem Eng Sci*. 2001;56:6341-6349.

10   Derksen JJ, Kooman JL, Van den Akker HEA. Parallel fluid flow simulation by means of a lattice-Boltzmann scheme. *Lect Notes Comput Sci*. 1997;125:524.

11   Derksen JJ, Van den Akker HEA, Sundaresan S. Two-way coupled large-eddy simulations of the gas-solid flow in cyclone separators. *AIChE J*. 2008;54:872-885.

12   Derksen JJ, Van den Akker HEA. Large eddy simulations on the flow driven by a Rushton turbine. *AIChE J*. 1999;45:209-221.

13   Derksen JJ. Assessment of large eddy simulations for agitated flows. *Trans IChemE*. 2001;79A:824-830.

14   Derksen JJ. Numerical simulation of solid suspension in a stirred tank. *AIChE J.* 2003;49:2700-2714.

15   Eggels JGM, Somers JA. Numerical simulations of free convective flow using the lattice-Boltzmann scheme. *Int J Heat Fluid Flow*. 1995;16:357-364.

16   Fares E. Unsteady flow simulation of the ahmed reference body using a lattice Boltzmann approach. *Comput Fluids*. 2006;35:940-950.

17   Geary NW, Rice RG. Bubble size prediction for rigid and flexible spargers. *AIChE J.* 1991;37:161-168.

18   Gogate, PR, Beenackers AACM, Pandit AB. Multiple-impeller systems with a special emphasis on bioreactor: A critical review. *Biochem Eng J.* 2000;6:109-144.

19   Goldstein D, Handler R, Sirovich L. Modeling a no-slip flow boundary with an external force field. *J Comput Phys*. 1993;105:354.

20   Hennick EA, Lightstone MF. A comparison of stochastic separated flow models for particle dispersion in turbulent flows. *Energ Fuel*. 2000;14:95-103.

21   Hoomans BPB, Kuipers JAM, Briels WJ, Van Swaaij WPM. Discrete particle simulation of bubble and slug formation in a two-dimensional gas-fluidised bed: A hard-sphere approach. *Chem Eng Sci*. 1996;51:99-118.

22   Hu G, Celik I. Eulerian-Lagrangian based large-eddy simulation of a partially aerated flat bubble column. *Chem Eng Sci*. 2008;63:253-271.

23   Khopkar AR, Rammohan AR, Ranade VV, Dudukovic MP. Gas-liquid flow generated by a Rushton turbine in stirred vessel: CARPT/CT measurements and CFD simulations. *Chem Eng Sci*. 2005;60:2215-2229.

24   Laakkonen M, Moilanen P, Alopaeus V, Aittamaa J. Modelling local bubble size distribution in agitated vessels. *Chem Eng Sci*. 2007;62:721-740.

25   Lehr F, Millies M, Mewes D. Bubble-size distribution and flow fields in bubble columns. *AIChE J*. 2002;48:2426-2443.

26   Loth E. Numerical approaches for motion of dispersed particles, droplets and bubbles. *Prog Ener Combust*. 2000;26:161-223.

27   Luo H, Svendsen HF. Theoretical model for drop and bubble breakup in turbulent dispersions. *AIChE J*. 1996;42:1225-1233.

28   Marshall EM, Bakker A. Computational fluid mixing. In: Paul EL, Atiemo-Obeng VA, Kresta SM. Handbook of Industrial Mixing: Science and Practice. New Jersey: Wiley-Interscience, 2004:257-344.

29   Montante G, Horn D, Paglianti A. Gas-liquid flow and bubble size distribution in stirred tanks. *Chem Eng Sci*. 2008;63:2107-2118.

30   Montante G, Paglianti A, Magelli F. Experimental analysis and computational modelling of gas-liquid stirred vessels. *Tran IChemE*. 2007;85:647-653.

31   Nemoda SDJ, Zivkovic GS. Modelling of bubble break-up in stirred tanks. *Thermal Science*. 2004;8:29-49.

32   Prince MJ, Blanch HW. Bubble coalescence and break-up in air-sparged bubble columns. *AIChE J*. 1990;36:1485-1499.

33   Ruprecht A, Helmrich T, Buntic I. Very large eddy simulation for the prediction of unsteady vortex motion. In: Conference on Modelling Fluid Flow. Budapest Hungary, 2003.

34   Smagorinsky J. General circulation experiments with the primitive equations: 1. The basic experiment. *Mon Weather Rev*. 1963;91:99.

35   Somers JA. Direct simulation of fluid flow with cellular automata and the lattice-Boltzmann equation. *J Appl Sci Res*. 1993;51:127-133.

36   Sommerfeld M, Bourloutski E, Broeder D. Euler/Lagrange calculations of bubbly flows with consideration of bubble coalescence. *Can J Chem Eng*. 2003;81:508-518.

37   Sommerfeld M. Kohnen G, Rueger M. Some open questions and inconsistencies of Lagrangian particle dispersion models. In: Proceedings of the Ninth Symposium on Turbulent Shear Flows. Kyoto Japan, 1993;Paper No. 15-1.

38   Sommerfeld M. Validation of a stochastic Lagrangian modeling approach for inter-particle collisions in homogeneous isotropic turbulence. *Int J Multiphas Flow*. 2001;27:1829-1858.

39   Spalding DB. A single formula for the law of the wall. *J Appl Mech*. 1961;28:455-458.

40   Succi S. The Lattice Boltzmann Equation for Fluid Dynamics and Beyond. Oxford: Clarondon Press; 2001.

41   Sungkorn R, Derksen JJ, Khinast JG. Modeling of turbulent gas-liquid bubble flows using stochastic Lagrangian model and lattice-Boltzmann scheme. *Accepted for publication in Chem Eng Sci*. 2011.

42   Tsuji Y, Tanaka T, Ishida T. Lagrangian numerical simulation of plug flow of cohesionless particles in a horizontal pipe. *Powder Technol*. 1992;71:239-250.

43   Unverdi SO, Trygvvason G. A front-tracking method for viscous, incompressible multi-fluid flow. *J Comput Phys*. 1992;100:25-37.

44   Van den Hengel EIV, Deen NG, Kuipers JAM. Application of coalescence and breakup models in a discrete bubble model for bubble columns. *Ind Eng Chem Res*. 2005;44:5233-5245.

45   Van Driest ER. On turbulent flow near a wall. *J Aeronautical Science*. 1956;23:1007.

46   Venneker BCH, Derksen JJ, Van den Akker HEA. Population balance modeling of aerated stirred vessels based on CFD. *AIChE J.* 2002;48:673-685.

47   Wu Z, Revstedt J, Fuchs L. LES of a two-phase turbulent stirred reactor. In: Lindborg E. Turbulence and Shear Flow Phenomena 2. Stockholm: KTH; 2001:529-34.

48   Zhang Y, Yang C, Mao Z-S. Large eddy simulation of the gas-liquid flow in a stirred tank. *AIChE J*. 2008;54:1963-1974.

3.6 Appendix

Table A 3.1. Expressions for the forces acting on a bubble.

Force	Closure
$\mathbf{F}_G = (\rho_p - \rho_l)V_p\mathbf{g}$	-
$\mathbf{F}_S = \rho_l V_p D_t\mathbf{u}$	-
$\mathbf{F}_D = -\dfrac{1}{2}C_D\rho_l\pi r_p^2\|\mathbf{u}_p - \mathbf{u}\|(\mathbf{u}_p - \mathbf{u})$	$C_D = \max\left[\min\left[\dfrac{24}{Re_p}\left(1+0.15Re_p^{0.687}\right),\dfrac{48}{Re_p}\right],\dfrac{8}{3}\dfrac{Eo}{Eo+4}\right]$
$\mathbf{F}_L = -C_L\rho_l V_p(\mathbf{u}_p - \mathbf{u})\times\nabla\times\mathbf{u}$	$C_L = \begin{cases} \min\left[0.288\tanh(0.121Re_p), f(Eo_d)\right], & Eo_d < 4 \\ f(Eo_d), & 4 < Eo_d \leq 10 \\ -0.29, & Eo_d > 10 \end{cases}$ $Eo_d = \dfrac{Eo}{E^{2/3}}, \quad E = \dfrac{1}{1+0.163Eo^{0.757}}$ $f(Eo_d) = 0.00105Eo_d^3 - 0.0159Eo_d^2 - 0.0204Eo_d + 0.474$
$\mathbf{F}_A = -C_A\rho_l V_p(D_t\mathbf{u}_p - D_t\mathbf{u})$	$C_A = 0.5$

Mapping function (Deen et al., 2004)

The so-called "cheap clipped fourth-order polynomial" mapping function is formulated as:

$$\varsigma(\mathbf{x} - \mathbf{x}_p) = \frac{15}{16}\left[\frac{(\mathbf{x} - \mathbf{x}_p)^4}{n^5} - 2\frac{(\mathbf{x} - \mathbf{x}_p)^2}{n^3} + \frac{1}{n}\right] \text{ with } |\mathbf{x} - \mathbf{x}_p| \leq n, \tag{A 3.1}$$

with $\mathbf{x}$ the position of a neighboring grid node and n half of the predefined influence diameter (set to $2d_p$ in this work).

Calculation of the eddy-particle interaction time (Hennick & Lightstone, 2000)

The time interval in which a bubble interacts with a randomly sampled velocity field, i.e., the eddy-particle interaction time t_e, is determined by the eddy lifetime t_{eddy} and the transit time t_{tr} as

$$t_e = \min(t_{eddy}, t_{tr}). \tag{A 3.2}$$

The eddy lifetime t_{eddy} is given by:

$$t_{eddy} = \frac{l_{eddy}}{|\mathbf{u}'|}, \tag{A 3.3}$$

with $\mathbf{u}'$ the liquid phase velocity fluctuation. The dissipation length scale l_{eddy} is estimated by:

$$l_{eddy} = 0.3 \frac{k^{1.5}}{\varepsilon}, \tag{A 3.4}$$

with k being the turbulent kinetic energy.

The transit time of a bubble is estimated based on the linearized form of the equation of motion of a bubble in uniform flow:

$$t_{tr} = -\tau_p \ln \left(1 - \frac{l_e}{\tau_p |\mathbf{u} - \mathbf{u}_p|} \right), \tag{A 3.5}$$

with the particle relaxation time τ_p

$$\tau_p = \frac{\rho_p d_p^2}{18 \rho \nu}. \tag{A 3.6}$$

4

MODELING OF AERATED STIRRED TANKS WITH NON-NEWTONIAN LIQUIDS[1]

A modeling technique for simulations of aerated stirred reactors with pseudoplastic liquids is presented. A truncated power-law model was used to account for the non-Newtonian, shear-thinning behavior of the liquid. To discretize the filtered conservation equations of the liquid phase, the lattice-Boltzmann scheme was used. An IBC was applied to model the effect of reactor components on the liquids phase. The motion of bubbles was tracked based on the Euler-Lagrange approach, and a bubble cluster concept was used with a point-volume assumption. The collision, breakup and coalescence of bubbles were computed as a stochastic event. The predicted flow field of a single-phase stirred tank with pseudoplastic liquid was compared to the experimental data, and a quantitative and qualitative good agreement was achieved. Furthermore, the simulation correctly reproduced the gas holdup distribution for an aerated stirred reactor experiment. The reactor was numerically studied. It was found that a change in rheology altered the number mean diameter, Sauter diameter and the shape of bubble size distribution. The presented modeling technique offers an alternative engineering tool with a sophisticated level of accuracy and an adequate computational cost to gain insights into the work of complex industrial-scale aerated stirred reactors with pseudoplastic liquids.

4.1   Introduction

Many processes in the chemical and biochemical industries involve aeration of liquids in stirred tank reactor. For example, in bioreactors oxygen is supplied to microorganisms or cell cultures via a sparger and, together with a substrate, is distributed by a turbulent liquid flow induced by an impeller. At the start of a fermentation the rheology of the liquid phase often exhibits Newtonian behavior and gradually changes to non-Newtonian behavior during the process. Consequently, a change in rheology may cause stagnant zones, insufficient oxygen transfer and poor bulk mixing. One of the most challenging tasks during these processes is to create adequate liquid mixing and a large interfacial contact area, while avoiding shear damage of microorganisms caused by too vigorous mixing (Arlov et al., 2008; Gogate et al., 2000).

Computational fluid dynamics (CFD) are widely perceived as a powerful method for gaining a detailed insight into the work of such reactors. Several researcher groups have attempted to establish a framework for modeling of aerated stirred reactors with a Newtonian liquid. Bakker & Van den Akker (1994) used a flow field obtained from a single-phase simulation as basis to solve the conservation equations of the gas phase (i.e., one-way coupling), taking the breakup and coalescence of bubbles into account. Ranade & Van den Akker (1994) proposed a computational snapshot approach to model the suction and ejection around impeller blades. In their work, a two-fluid model was employed to describe gas-liquid flow, and the standard k-ε model was used as the closure for turbulence. The simulation predicted gas flow around the blades and the accumulation of gas behind them. Deen et al. (2002) used a sliding grid method. The predicted mean and root-mean-square liquid velocity components in the impeller region agreed well with their measured data. Lane et al. (2005) employed a multi-reference frame technique to predict a gas-liquid flow field induced by the impellers. The breakup and coalescence of bubbles were taken into consideration via a bubble number density equation. Montante et al. (2007; 2008) solved a population balance equation (PBE) with breakup and coalescence models to predict the local bubble size distribution (BSD). Zhang et al. (2008) employed an inner-outer iterative algorithm to model the fluid motion induced by the impeller blades. They concluded that large eddy simulation (LES) provided a greater accuracy than the standard k-ε model for the prediction of the mean liquid flow field and the gas holdup. In the above studies, both gas and liquid phases were treated as interpenetrating continua (Euler-Euler (EE) approach), which is preferred for the simulation of large-scale units due to its relatively low computational demand.   However, it fails to offer accurate bubble-level

information, such as the information regarding the interaction between bubbles and reactor components and the bubble size distribution.

Recently, with advances in computational hardware, an Euler-Lagrange (EL) approach, under which each individual bubble is treated as a single point, gained increasing popularity among researchers. Derksen (2003)[10] employed a two-way coupled Lagrangian particle tracking (LPT) model with LES to study the suspension of solid particles in a stirred reactor. The effect of the impeller and other reactor components were modeled using an immersed boundary condition (IBC). A two-way coupled LPT model with a mono-disperse assumption and LES were used by Arlov et al. (2008) to study gas-liquid flows in an aerated stirred reactor. A volume-of-solid method was employed to model the motion of the rotating impeller. Most recently, Sungkorn et al. (2011b) extended the work of Derksen (2003) by tracking the motion of bubbles, including the breakup and coalescence phenomena, using the stochastic model of Sommerfeld (2001) and Sommerfeld et al. (2003). They suggested that this was an alternative technique to simulate large-scale reactors and to numerically study the effects of operating conditions and reactor configurations.

In contrast to the modeling of aerated stirred reactors with a Newtonian liquid, references to modeling of aerated stirred reactors with a non-Newtonian liquid are rarely found in the literature. Venneker et al. (2002) studied the dispersion of gas in pseudoplastic Xanthan solutions. A single-phase flow field was scaled with the drop of power consumption to obtain a gas-liquid flow field. They termed this method a 1½ -way coupling. A black-box approach was used to model the flow in the impeller region. The correlation closure for the drag coefficient derived from an experiment with non-Newtonian liquid was employed. The breakup and coalescence of bubbles were taken into account via PBE. Moilanen et al. (2006; 2007) employed an EE approach with PBE to study fermentors with pseudoplastic liquids. Several turbulence models for Reynolds-averaged Navier-Stokes (RANS) equations were tested. Typical phenomena in pseudoplastic liquids, such as cavern formation and gas-slugs, were reproduced in their simulations. The studies cited above were limited to the EE approach based on RANS models. It is well-known that time-dependent, anisotropic turbulence characteristics, which directly relate to the breakup and coalescence of bubbles, cannot be accurately captured by RANS models. Therefore, a more sophisticated modeling technique is required to correctly predict the flow field in a stirred reactor, as well as the evolution of bubbles in terms of trajectory, velocity and size.

The objective of this work was to develop a modeling technique that provides detailed information concerning the evolution of bubbles and liquid hydrodynamics in aerated non-

Newtonian liquids. Our approach is based on an EL approach presented by Sungkorn et al. (2011a; 2011b) A variation of a lattice-Boltzmann (LB) scheme by Somers (1993) (see also Eggels & Somers (1995) and Derksen & Van den Akker (1999)) was used to discretize the liquid phase conservation equations. Non-Newtonian liquid behavior according to the power-law fluid model was incorporated in the LB scheme via an *ad hoc* modification suggested by Gabbanelli et al. (2005). The effect of the impeller and other reactor components was modeled using the IBC proposed by Derksen (2003).

4.2   Numerical Modeling

4.2.1   Non-Newtonian liquids

The so-called generalized Newtonian model is used in engineering practice to describe steady-state shear flows of non-Newtonian liquids (Bird et al., 2007). It simply replaces the constant viscosity with the (non-Newtonian) apparent viscosity μ_{app}, which relates to the magnitude of the rate-of-strain tensor $S = \sqrt{2S_{ij}S_{ij}}$. The rate-of-strain tensor S_{ij} is defined by:

$$S_{ij} = \frac{1}{2}\left(\frac{\partial u_i}{\partial x_j} + \frac{\partial u_j}{\partial x_i}\right). \qquad (4.1)$$

The simplest empirical model for μ_{app} is the power-law model expressed as $\mu_{app} = KS^{n-1}$, where K is the consistency coefficient, and n is the power-law index. $n < 1$ corresponds to shear-thinning (pseudoplastic) liquids, $n = 1$ to Newtonian liquids, and $n > 1$ to shear-thickening (dilatant) liquids. However, the power-law model may yield unphysical viscosity, e.g., a mathematic singularity occurs when the shear-thinning liquid is at rest (i.e., when $S = 0$). In order to overcome this problem, Gabbanelli et al. (2005) proposed that the liquid assumes non-Newtonian behavior only within a limited range of S, with a constant value outside the range. They proposed a truncated power-law model with an *ad hoc* modification as:

$$\mu_{app} = \begin{cases} KS_0^{n-1}, & S < S_0 \\ KS^{n-1}, & S_0 < S < S_\infty \\ KS_\infty^{n-1}, & S > S_\infty \end{cases} \qquad (4.2)$$

where S_0 and S_∞ represent the predefined minimum and maximum magnitude of the rate-of-strain tensor, respectively. This model was adopted in our LB scheme to calculate the apparent viscosity. Based on the LB scheme, the values of S_0 and S_∞ were estimated according to the

numerical stability criteria, i.e., the kinematic apparent viscosity $\nu_{app} = \mu_{app}/\rho$. Our preliminary results suggested that the value of ν_{app} for a stable simulation was in the range between 1.0×10^{-7} and 1.0×10^{-3} (in lattice unit).

4.2.2 Lattice-Boltzmann scheme

The fundamental idea of the LB scheme is to use a many-particle system governed by mass and momentum conservation laws to simulate macroscopic flows obeying the same conservation laws. A set of (fictitious) particles residing on a lattice propagates to its neighbor sites and exchanges momentum with particles coming its way. The Navier-Stokes equations (within the incompressible limit) are solved via appropriately designed collision rules and topology of the lattice.

The specific LB scheme used in this work was proposed by Somers (1993) (see also Eggels & Somers (1995) and Derksen & Van den Akker (1999)). It is based on the staggered formulation and utilizes so-called filter matrices and solution vectors. The scheme was chosen because of its robustness at low viscosities due to its treatment of high-order terms. Particularly, the information of the flow field required for the turbulence model and the generalized Newtonian model, e.g., the magnitude of the rate-of-strain tensor S, can be explicitly obtained from the solution vector stored locally at each grid node.

4.2.3 Liquid phase hydrodynamics

Flow structures in a single-phase stirred reactor are known to be highly complex due to time-dependent, three-dimensional phenomena covering a wide range of spatial and temporal scales (Derksen & Van den Akker, 1999). under typical operating conditions for low-viscosity fluids, the impeller Reynolds number Re_r, defined as $Re_r = ND^2/\nu$, is in the transition $(100 < Re_r < 10,000)$ and turbulent regime $(Re_r > 10,000)$ (Hemrajani & Tatterson, 2004). During the last decades, much progress was made in understanding and modeling of turbulence in single-phase stirred reactors with Newtonian liquids (Sommerfeld & Decker, 2004; Murthy & Joshi, 2008; Hartmann et al., 2004). In contrast, turbulence in non-Newtonian liquids is currently considered an area of ongoing research. For example, turbulence modeling in non-Newtonian liquids is performed by using direct numerical simulations or by adopting an existing turbulence model for Newtonian liquids. Based on the concept of Reynolds number similarity, Venneker (1999) postulated that turbulence dynamics are not affected by the non-Newtonian behavior of the liquid, at least in the bulk. He further assumed that turbulent non-

Newtonian flows could be treated similarly to turbulent Newtonian flows, unless a reliable turbulence model for non-Newtonian liquids is available. The complexity drastically increases when gas is dispersed into a turbulent flow. With only a moderate amount of bubbles in a system, bubbles may induce so-called pseudo-turbulence caused by fluctuation, i.e., the motion of bubbles relative to the liquid that results in a turbulent-like flow structure. The intensity of pseudo-turbulence increases with increasing amount of bubbles in a system.

In this work, the evolution of large-scale motions was addressed by applying a filtering process to the conservation equations of the liquid phase, i.e., we performed Large Eddy Simulations (LES) based on the Lattice-Boltzmann scheme. The effect of the residual motion for scales smaller than the filter width was modeled using the subgrid-scale (SGS) model by Smagorinsky (1963). SGS motion is considered to be purely diffusive, and the model only drains energy from the resolved motion without feedback. Based on the suggestion of Venneker (1999), the SGS viscous stress for the non-Newtonian liquids was treated in the same manner as for Newtonian liquids. It was further assumed that, within a dilute dispersion limit, the pseudo-turbulence induced by bubbles resembles the liquid phase SGS motion and can be modeled using a similar SGS model. The eddy viscosity concept represents the effect of the SGS motion as

$$\nu_t = \left(C_S \Delta\right)^2 S, \tag{4.3}$$

where C_S is the Smagorinsky constant, and Δ is the filter width (with size equal to the grid spacing h). The value of C_S was set to 0.10 throughout this work. Note that hereinafter S in Eq. (4.2) and (4.3) represents the resolved rate-of-strain tensor and that properties involving a liquid flow field discussed below are resolved properties, unless stated otherwise. Hence, the effective viscosity in the conservation equations, which is a summation of the apparent viscosity and the eddy viscosity ($\nu_{eff} = \nu_{app} + \nu_t$), is a function of the resolved flow field.

Since the systems under consideration have a global gas phase fraction of only up to 3%, it was assumed that the void fraction term in the conservation equations of the liquid phase had only a marginal effect on the flow and that the filtered conservation equations for a single-phase flow were approximately valid (Sungkorn et al., 2011a; 2011b; Hu & Celik, 2008). The effect of the reactor components, i.e., impeller, baffles and tank wall, on the liquid phase was modeled using an immersed boundary condition (IBC) approach, under which the forces exerted by the reactor components were included in the conservation equations via source terms (Goldstein et al., 1993; Derksen et al., 1997). From a theoretical point of view, the assumptions proposed above were conjectural. However, it is well-known that, to date, no reliable and

accurate model of a multiphase flow with non-Newtonian liquids is available. Thus, the validity of the presented modeling technique was substantiated by the results discussed below.

4.2.4   Bubble dynamics

A bubble cluster concept with a point-volume assumption, under which each parcel represents a group of bubbles with an identical diameter and velocity, was employed in this work. The motion of bubbles within a parcel was tracked in a Lagrangian manner by solving Newton's equation of motion, including all relevant forces, such as net gravity force $\mathbf{F}_G$, forces due to stress gradients $\mathbf{F}_S$, drag $\mathbf{F}_D$, net transverse lift $\mathbf{F}_L$ and added mass force $\mathbf{F}_A$. The following set of equations was solved as:

$$d_t\mathbf{x}_p = \mathbf{u}_p, \tag{4.4}$$

$$\rho_p V_p d_t\mathbf{u}_p = \mathbf{F}_G + \mathbf{F}_S + \mathbf{F}_D + \mathbf{F}_L + \mathbf{F}_A, \tag{4.5}$$

where $\mathbf{x}_p$ is the centroid position of the parcel, $\mathbf{u}_p$ is the bubble velocity, and ρ_p is the bubble density. Expressions of the forces acting on a bubble and their coefficients are summarized in Table 4.1. The drag coefficient C_D was estimated using a correlation derived from the experimental drag curve as a function of the bubble's Reynolds number $\mathrm{Re}_p = \rho_l|\mathbf{u}_p - \mathbf{u}|^{2-n}d_p^n/K$ with ρ_l being the liquid density, $\mathbf{u}$ the liquid velocity at the centroid of the parcel and d_p the bubble diameter (Dewsbury et al., 1999). The Eötvös number that appeared in the correlation for the lift coefficient C_L was defined as $\mathrm{Eo} = (\rho_l - \rho_p)|\mathbf{g}|d_p^2/\sigma$ with $\mathbf{g}$ and σ being the gravitational acceleration and the surface tension, respectively. The liquid velocity appearing in Newton's equation of motion was the resolved liquid velocity $\tilde{\mathbf{u}}$ and the residual liquid fluctuating component $\mathbf{u}'$, i.e., $\mathbf{u} = \tilde{\mathbf{u}} + \mathbf{u}'$. The first component was interpolated from the Eulerian grid nodes, and the fluctuating component was obtained by solving a Langevin-type model by Sommerfeld (1993). The effect of bubbles (on the Lagrangian reference frame) on the liquid phase (on the Eulerian grid) and vice versa, i.e., the two-way coupling, was accounted for using fourth-order polynomial mapping functions (Deen et al., 2004). The forces exerted by the bubbles on the liquid phase consisted of drag, lift and the added mass force.

Force	Closure
$\mathbf{F}_G = (\rho_p - \rho_l)V_p\mathbf{g}$	-
$\mathbf{F}_S = \rho_l V_p D_t \mathbf{u}$	-
$\mathbf{F}_D = -\dfrac{1}{2}C_D\rho_l\pi r_p^2 \lvert \mathbf{u}_p - \mathbf{u}\rvert(\mathbf{u}_p - \mathbf{u})$	$C_D = \dfrac{16}{Re_p}\left(1+0.173Re_p^{0.657}\right)+\dfrac{0.413}{1+16300Re_p^{-1.09}}$
$\mathbf{F}_L = -C_L\rho_l V_p(\mathbf{u}_p - \mathbf{u})\times\nabla\times\mathbf{u}$	$C_L = \begin{cases}\min\left[0.288\tanh(0.121Re_p), f(Eo_d)\right], & Eo_d < 4 \\ f(Eo_d), & 4 < Eo_d \le 10 \\ -0.29, & Eo_d > 10\end{cases}$ $Eo_d = \dfrac{Eo}{E^{2/3}}, \quad E = \dfrac{1}{1+0.163Eo^{0.757}}$ $f(Eo_d) = 0.00105Eo_d^3 - 0.0159Eo_d^2 - 0.0204Eo_d + 0.474$
$\mathbf{F}_A = -C_A\rho_l V_p(D_t\mathbf{u}_p - D_t\mathbf{u})$	$C_A = 0.5$

Table 4.1. Expressions for forces acting on a bubble.

Bubble-bubble collisions were calculated using the stochastic inter-particle collision model of Sommerfeld (Sommerfeld, 2001; Sommerfeld et al., 2003). The model describes the collision between a bubble and its fictitious collision partner generated based on the statistics stored at Eulerian grid nodes. As a result of the collision, the coalescence of the bubbles takes place when the contact time τ_{ij} is shorter than the film drainage time t_{ij}. Otherwise, a momentum exchange and bouncing of the bubbles occur. The contact time was expressed as:

$$\tau_{ij} = \frac{C_C R_{ij}}{u_n}, \tag{4.6}$$

with the equivalent bubble radius R_{ij}

$$R_{ij} = 2.0\left(\frac{2}{d_p}+\frac{2}{d_{fict}}\right)^{-1}, \tag{4.7}$$

where u_n is the relative approaching velocity in a normal direction, and the subscription *fict* represents properties of the bubbles in a fictitious parcel. C_C is the deformation distance as a fraction of the effective bubble radius set to 0.25.[35] The film drainage time was described by neglecting the effects due to surfactants and Hamaker forces as

$$t_{ij} = \sqrt{\frac{R_{ij}^3 \rho}{16\sigma}} \ln\left(\frac{h_0}{h_f}\right). \tag{4.8}$$

The initial film thickness h_0 and the final film thickness before rupture h_f were assumed to be equal to that in an air-water system, i.e., 0.1 [mm] and 0.01 [μm], respectively. A more accurate value for h_0 and h_f may be estimated from the correlations suggested by Chesters (Chester 1975; 1991) but would require additional computational time. Properties of the bubbles after coalescence were calculated based on the mass and momentum balance. The resulting bubble diameter was calculated as $d_{p,new} = \left(d_{p,old}^3 + d_{fict}^3\right)^{1/3}$ and the number of bubbles in a parcel as $n_{p,new} = n_{p,old}\left(d_{p,old}/d_{p,new}\right)^3$.

Bubble breakup was assumed to be due to bubble interaction with turbulent eddies. It was further assumed that only eddies whose size was smaller or equal to the bubble diameter participated in the breakup mechanism. Larger eddies simply transported the bubble without causing a breakup. The breakup model by Luo & Svendsen (1996) was modified to include the apparent viscosity in order to calculate the breakup rate of a bubble in non-Newtonian liquids. The rate of breakup of a bubble with volume V_p into a bubble with a volume of $V_p f_{BV}$ and $V_p\left(1-f_{BV}\right)$ when colliding by turbulent eddies of the size ranging from λ_{min} to d_p was expressed by:

$$\frac{\Omega_B\left(V_p : V_p f_{BV}\right)}{\left(1-\alpha_g\right)n_p} = 0.923\left(\frac{\varepsilon}{d_p^2}\right)^{1/3} \int_{\xi_{min}}^{1} \frac{(1+\xi)^2}{\xi^{11/3}} \exp\left(-\frac{2c_f\sigma}{\rho\varepsilon^{2/3} d_p^{5/3} \xi^{11/3}}\right) d\xi, \tag{4.9}$$

where α_g is the gas phase volume fraction, ε is the energy dissipation at the centroid of the parcel and $\xi_{min} = \lambda_{min}/d_p$. The breakage volume f_{BV} was randomly chosen from the U-shape distribution:

$$f_{BV} = 0.5 + 0.5\tanh\left(10\frac{(RN-0.5)}{\pi}\right), \tag{4.10}$$

where RN is a uniform random number within the interval [0,1]. The value of f_{BV} was limited in the interval [0.2, 0.8]. Accordingly, the increase of surface area c_f was computed from $c_f = f_{BV}^{2/3} + \left(1-f_{Bv}\right)^{2/3} - 1$. The minimal size of the turbulent eddies λ_{min} was assumed to be proportional to the length of micro-scale eddies λ_{ms} as $\lambda_{min} = 11.4\lambda_{ms}$. Instead of a constant kinematic viscosity for a Newtonian liquid, the apparent viscosity was used to estimate λ_{ms} as:

$$\lambda_{ms} = \left(\frac{v_{app}^3}{\varepsilon} \right)^{1/4}.$$
(4.11)

Bubble breakup was considered to be a stochastic event. The breakage volume randomly generated in Eq. (3.16) was used to calculate the breakup rate of a bubble into a new volume $V_p f_{BV}$. The success of the breakup was determined by comparing the breakup rate during the specified time interval with a uniform random number in the interval [0,1]. The number of bubbles in a parcel after the breakup was calculated similarly to how the coalescence of bubbles is calculated. To avoid unphysical consecutive breakups of the bubbles (especially in the impeller region where turbulence intensity is relatively high) and to obtain a time-step resolution-independent solution, the breakup event was bounded by the particle-eddy interaction time t_e. That is, only one group of eddies interacted with the parcel in question for the duration of the particle-eddy interaction time. The next calculation of the breakup rate was carried out after t_e [s]. The expressions for t_e are summarized in the Appendix.

Case	N [rpm]	K [kg / m s^{2-n}]	n [-]	Re$_r$ [-]	nx×ny×nz
A1	480	0.0119	0.68	2,600	88×88×88
A2	480	0.0119	0.68	2,600	66×66×66
A3	480	0.0119	0.68	2,600	112×112×112

Table 4.2. Overview of single-phase simulation cases.

4.2.5   Practical aspects of the simulations

Aerated stirred reactors as described in the work of Venneker (1999) and Venneker et al. (2002) were used to validate the present modeling technique as well as the numerical model of the reactor. The reactor had a standard configuration and consisted of a cylindrical, flat-bottomed, baffled vessel with diameters $T = 0.286$ and $T = 0.441$ [m] in the single- and multiphase study cases, respectively. In all cases, the liquid fill-level was equal to the reactor diameter, i.e., $H = T$. The reactor was equipped with a standard Rushton turbine with a diameter $D = T/3$ located at a distance from the bottom $C = D$. In case of aeration, a ring sparger was placed

midway between the impeller and the tank bottom. The impeller Reynolds number for pseudoplastic liquids was computed as $Re_r = \rho N^{(2-n)} D^2 / K k_s^{(n-1)}$ with k_s being the Metzner-Otto constant chosen to be equal to 11 (Grenville et al., 2004). Settings of single- and multiphase simulation cases are summarized in Table 4.2 and Table 4.3, respectively.

For all simulations, a no-slip (wall) boundary condition was applied at all surfaces except for the top one, for which a free-slip boundary condition was employed to mimic a free surface flow. The reactor components were represented by sets of control points according to the immersed boundary condition. The diameter of the impeller was 30 times the size of grid spacing. The distance between two control points at the impeller surface was $0.7h$. The fluid domain was discretized by a uniform cubic grid of 88^3 lattices (except some simulations in the grid sensitivity study), which corresponded to a grid spacing h of 3.3×10^{-3} and 5×10^{-3} [m] in the single- and multiphase cases, respectively. The simulations began at a standstill and proceeded with a time step of 1.1×10^{-5} [s] for the single-phase simulations. In the multiphase cases, a liquid phase time step of 1.8×10^{-5} [s] and a sub-time step of 3.5×10^{-6} [s] for the calculation of the bubble motion were used. After 30 impeller revolutions, information concerning the liquid phase and bubbles was collected after 30 and 60 impeller revolutions for the single- and multiphase simulations, respectively, and proceeded statistically.

The initial bubble diameter was assumed to be uniform at 8 [mm] in every case with aeration. This corresponded to the grid-spacing-to-bubble-diameter ratio h/d_p of 0.625. Theoretically, the h/d_p ratio should be less than unity when the point-volume assumption is employed. Nevertheless, Sungkorn et al. (2011a) demonstrated that this restriction could be relaxed, i.e., h/d_p can be less than unity but should be greater than 0.5 for a small number of bubbles presented in the system. Therefore, the size of bubbles was limited to 0.05-10 [mm], corresponding to the range of 0.1-2.0 for grid spacing.

All simulations were run in parallel, following the strategy introduced by Derksen et al. (1999) and Sungkorn et al. (2011b) The wall-clock time for simulating of one impeller revolution was approximately 1,5 hours when 4 Intel® Xeon® E5504 (at 2.0 GHz) processors were used.

Case	N [rpm]	Q_g [L/s]	K [kg / m s^{2-n}]	n [-]	Re$_r$ [-]
B1	300	1.0	0.0367	0.65	12,000
B2	300	-	0.0367	0.65	12,000
B3	300	1.0	0.0010	1.00	112,000
B4	300	1.0	0.0132	0.65	33,000
B5	300	1.0	0.0748	0.65	6,000
B6	300	1.0	0.0367	0.56	17,000
B7	300	1.0	0.0367	0.85	5,300

Table 4.3. Overview of multiphase simulation cases.

4.3   Results and Discussion

4.3.1   Single-phase stirred reactor

Flow hydrodynamics

Simulations were carried out following the settings of the A1 case in . The predicted instantaneous and long-term averaged liquid flow fields in the mid-plane between the baffles are shown in Figure 4.1. A radial jet-like outflow with trailing vortices in the impeller plane can be observed, as it is expected for a Rushton disk turbine. The radial outflow significantly interacts with the tank wall inducing two recirculation loops in the region above and below the impeller level. Moreover, eddy-like structures could be observed in the bulk. Since the impeller was located close to the tank bottom, the lower recirculation loop interacted with the tank bottom and had a smaller size than the upper one. The upper recirculation loop was not strong enough to entirely cover the tank above the impeller, creating a stagnant zone (referred to as a region with relatively low liquid motion) near the liquid surface, i.e., above two-thirds of the reactor height. Similar flow structures could be observed in the long-term averaged flow field with a more pronounced stagnant zone in the region near the liquid surface. Note, that this flow

structure should not be considered a cavern formation typically found in very viscous, highly shear-thinning liquids (with n value of 0.3 or less) (Grenville et al., 2004). Rather, these flow structures are caused by such factors as the position of the impeller, the (moderate) shear-thinning behavior of the liquid and the impeller Reynolds number Re_r in the transition regime.
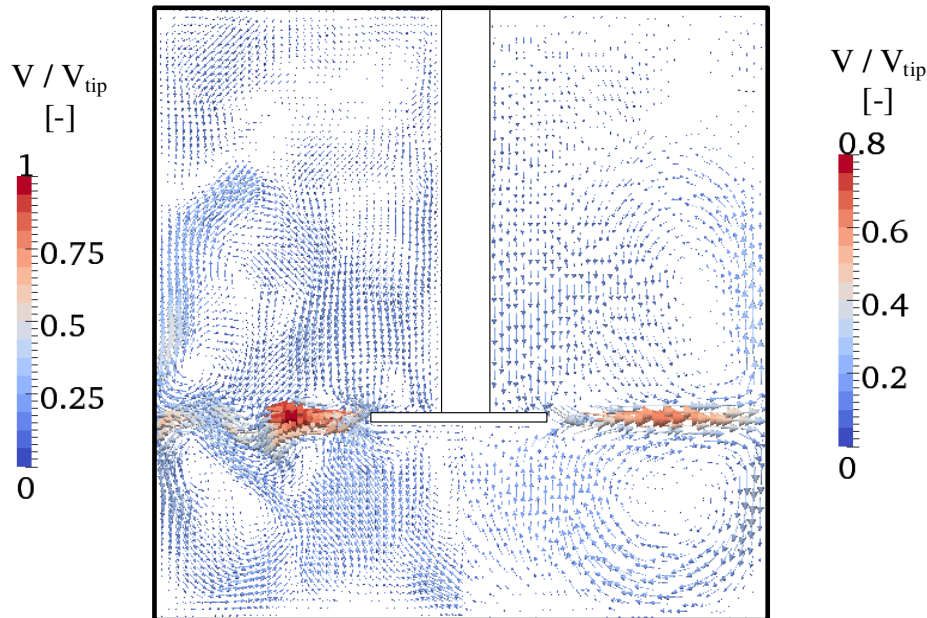
Figure 4.1. Predicted instantaneous (left) and long-term averaged (right) velocity vector field in the mid-plane between the baffles (case A1).

In Figure 4.2, the predicted axial and radial long-term averaged liquid velocity components are compared with the experimental data of Venneker (1999). The comparison was made in the plane of the baffle for the radial velocity profiles at various heights. Despite a coarse grid spacing employed during the simulation, the predicted flow field was in good quantitative and qualitative agreement with the experimental data, because the reactor had only a moderate impeller Reynolds number in this case $\left(Re_r = 2,500\right)$ and the liquid exhibited only moderate shear-thinning behavior with $n = 0.68$. Additionally, the energy-containing eddies were at the scale corresponding to the impeller diameter. As such, most of the energy of the flow field was resolved during the simulation and the main features of the flow field were accurately captured.

Figure 4.3 shows that the long-term averaged apparent liquid viscosity calculated using Eq. (4.2) varied within a small range. The lowest viscosity occurred in the impeller-swept region, under which the highest liquid deformation took place, and increased along the radial

outflow. The highest viscosity was on the edge of the reactor and near the wall next to the upper recirculation loop, where almost no liquid motion was observed.

Grid sensitivity study

Effects of the grid resolution, i.e., of grid spacing h, were studied by performing simulations with coarser (case A2 in Table 2) and finer grids (case A3). A comparison of the predicted axial and radial long-term averaged liquid velocity components with the experimental data is shown in Figure 4.4. It can be observed that a good agreement was achieved for all simulations. The agreement that was achieved for the simulation with the finest grid spacing (case A3) was only a slightly better, which demonstrates a grid-independent behavior of the reactor simulation. However, in case A2 (coarse grid) significant deviations were found especially at larger radii. Thus, case A1 is deemed a sufficiently fine resolution of the flow at this Reynolds number.
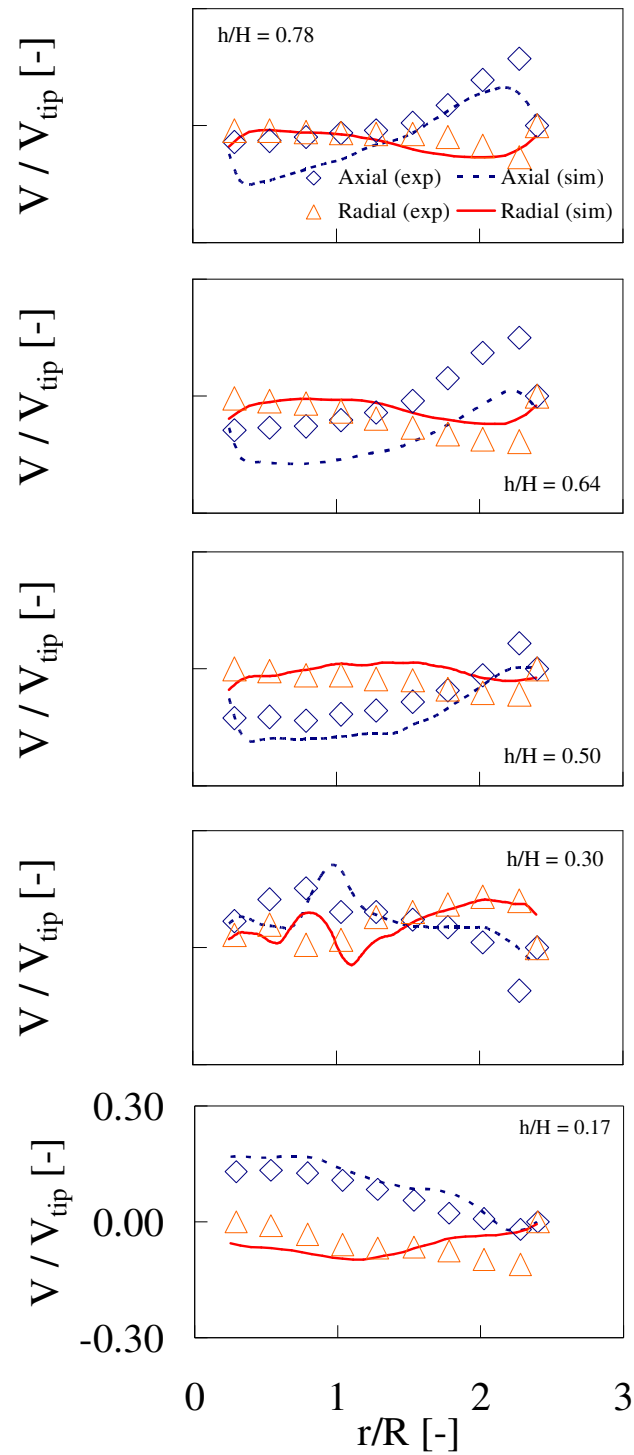
Figure 4.2. Experimental and predicted (case A1) axial and radial long-term averaged velocity components in the baffle plane at various heights.
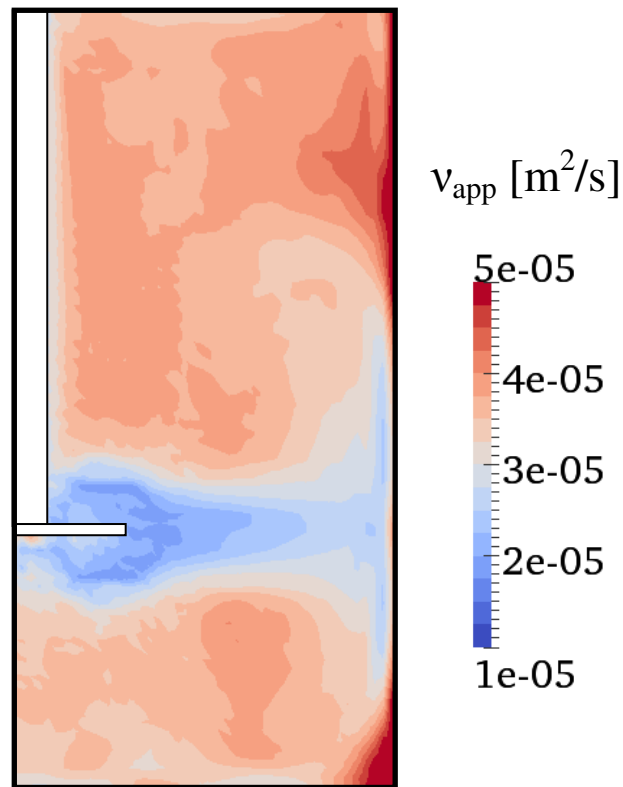
Figure 4.3. Predicted long-term averaged apparent viscosity in the mid-plane between the baffles (case A1).

Within the limitations of the Re_r value and shear-thinning behavior, the simulation results support the assumption proposed by Venneker (1999) that the SGS viscous stress in non-Newtonian liquids can be treated in a similar manner as it is in Newtonian liquids. However, in order to develop a predictive turbulence model for non-Newtonian liquids, detailed experimental data concerning a liquid flow field in a stirred reactor with a high Re_r value and various liquid rheologies are required.

In summary, we postulate that the presented modeling technique is a valid approximation for such simulations. It was also shown that the choice of the grid spacing, which is restricted by the bubble diameter (as discussed earlier but not considered in the single-phase simulations), had only a marginal effect on the main features of the liquid flow field. Future studies will focus on a further refinement of our modeling technique, e.g., a non-Newtonian turbulence model and a more sophisticated non-Newtonian liquid model.
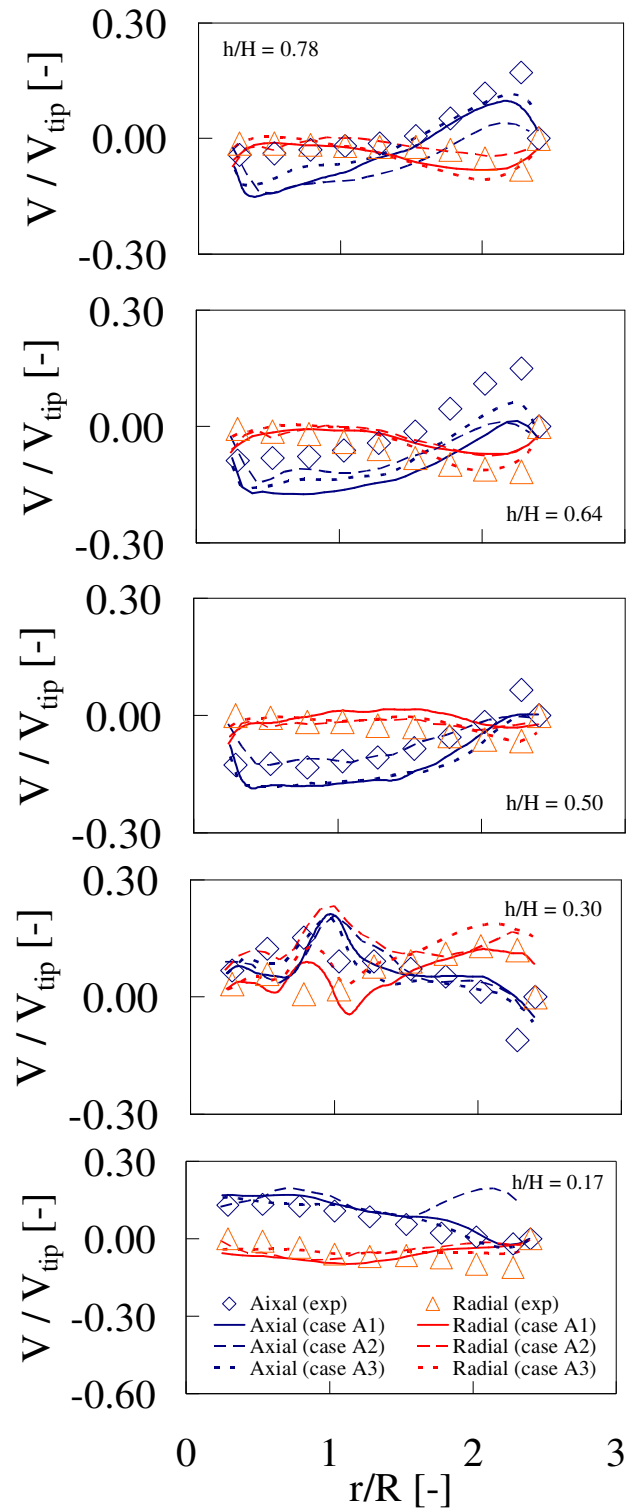
Figure 4.4. Experimental and predicted (case A1, A2 and A3) axial and radial long-term averaged velocity components in the baffle plane at various heights.

4.3.2 Multiphase stirred reactor

Gas-liquid flow hydrodynamics

Simulations for aerated systems were carried out and parameters for the case B1 are summarized in Table 4.3. The resolution was identical to case A1. Snapshots of the predicted bubble dispersion pattern and liquid velocity field in the mid-plane between the baffles are shown in Figure 4.5. The snapshots in both Figures were taken from similar time steps. As in the single-phase stirred reactor, a radial jet-like outflow from the Rushton turbine can be observed in the vertical plane between the baffles. The flow had the highest magnitude near the impeller's blades and decreased in the radial direction towards the tank wall. The radial outflow induced two primary recirculation loops in the region above and below the impeller level. The influence of the sparger on the liquid flow field was also observed. Eddy-like structures were more pronounced in the bulk above the impeller than that at the bottom, and near the liquid surface there was a stagnant zone. The temporal behavior of the liquid flow showed time-dependent flow structures. Bubbles were injected into the top surface of the ring sparger with a uniform initial diameter of 8 [mm], as discussed earlier. The bubbles fluctuated within a small range before they were drawn into the impeller-swept area. Most of the bubble breakup occurred in the impeller-swept area where small eddies reside. Small bubbles tended to follow the recirculation loop to the lower part of the reactor, while larger bubbles tended to rise as their buoyancy was high enough to overcome the downwards liquid flow. In the volume above the impeller, some fraction of the bubbles was drawn into the upper recirculation loop resulting in a recycling into the upper impeller-swept region and, consequently, in a secondary breakup of the bubbles. Furthermore, the bubbles accumulated near the impeller's shaft due to the viscosity and pressure gradient in the impeller's shaft region. Additionally, the downwards flow in that region prevented the bubbles from rising to the liquid surface.
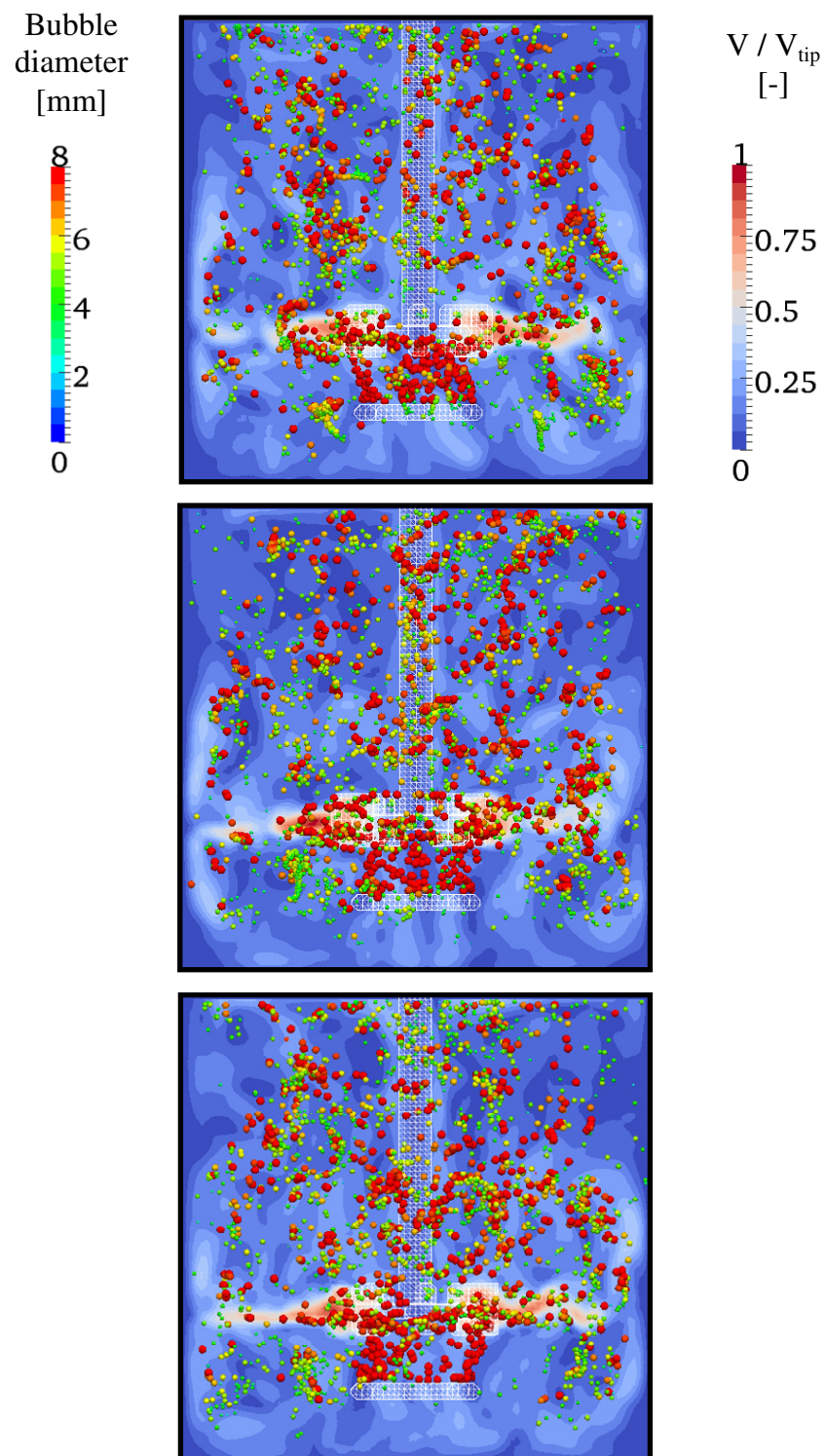
Figure 4.5. Three snapshots of bubble dispersion pattern and liquid velocity magnitude in the mid-plane between the baffles (case B1). Bubbles are highlighted and scaled by diameter.
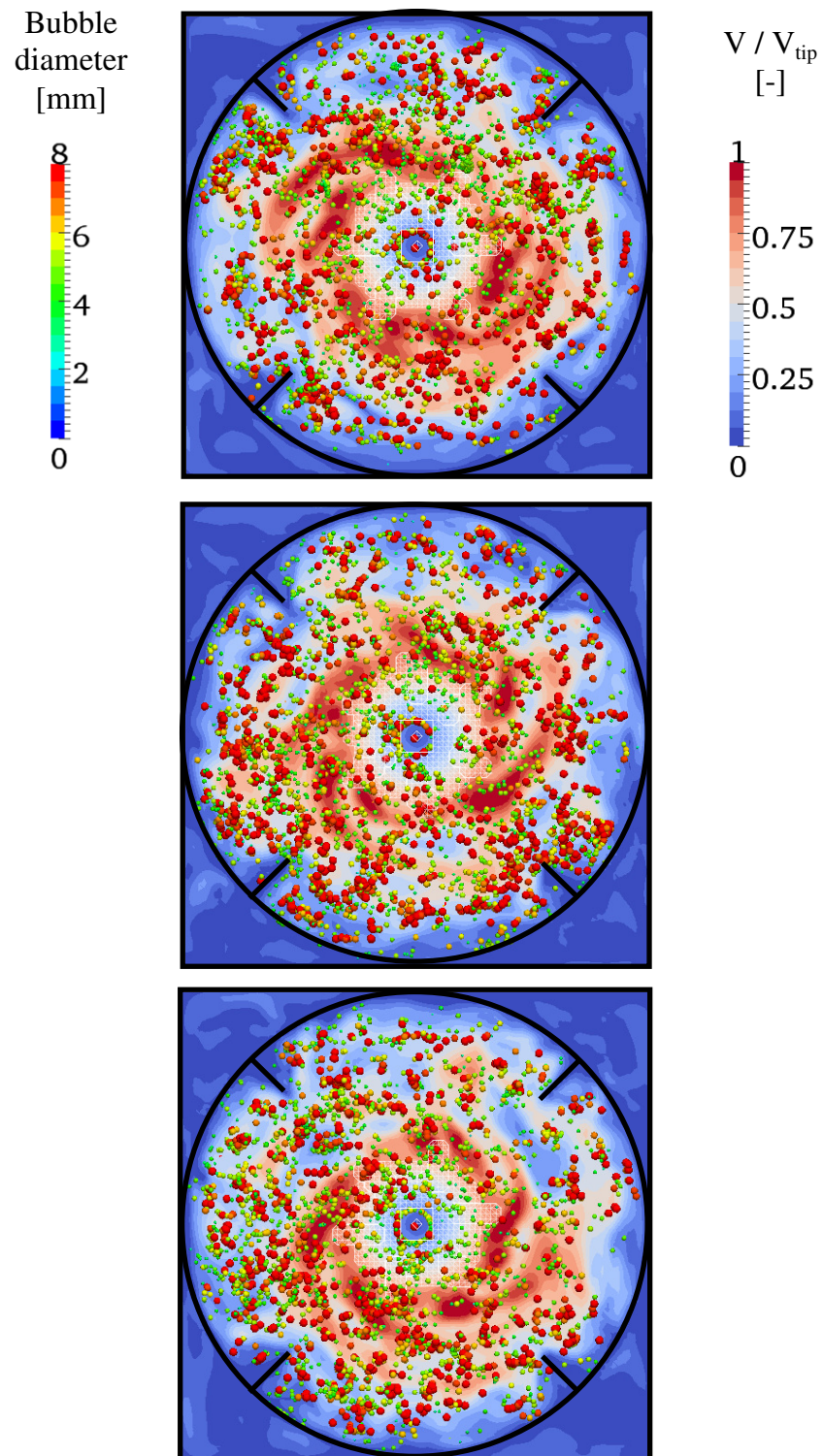
Figure 4.6. Three snapshots of bubble dispersion pattern and liquid velocity magnitude at a cross section at the impeller disc (case B1). Bubbles are highlighted and scaled by diameter.

Snapshots of the predicted bubble dispersion pattern and liquid velocity field at the cross section just below the impeller disc are shown in Figure 4.6. The impeller rotates in counterclockwise direction. From the animated results (data available upon request), it can be observed that the liquid wakes behind the impeller blades have a magnitude that is slightly higher than the impeller tip speed. An interaction between the wakes and the baffles is also observed. Furthermore, the low pressure region behind the blades formed so-called ventilated cavities (Middleton & Smith, 2004). The bubbles were dispersed throughout the cross-section following the wakes. An accumulation of the bubbles near the impeller's shaft and on the windward side of the baffles can be seen on the snapshots.
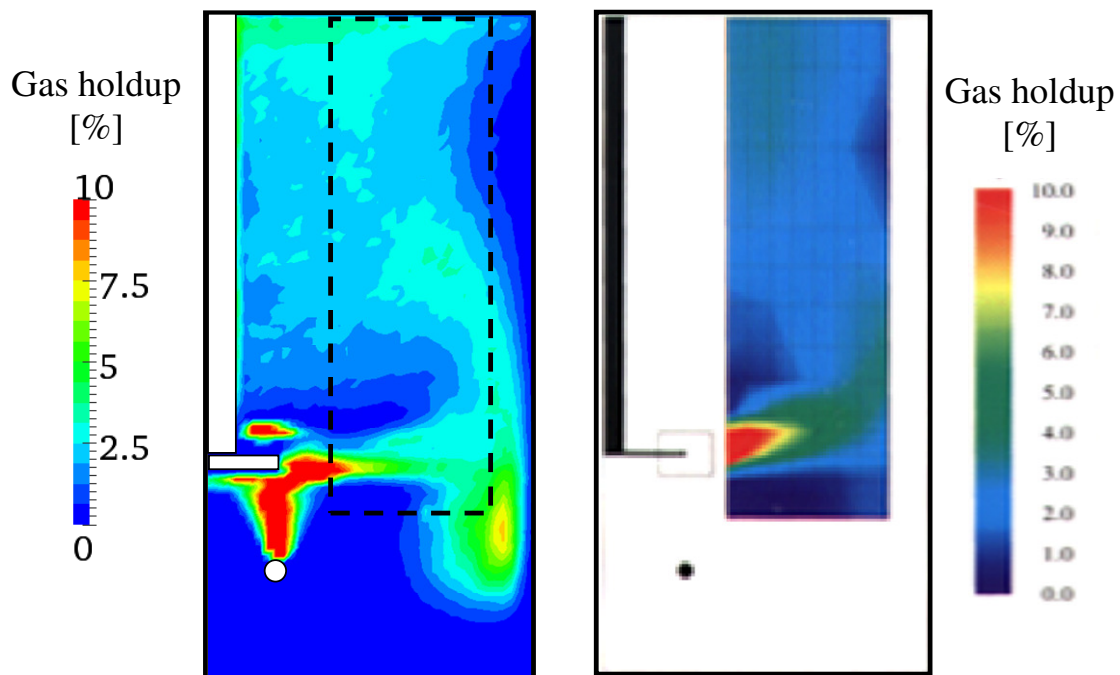
Figure 4.7. Predicted (left) and experimental (right) long-term averaged local gas holdup (case B1).

The predicted and experimental long-term averaged gas holdup contour plots are shown in Figure 4.7. The experimental data were measured with an optical fiber probe (Venneker, 1999) whose (depth of the) measurement plane greatly depends on the measured bubble size and the approaching angle of the bubble to the probe. A specific plane cannot be defined by such a measurement method. However, with a long enough averaging period, the phase-averaged procedure may be used for a comparison between the simulation and experimental results. As can be seen, a qualitatively good agreement between our predictions and experimental results was achieved. A radial stream of gas bubbles towards the reactor wall was reproduced in the

simulation, and the absence of significant gas holdup above and below the outflow stream was predicted. Moreover, the gas holdup near the wall towards the center axis at the liquid surface was correctly captured. Additionally, the simulation showed a high concentration of gas in the sparger's outflow, the impeller swept region and the region next to the impeller's shaft. Interestingly, a region of high concentration was also found above the impeller's blades due to an equilibrium between the bubbles' buoyancy and the downward liquid flow resulting in a long bubble residence time. This behavior was also observed in our experiments.

Figure 4.8 shows the predicted and experimental long-term averaged radial profile of the gas holdup at various heights. Again, a good agreement between the simulation and experimental results was achieved. There were some deviations in the region right above and below the impeller, which could have been caused by such factors as the spherical bubble assumption, the lack of accurate methods to describe the interaction between the impeller and bubbles in non-Newtonian liquids, a relatively coarse grid spacing employed in the simulation, the lack of a reliable turbulence model for non-Newtonian liquids or also the inaccuracy of the intrusive measurement method. The latter unavoidably disturbs the flow field and may cause a significant deviation when the attack angle of the bubble is greater than 90 degrees, as demonstrated by Bombac et al. (1997) for a conductivity-based probe.

The predicted long-term averaged bubble size distribution (BSD) in the region above and below the impeller is shown in Figure 4.9. Both BSDs had a bimodal distribution with one mode having a diameter approximately half of the initial diameter and the other one having a diameter equal to the bubble's initial diameter. The lower part of the reactor had a slightly larger number mean diameter d_{10} and Sauter diameter d_{32} due to the presence of sparger in the lower part. Bubbles with a diameter larger than the initial bubble size were rarely found, obviously because of the restriction of the maximum bubble size set in this work (i.e., only a coalescence of bubbles smaller than 2 times the grid spacing or a coalescence that would result in a bubble smaller than 2 times the grid spacing were allowed in the simulations). Hence, a bubble with a diameter of 8 [mm], corresponding to 1.6 times the grid spacing, would rarely coalesce. If the restriction were omitted, a smoother distribution around the larger mode would be obtained. However, it would only slightly affect the overall BSD.
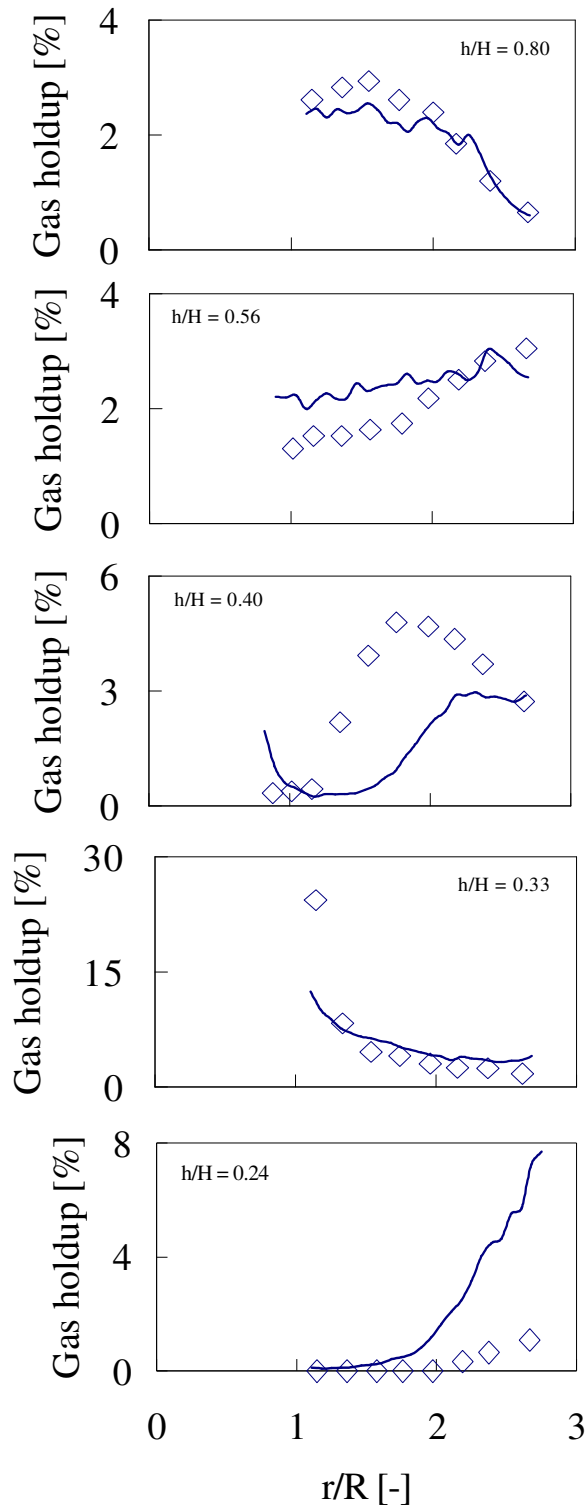
Figure 4.8. Experimental and predicted (case B1) long-term averaged radial gas holdup profile at various heights.
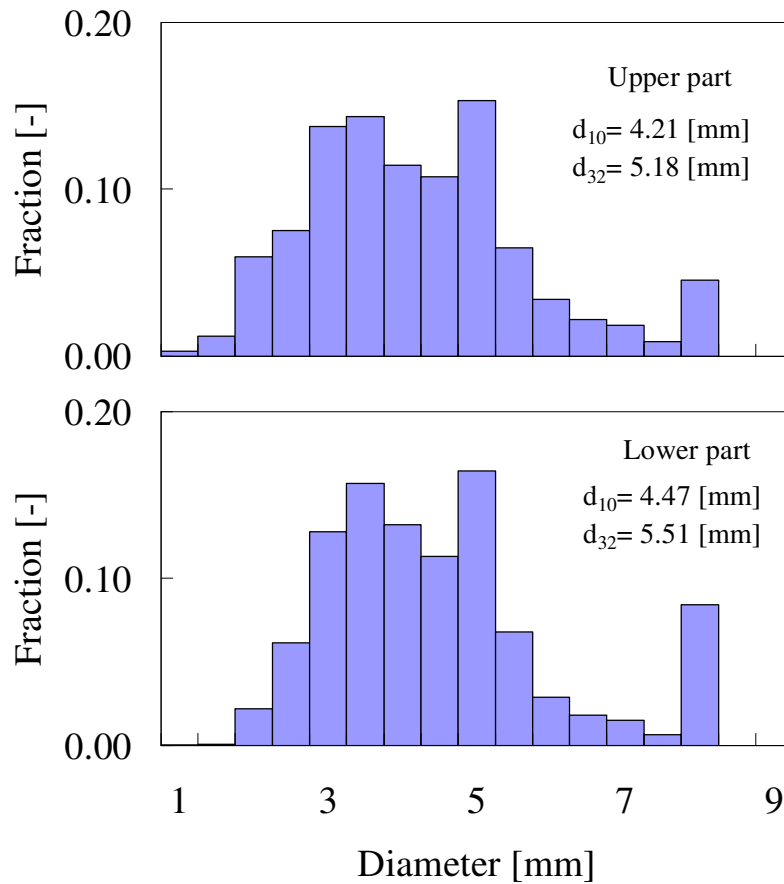
Figure 4.9. Predicted long-term averaged bubble size distribution for case B1 in the region above (top) and below the impeller (bottom).

The predicted long-term averaged liquid and apparent viscosities in the mid-plane between the baffles are shown in Figure 4.10. The radial jet-like outflow induced by the Rushton turbine with two primary recirculation loops in the region above and below the impeller can be seen. Again, the radial outflow away from the impeller was not strong enough to create significant liquid motion near the surface, resulting in a stagnant zone near the liquid surface. The apparent viscosity showed a similar trend, with the lowest viscosity in the impeller-swept region and the highest viscosity in the lower corner of the reactor.
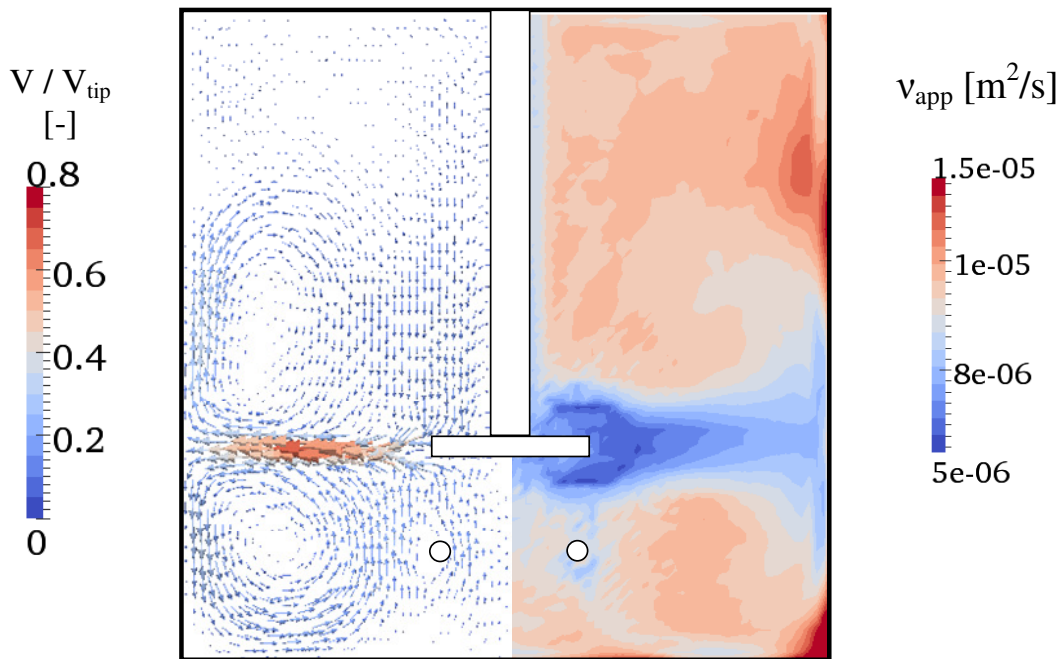
Figure 4.10. Predicted long-term averaged liquid velocity (left) and apparent viscosity (right) in the mid-plane between the baffles (case B1).
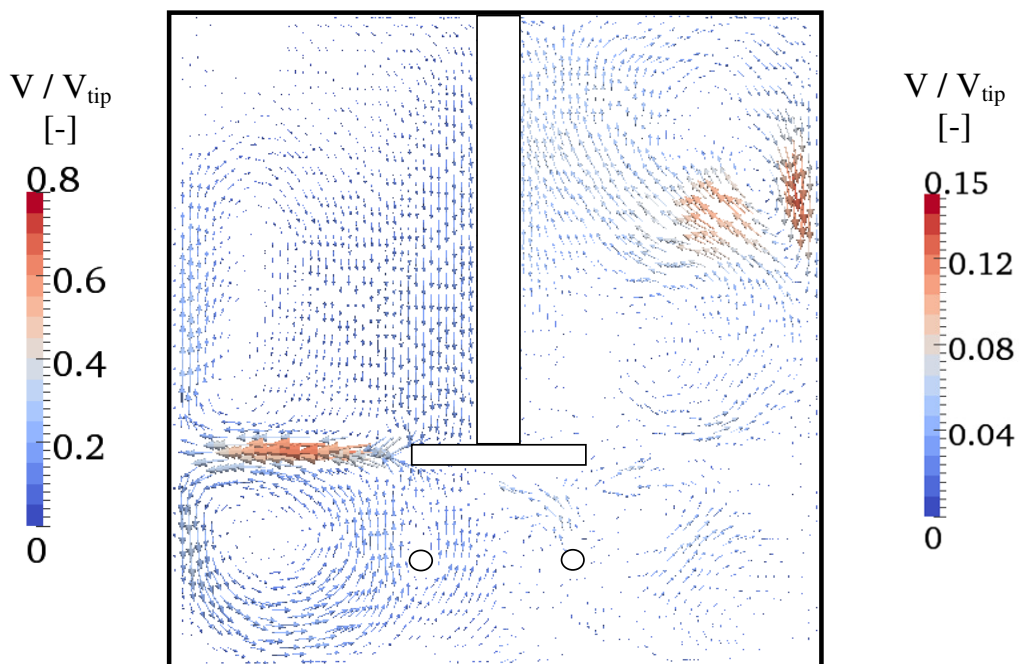
Figure 4.11. Predicted long-term averaged liquid velocity from simulation without aeration (case B2) (right) and the difference between liquid velocity for aerated (case B1) and unaerated condition (case B2) in the mid-plane between the baffles.

The effect of bubbles on the liquid flow field was determined by performing a simulation without aeration (case B2). The predicted long-term averaged liquid velocity from the case B2 and the difference between the liquid velocity, aerated (case B1) and unaerated (case B2), in the mid-plane between the baffles, are shown in Figure 4.11. Differences can be noticed in the upper part of the reactor, especially in the region near the wall. Bubbles at the impeller's blades reduce the pumping capacity of the impeller resulting in a weaker liquid stream and, consequently, in a weaker and smaller recirculation loop.
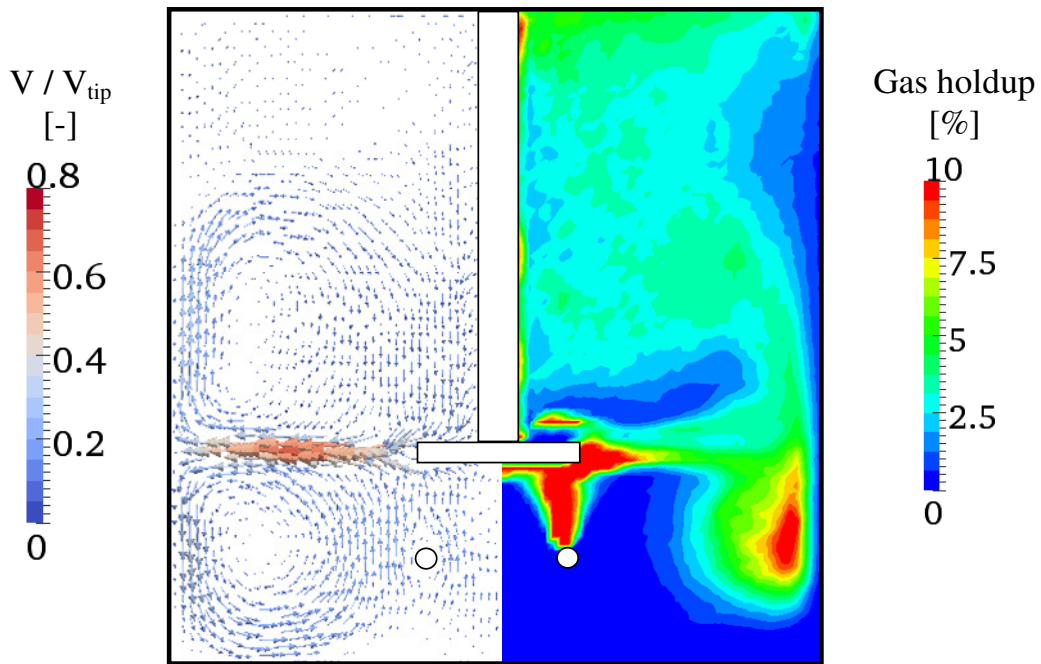
Figure 4.12. Predicted long-term averaged liquid velocity (right) and gas holdup (right) in the mid-plane between the baffles from simulation case with a Newtonian liquid (case B3).
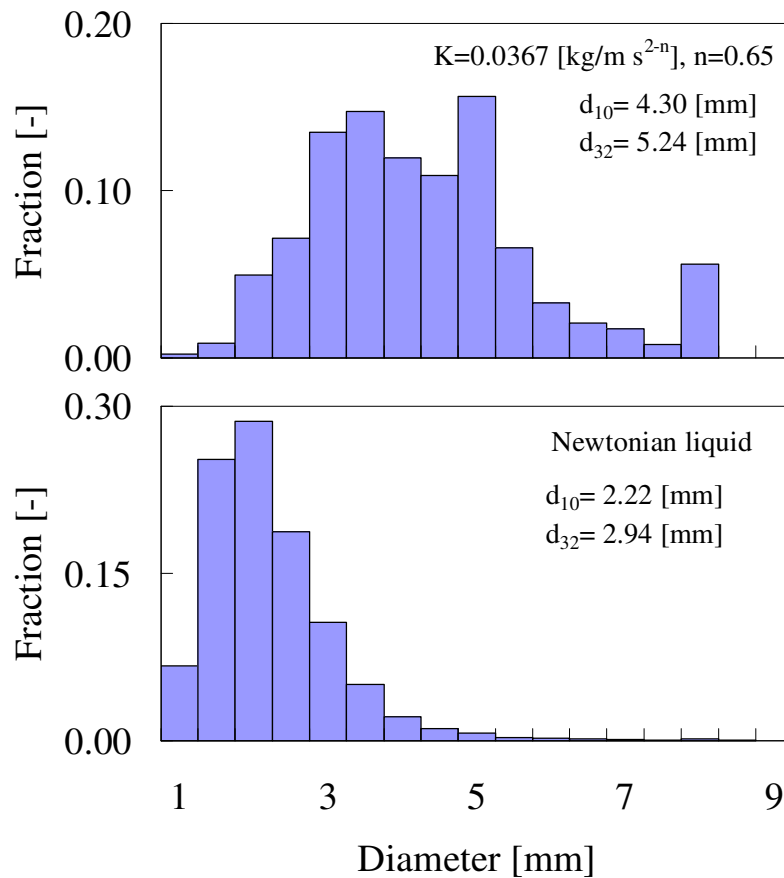
Figure 4.13. Predicted long-term averaged bubble size distribution within the reactor from simulations with non-Newtonian (case B1) (top) and Newtonian liquids (case B3) (bottom).

Effects of liquid rheology

The effect of the non-Newtonian behavior was determined by comparing the simulation for a non-Newtonian liquid (case B1) with a simulation for a Newtonian liquid (case B3). Note that, in this work, we aimed at studying the effects of liquid rheology, therefore the impeller rotational speed and the gas flow rate were kept constant while liquid rheology was varied. The predicted long-term averaged liquid velocity and gas holdup in the mid-plane between the baffles for case B3 are displayed in Figure 4.12 showing only a marginal difference in the liquid flow field between the cases. In reality, this would result in a significant difference in power input. Nevertheless, in our work we focused only on the flow hydrodynamics. A significant difference could be observed when comparing the gas holdup distribution profiles. A higher gas concentration and larger dispersion area were obtained for a Newtonian liquid. The predicted long-term averaged BSDs in the reactor for both cases are shown in Figure 4.13. The BSD had a

bimodal distribution shape for a non-Newtonian liquid, while the BSD for a Newtonian liquid had a log-normal distribution shape. The value of d_{10} and d_{32} significantly decreased from 4.30 and 5.24 [mm] in the former case to 2.22 and 2.94 [mm] in the latter case. This is due to a higher Re_r value in the latter case which results in a higher turbulence intensity and, consequently, a greater amount of small eddies participating in the bubble breakage mechanism.
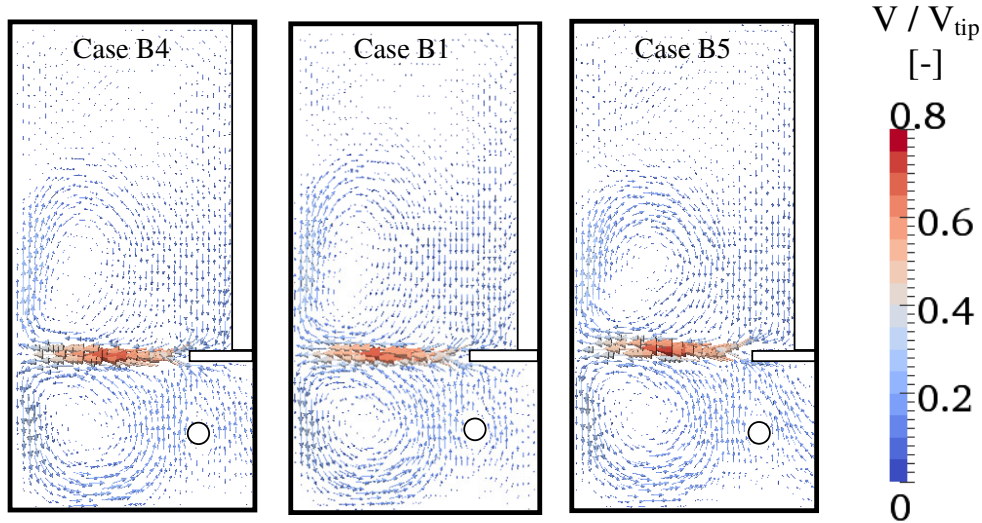
Figure 4.14. Comparison of long-term averaged liquid velocity in the mid-plane between the baffles with increasing consistency coefficient from left to right (i.e., case B4, B1 and B5, respectively).
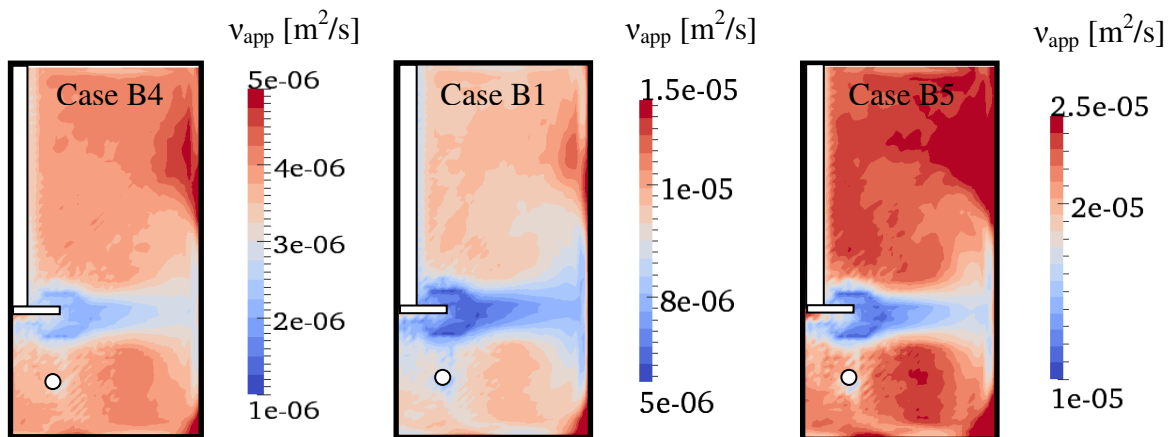
Figure 4.15. Comparison of long-term averaged apparent viscosity in the mid-plane between the baffles with increasing consistency coefficient from left to right (i.e., case B4, B1 and B5, respectively).
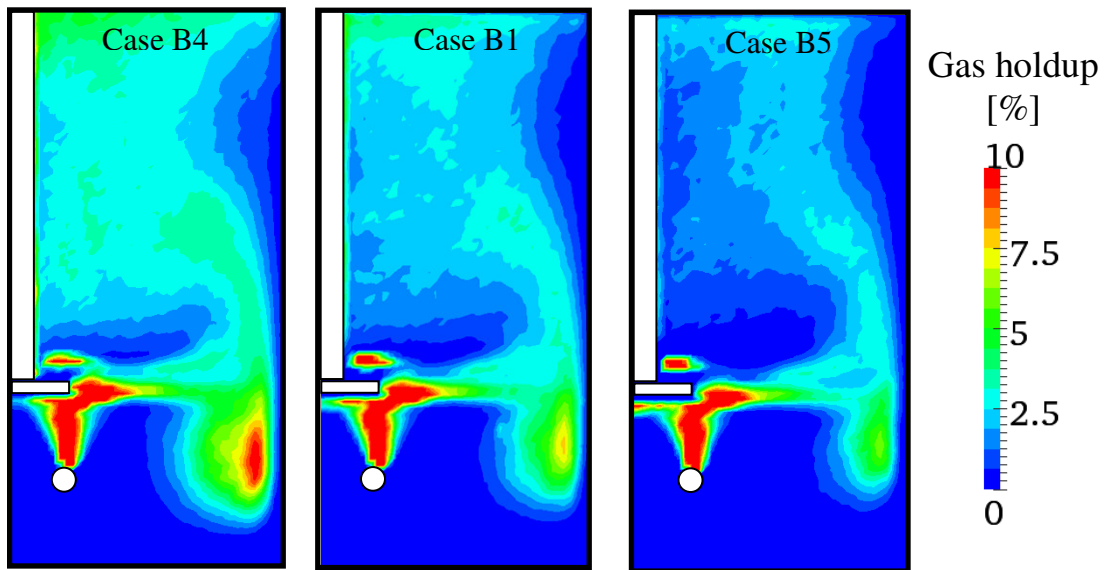
Figure 4.16. Comparison of long-term averaged local gas holdup in the mid-plane between the baffles with increasing consistency coefficient from left to right (i.e., case B4, B1 and B5, respectively).

In the next case study, only the consistency coefficient was varied from 0.0367 [kg / m s^{2-n}] for case B1 to a lower value for case B4 and a higher value for case B5. Correspondingly, the Re_r value changed from 12,000 for case B1 to 33,000 and 6,000 for cases B4 and B5, respectively. Figure 4.14 shows the predicted long-term averaged liquid velocity in the mid-plane between the baffles for the simulation cases described above. The Figure was arranged such that the consistency coefficient increases from left to right. As can be seen, there was only a marginal difference between the liquid flow fields. The predicted long-term averaged apparent viscosity is shown in Figure 4.15. For all simulations, the viscosity profile exhibited a similar trend, i.e., the lowest viscosity occurred in the impeller-swept region, increased along the outflow and had the minimum value on the edge of the reactor. However, as expected, the magnitude of the viscosity increased while the range of the viscosity decreased with the increased consistency coefficient. A significant difference in the gas holdup distribution was observed (Figure 4.16). The increase in the consistency coefficient resulted in a lower concentration and a smaller dispersion area. The predicted BSD depicted in Figure 4.17 shows that the decrease of the consistency coefficient from case B1 to case B4 led to a more pronounced bubble breakage, as can be noticed in the change of the BSD from a bimodal to a log-normal distribution with smaller d_{10} and d_{32} values. Additionally, an increase of the consistency coefficient led to a lower bubble breakage, as the bimodal distribution shape

112

obtained for case B5 demonstrates. The behavior might be caused by several factors, as previously discussed.
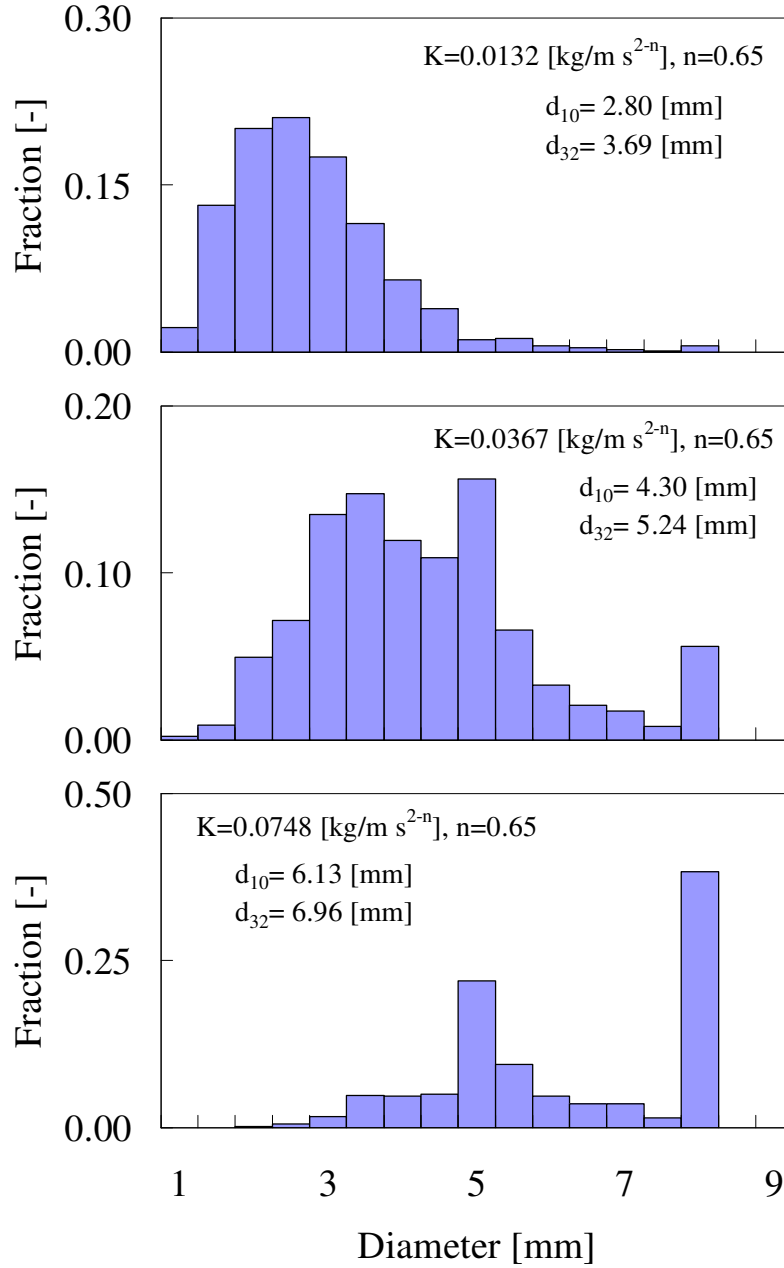
Figure 4.17. Comparison of long-term averaged bubble size distribution with increasing consistency coefficient from top to bottom (i.e., case B4, B1 and B5, respectively).
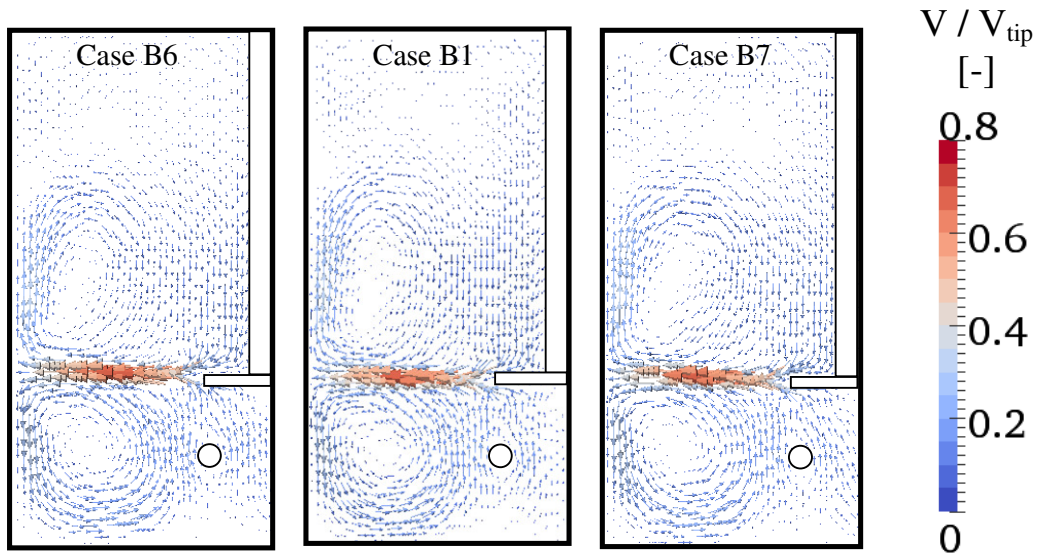
Figure 4.18. Comparison of long-term averaged liquid velocity in the mid-plane between the baffles with increasing power-law index from left to right (i.e., case B6, B1 and B7, respectively).
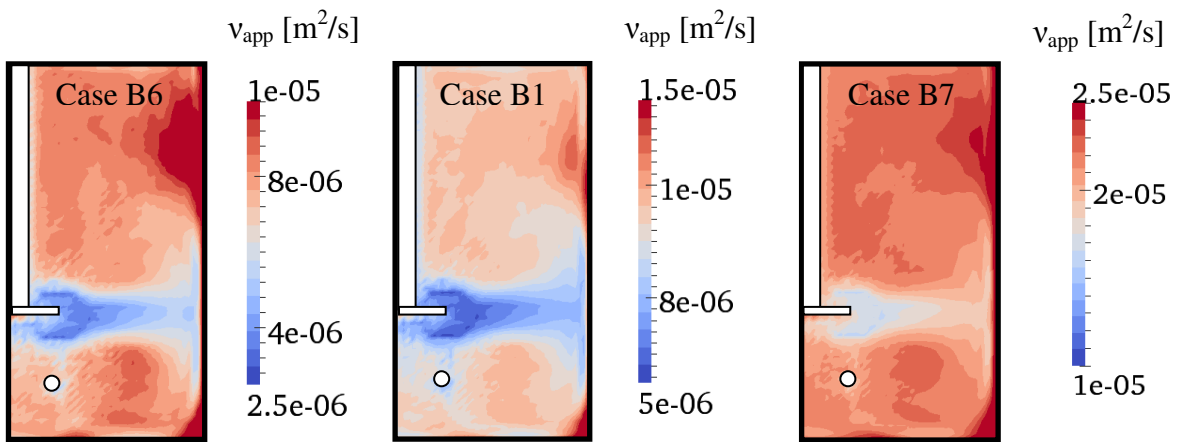
Figure 4.19. Comparison of the long-term averaged apparent viscosity in the mid-plane between the baffles to increased power-law index from left to right (i.e., case B6, B1 and B7, respectively).
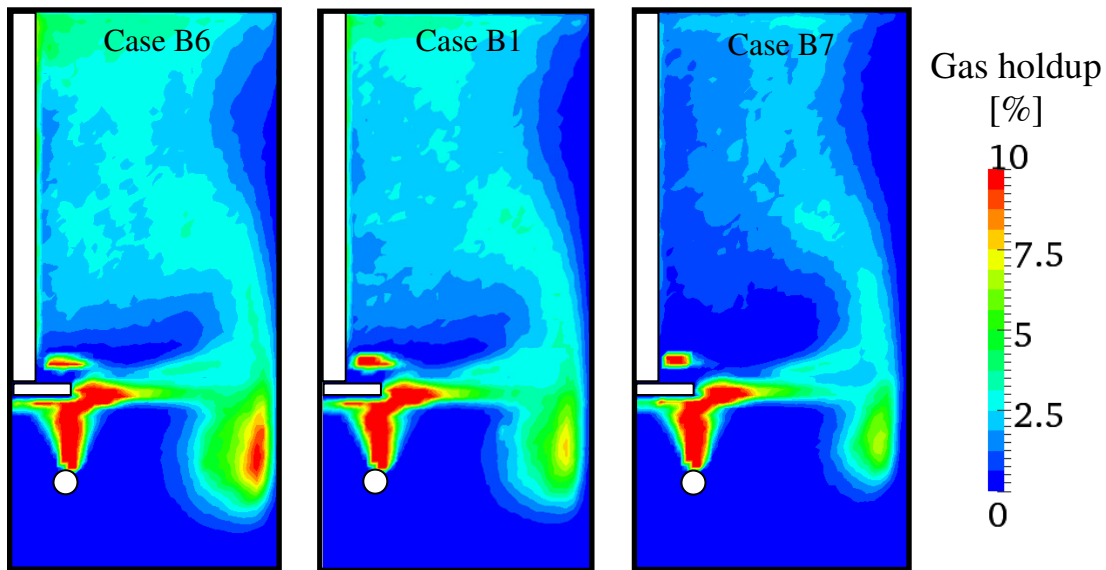
Figure 4.20. Comparison of the long-term averaged local gas holdup in the mid-plane between the baffles to the increased power-law index from left to right (i.e., case B6, B1 and B7, respectively).

Furthermore, we numerically studied the effects of the power-law index n in pseudoplastic liquids. The value of n was varied from 0.65 in case B1 to 0.56 and 0.85 in cases B6 and B7, respectively. Other parameters, i.e., the consistency coefficient, Fr and Fl number, were kept constant. A decrease in n value implies that the liquid exhibits higher shear-thinning behavior. Accordingly, the Re_r value changed from 12,000 in case B1 to 17,000 and 5,300 in cases B6 and B7, respectively. Plots of the long-term averaged liquid velocity are shown in Figure 4.18. Again, only a marginal change between the cases was observed. Venneker et al. (2010) measured liquid velocity components at the level of the impeller disc in a single-phase stirred reactor with shear-thinning fluids and concluded that the values of Re_r and n had no effect on the measured mean radial and tangential velocity components. Only the axial velocity component depended on the Re_r value. As stated in the previous Section, the presence of bubbles for the range of aeration rate considered in this study only had a marginal effect on the liquid flow field. Plots of the predicted long-term averaged apparent viscosity in Figure 4.19 show that an increase in n value resulted in an increase in the viscosity and a decrease in the viscosity range. The trend for the viscosity was qualitatively similar for all cases. The difference between the viscosity in the impeller-swept region and the bulk was decreased at a higher n value. The predicted long-term averaged gas holdup is depicted in Figure 4.20. It can be clearly seen that the concentration and dispersion areas decreased with the increase of n value. In the

case B7, bubbles rarely disperse in the reactor, and most of them rise towards the liquid surface. The predicted long-term averaged BSD in the reactor is shown in Figure 4.21. The d_{10} and d_{32} values increase with the increased n value. Significant differences were observed between cases B1 and B7: BSD for case B7 shows that almost no breakup occurred in the reactor resulting in high values of d_{10} and d_{32}. Thus, the n-value has the most significant impact on the bubble size distribution.
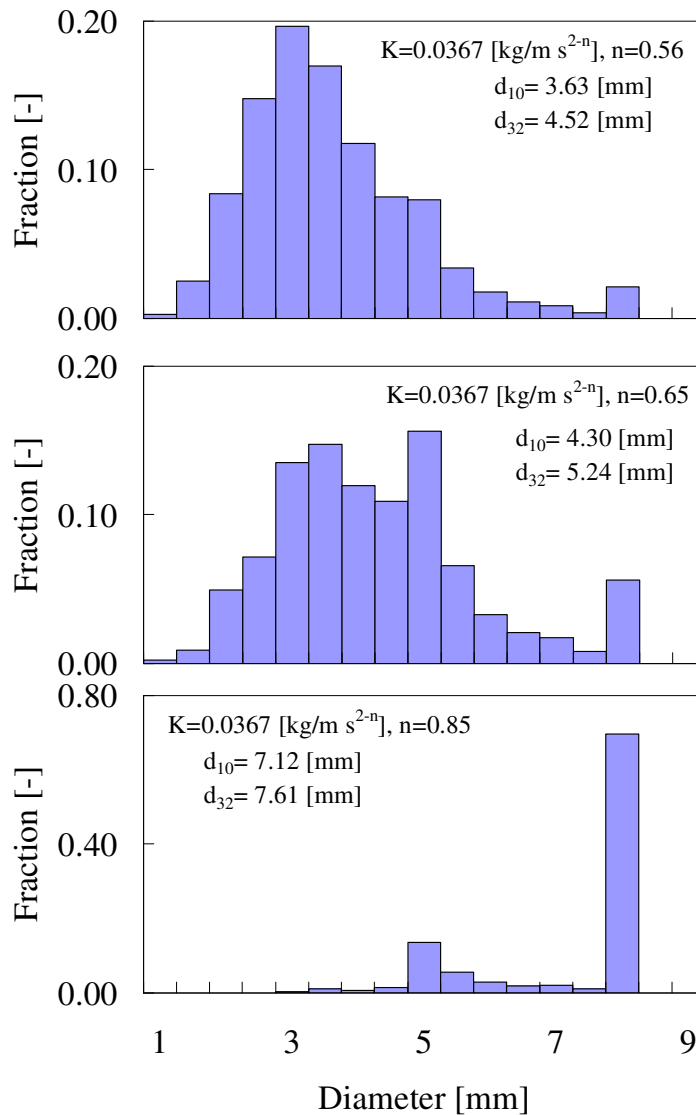
Figure 4.21. Comparison of the long-term averaged bubble size distribution within the reactor to the increased power-law index from top to bottom (i.e., case B6, B1, and B7, respectively).

4.4   Conclusions

In this study, we expanded our previous work (Derksen, 2003; Sungkorn et al., 2011a; 2011b; Derksen & Van den Akker, 1999) to develop a modeling technique for simulations of aerated stirred reactors with pseudoplastic liquids. The proposed model accounted for the bubble breakup and coalescence, and the non-Newtonian behavior was modeled using a truncated power-law model (Gabbanelli et al., 2005). A variation of the LB scheme of Somers (1993) was used to discretize the filtered conservation equations of the liquid phase. A bubble cluster concept was employed with a point-volume assumption to track the bubble motion. The drag force was calculated using the correlation derived from experiments with pseudoplastic liquids (Dewbury et al., 1999). The collision, coalescence and breakup of the bubbles were treated as a stochastic event. The IBC by Derksen (1997) was applied to describe the effect of the moving reactor components on the liquid phase and on the bubbles.

The comparison between the predicted and experimental liquid flow fields of a single-phase stirred reactor with a pseudoplastic liquid showed that the simulation accurately captured the main features of the flow field. A grid sensitivity study suggested that finer grid spacing, i.e., higher cell numbers, provided only a slightly better prediction. It was also found that coarser grid spacing captured most of the main flow features, e.g., a radial outflow and recirculation loops above and below the impeller. The study was performed with a moderate impeller Reynolds number, i.e., $\mathrm{Re}_r = 2,500$. Hence, the validity range was justified within the limitations of Re_r and liquid rheology. In order to further justify the validity and develop a reliable modeling technique, detailed experimental data of a stirred reactor with high Re_r and a diverse liquid rheology are required. However, we assumed that our modeling technique was sufficiently valid for the simulations carried out in this work, at least with regard to capturing the main flow features.

When the predicted gas holdup of an aerated stirred reactor with a pseudoplastic liquid was compared to the experimental data of Venneker et al. (2002), a qualitatively and quantitatively good agreement was achieved. It was numerically demonstrated that the presence of bubbles, within the aeration rate employed in this work, had an effect mainly on the liquid flow field in the upper part of the reactor and especially near wall.

Furthermore, the presented modeling technique was used to study the effect of liquid rheology on the flow hydrodynamics, the bubble dispersion pattern and BSD. It was found that the increase in the consistency coefficient (i.e., viscosity) and the power-law index (i.e., shear-thinning behavior) resulted in the decrease in the concentration and dispersion areas of the

bubbles. Accordingly, the BSD changed significantly from bimodal to log-normal distribution shape in some cases. It is known that the change in the liquid rheology resulted in the change of the Re_r value and, consequently, in the turbulence intensity, the size of eddies and the viscosity distribution within the reactor. As such, these factors affect the breakage of the bubbles, as well as their rise velocity and dispersion pattern. It is not yet clear if the dispersion pattern and BSD only depend on the Re_r value or if they interact with the liquid rheology and Re_r value in a more complex way. In the future we plan to study the subject both numerically and experimentally to gain more understanding.

Some of the assumptions employed in this work were conjectural. However, from an engineering point of view, they are sufficient to gain a preliminary understanding of the phenomena within a complex aerated stirred reactor with pseudoplastic liquids. Since the presented modeling technique utilizes elementary physical principles, it can be considered an alternative engineering tool to gain detailed insights into complex industrial-scale reactors.

4.5   References

1   Arlov D, Revstedt J, Fuchs L. Numerical simulation of gas-liquid Rushton stirred reactor – LES and LPT. *Computers & Fluids*. 2008;37:793-801.

2   Bakker A, Van den Akker HEA. A computational model for the gas-liquid flow in stirred reactors. *Trans Inst Chem Eng*. 1994;72:594-606.

3   Bird RB, Stewart WE, Lightfoot EN. *Transport phenomena*; John Wiley & Sons: New York, 2nd Ed., 2007.

4   Bombac A, Zun I, Filipic B, Zumer M. Gas-filled cavity structures and local void fraction distribution in aerated stirred vessel. *AIChE J*. 1997;43:2921-2931.

5   Chesters AK. The applicability of dynamic-similarity criteria to isothermal, liquid-gas, two-phase flows without mass transfer. *Int J Multiphas Flow*. 1975;2:191.

6   Chesters AK. The modeling of coalescence processes in fluid-liquid dispersions: A review of current understanding. *Trans Inst Chem Eng*. 1991;69:25.

7   Darmana D, Deen NG, Kuipers JAM. Numerical study of homogeneous bubbly flow: Influence of the inlet conditions to the hydrodynamic behavior. *Int J Multiphase Flow*. 2009;35:1077-1099.

8   Deen NG, Solberg T, Hjertager BH. Flow generated by an aerated Rushton impeller: Two-phase PIV experiments and numerical simulations. *Can J Chem Eng*. 2002;80:1-15.

9   Deen NG, Van Sint Annaland M, Kuipers JAM. Multi-scale modeling of dispersed gas-liquid two-phase flow. *Chem Eng Sci*. 2004;59:1853-1861.

10   Derksen JJ. Numerical simulation of solids suspension in a stirred tank. *AIChE J*. 2003;49:2700-2714.

11   Derksen JJ, Kooman JL, Van den Akker HEA. Parallel fluid flow simulation by means of a lattice-Boltzmann scheme. *Lect Notes Comput Sci*. 1997;125:524.

12   Derksen JJ, Van den Akker HEA. Large eddy simulation on the flow driven by a Rushton turbine. *AIChE J*. 1999;45:209-221.

13   Dewsbury K, Karamanev D, Margaritis A. Hydrodynamic characteristics of free rise of light solid particles and gas bubbles in non-Newtonian liquids. *Chem Eng Sci*. 1999;54:4825-4830.

14   Eggels JGM, Somers JA. Numerical simulations of free convective flow using the lattice-Boltzmann scheme. *Int J Heat Fluid Flow*. 1995;16:357-364.

15   Gabbanelli S, Drazer G, Koplik J. Lattice Boltzmann method for non-Newtonian (power-law) fluids. *Phy Rev E*. 2005;72:046312.

16 Gogate PR, Beenackers AACM, Pandit AB. Multiple-impeller systems with a special emphasis on bioreactor: A critical review. *Biochem Eng J*. 2000;6:109-144.

17 Goldstein D, Handler R, Sirovich L. Modeling a no-slip flow boundary with an external force field. *J Comput Phys*. 1993;105:354.

18 Grenville RK, Nienow AW. Blending of miscible liquids. In *Handbook of Industrial Mixing: Science and Practice*; Paul EL, Atiemo-Obeng VA, Kresta SM. Eds.; Wiley: New York, 2004.

19 Hartmann H, Derksen JJ, Montavon C, Pearson J, Hamill IS, Van den Akker HEA. Assessment of large eddy and RANS stirred tank simulations by means of LDA. *Chem Eng Sci*. 2004;59:2419-2432.

20 Hemrajani RR, Tatterson GB. Mechanically stirred vessels. In *Handbook of Industrial Mixing: Science and Practice*; Paul EL, Atiemo-Obeng VA, Kresta SM. Eds.; Wiley: New York, 2004.

21 Hennick EA, Lightstone MF. A comparison of stochastic separated flow models for particle dispersion in turbulent flows. *Energ Fuel*. 2000;14:95-103.

22 Hu G, Celik I. Eulerian-Lagrangian based large-eddy simulation of a partially aerated flat bubble column. *Chem Eng Sci*. 2008;63:253-271.

23 Lane GL, Schwarz MP, Evans GM. Numerical modelling of gas-liquid flow in stirred tanks. *Chem Eng Sci*. 2005;60:2203-2214.

24 Luo H, Svendsen HF. Theoretical model for drop and bubble breakup in turbulent dispersions. *AIChE J*. 1996;42:1225-1233.

25 Middleton JC, Smith JM. Gas-liquid mixing in turbulent systems. In *Handbook of Industrial Mixing: Science and Practice*; Paul EL, Atiemo-Obeng VA, Kresta SM. Eds.; Wiley: New York, 2004.

26 Moilanen P, Laakkonen M, Aittamaa J. Modeling aerated fermenters with computational fluid dynamics. *Ind Eng Chem Res*. 2006;45:8656-8663.

27 Moilanen P, Laakkonen M, Visuri O, Aittamaa J. Modeling local gas-liquid mass transfer in agitated viscous shear-thinning dispersions with CFD. *Ind Eng Chem Res*. 2007;46:7289-7299.

28 Montante G, Horn D, Paglianti A. Gas-liquid flow and bubble size distribution in stirred tanks. *Chem Eng Sci*. 2008;63:2107-2118.

29 Montante G, Paglianti A, Magelli F. Experimental analysis and computational modelling of gas-liquid stirred vessels. *Tran IChemE*. 2007;85:647-653.

30   Murthy BN, Joshi JB. Assessment of standard k-ε, RSM and LES turbulence models in a baffled stirred vessel agitated by various impeller designs. *Chem Eng Sci*. 2008;63:5468-5495.

31   Ranade VV, Van den Akker HEA. A Computational snapshot of gas-liquid flow in based stirred reactors. *Chem Eng Sci*. 1994;49:5175-5192.

32   Smagorinsky J. General circulation experiments with the primitive equations: 1. The basic experiment. *Mon Weather Rev*. 1963;91:99.

33   Somers JA. Direct simulation of fluid flow with cellular automata and the lattice-Boltzmann equation. *J Appl Sci Res*. 1993;51:127-133.

34   Sommerfeld M. Validation of a stochastic Lagrangian modeling approach for inter-particle collisions in homogeneous isotropic turbulence. *Int J Multiphas Flow*. 2001;27:1829-1858.

35   Sommerfeld M, Bourloutski E, Broeder D. Euler/Lagrange calculations of bubbly flows with consideration of bubble coalescence. *Can J Chem Eng*. 2003;81:508-518.

36   Sommerfeld M, Decker S. State of the art and future trends in CFD simulation of stirred vessel hydrodynamics. *Chem Eng Technol*. 2004;27:215-224.

37   Sommerfeld M, Kohnen G, Rueger M. Some open questions and inconsistencies of Lagrangian particle dispersion models. In *Proceedings of the Ninth Symposium on Turbulent Shear Flows*, Kyoto, Japan, 1993.

38   Sungkorn R, Derksen JJ, Khinast JG. Euler-Lagrange modeling of a gas-liquid stirred ractor with consideration of bubble breakage and coalescence, Submitted to *AIChE J.* (2011b).

39   Sungkorn R, Derksen JJ, Khinast JG. Modeling of turbulent gas-liquid bubbly flows using stochastic Lagrangian model and lattice-Boltzmann scheme. Accepted for publication in *Chem Eng Sci*. (2011a).

40   Venneker BCH. *Turbulent non-Newtonian fluid flow and gas dispersion in stirred vessels*, Ph.D. Thesis. University of Delft, The Netherlands, 1999.

41   Venneker BCH, Derksen JJ, Van den Akker HEA. Population balance modeling of aerated stirred vessels based on CFD. *AIChE J*. 2002;48:673-685.

42   Venneker BCH, Derksen JJ, Van den Akker HEA. Turbulent flow of shear-thinning liquids in stirred tanks – The effects of Reynolds number and flow index. *Chem Eng Res Des*. 2010;88:827-843.

43   Zhang Y, Yang C, Mao Z-S. Large eddy simulation of the gas-liquid flow in a stirred tank. *AIChE J*. 2008;54:1963-1974.

4.6 Appendix

Calculation of the Eddy-Particle Interaction Time (Hennick & Lightstone, 2000)

The time interval in which a bubble interacts with a randomly sampled velocity field, i.e., the eddy-particle interaction time t_e, is determined by the eddy lifetime t_{eddy} and the transit time t_{tr} as

$$t_e = \min\left(t_{eddy}, t_{tr}\right). \tag{A 4.1}$$

The eddy lifetime t_{eddy} is given by:

$$t_{eddy} = \frac{l_{eddy}}{|\mathbf{u}'|}, \tag{A 4.2}$$

with $\mathbf{u}'$ being the liquid phase velocity fluctuation. The dissipation length scale l_{eddy} is estimated by:

$$l_{eddy} = 0.3 \frac{k^{1.5}}{\varepsilon}, \tag{A 4.3}$$

with k being the turbulent kinetic energy.

The transit time of a bubble was simply estimated based on a linearized form of the equation of motion of the bubble in a uniform flow:

$$t_{tr} = -\tau_p \ln\left(1 - \frac{l_e}{\tau_p |\mathbf{u} - \mathbf{u}_p|}\right), \tag{A 4.4}$$

with the particle relaxation time τ_p

$$\tau_p = \frac{\rho_p d_p^2}{18 \rho \nu_{app}}. \tag{A 4.5}$$

5

CONCLUSIONS AND OUTLOOK

5.1   Summary

In this study, a novel modeling technique for a transient, full three-dimensional simulation of aerated stirred reactors within the dilute limit has been developed. The proposed model accounted for the underlying phenomena in both phases as well as the interactions between them. The model includes the following elements:

- The continuous phase is modeled using a variation of lattice-Boltzmann (LB) scheme due to Somers (1993) (see also Eggels & Somers, 1995; Derksen & Van den Akker, 1999). The scheme solves for the large-scale motions of the turbulent flow using the filtered conservation equations, where the Smagorinsky subgrid-scale model (Smagorinsky, 1963) has been used to model the effects of the sub-filter scales. The scheme has inherently high computational efficiency, especially on parallel platform, due to the locality of operations.

- An adaptive force-field procedure, also known as an immersed boundary method, due to Derksen et al. (1997) is used for describing the action of the reactor components (e.g., the impeller and tank wall) on the liquid flow field.

- A truncated power-law model introduced by Gabbanelli et al. (2005) is adopted to describe non-Newtonian behavior. Predefined maximum and minimum magnitude of the rate-of-strain-tensor were assumed to avoid mathematic singularity that can occur in the power-law model.

- The motion of the individual bubbles are computed by Lagrangian particle tracking model taking into account the sum of involving forces (e.g., stress gradients, net gravity and drag). The momentum transfer between phases is achieved by the mapping function with the virtual diameter concept introduced by Deen et al. (2004).

- Collisions of bubbles are governed by the so-called stochastic inter-particle collision (Sommerfeld, 2001). Based on the stochastic model, coalescence of bubbles is determined by comparing the film drainage time with the bubble contact time (Sommerfeld et al., 2003). Breakup of bubbles is accounted for using a theoretical model derived from the theory of isotropic turbulence (Luo & Svendsen, 1996). It is assumed that breakup is caused mainly by the interaction of bubbles with turbulent eddies.

5.2 Achievements and Conclusions

The major achievements of the presented work can be summarized as follows:

- The presented model has been validated with cases ranging from a case associated with simple to complex underlying phenomena, i.e., a bubble column (Chapter 2), an aerated stirred reactor with Newtonian liquid (Chapter 3) and an aerated stirred reactor with non-Newtonian liquid (Chapter 4). The validation results can be concluded as follows:

  o For Newtonian liquids, despite the limitation of grid resolution both mean and fluctuating liquid velocities are in excellent quantitative and qualitative agreement with the measured data from the literature. Thus, the modeling technique can be used with confidence to obtain detailed, quantitative insight into the dynamics of the continuous liquid phase.

  o For a single phase stirred reactor with non-Newtonian liquids, the averaged flow field can be accurately captured by the simulation. Due to the lack of turbulence model of non-Newtonian liquid and the lack of measured data in the range of interest, the accuracy of the predicted fluctuating liquid velocities (i.e., the second order statistic of the flow) is subjected to future research.

  o The stochastic inter-particle collision model was successfully incorporated into the model to take into account for the collisions between bubbles (or parcels of bubbles). The collision mode dramatically decreases computing time compared to the direct collision method and provide excellent computational efficiency on parallel platforms. Accordingly, collision statistic was used to determine coalescence between bubbles. Breakup of bubbles was treated as a stochastic event. Additional conditions have been proposed to obtain a correct breakup statistic. A good agreement between the predicted and measured bubble size distribution (BSD) has been achieved in the simulation of aerated stirred reactors with Newtonian liquids.

- In this work, it was demonstrated that a simulation with the grid size over bubble diameter ratio less than unity provides comparable accurate prediction with a simulation with the grid size over bubble diameter greater than unity. Note that, the ratio was typically restricted to a value greater than unity.

- The speedup and the scalability of the presented modeling technique on parallel platforms have been analyzed (Chapter 2). Excellent overall parallelization performance and scalability of the program were achieved. It was suggested that the maximum benefit of the presented modeling technique can be obtained when a large-scale simulation, in which the

ratio between the characteristic length and the bubble diameter is several order higher (i.e., industrial-scale reactors) and a massively parallelization are realized.

5.3   Future Work

It is clear that further development is required before the presented modeling technique can be used for design, scale-up and optimization of industrial-scale reactors. The following recommendations can be made for further study:

- The lattice-Boltzmann scheme which currently solves the single-phase conservation equations should be extended to include the void fraction, i.e., to recover the volume averaged conservation equations. This will enable us to study a multiphase reactor within the dense regime.

- Reliable subgrid scale models for multiphase flows as well as for non-Newtonian (multiphase-if possible) flows are to be developed and verified. This will require a use of a sophisticated first principle modeling approach.

- Due to the restriction of the grid size over bubble diameter ratio which limits us to use only coarse grid resolution (at least, in the study of laboratory-scale reactors), an alternative approach such as very-large-eddy simulation (VLES) should be employed to obtain a better turbulence prediction, especially in the near wall region.

- A more accurate daughter size distribution for the bubble breakup model should be determined. This can be done by the use of a first principle modeling approach.

- In order to study mixing in a stirred reactor, a modeling approach with high parallel efficiency, such as the lattice-Boltzmann scheme for advection-diffusion equations introduced by Ginzburg (2007) should be incorporated into the simulation.

- A program which utilizes the general purpose graphic processing units (GPGPUs), such as NVIDIA's CUDA environment, should be used to obtain massively parallelization and dramatically speedup of the simulation. This will also require a development of a (more) efficient parallelization strategy.

5.4   References

1   Deen NG, Van Sint Annaland M, Kuipers JAM. Multi-scale modeling of dispersed gas-liquid two-phase flow. *Chem Eng Sci*. 2004;59:1853-1861.

2   Derksen JJ, Kooman JL, Van den Akker HEA. Parallel fluid flow simulation by means of a lattice-Boltzmann scheme. *Lect Notes Comput Sci*. 1997;125:524.

3   Derksen JJ, Van den Akker HEA. Large eddy simulation on the flow driven by a Rushton turbine. *AIChE J*. 1999;45:209-221.

4   Eggels JGM, Somers JA. Numerical simulations of free convective flow using the lattice-Boltzmann scheme. *Int J Heat Fluid Flow*. 1995;16:357-364.

5   Gabbanelli S, Drazer G, Koplik J. Lattice Boltzmann method for non-Newtonian (power-law) fluids. *Phy Rev E*. 2005;72:046312.

6   Ginzburd I. Lattice Boltzmann modeling with discontinuous collision components: Hydrodynamic and advection-diffusion equations. *Journal of Statistical Physics*. 2007;126:157-206.

7   Luo H, Svendsen HF. Theoretical model for drop and bubble breakup in turbulent dispersions. *AIChE J*. 1996;42:1225-1233.

8   Smagorinsky J. General circulation experiments with the primitive equations: 1. The basic experiment. *Mon Weather Rev*. 1963;91:99.

9   Somers JA. Direct simulation of fluid flow with cellular automata and the lattice-Boltzmann equation. *J Appl Sci Res*. 1993;51:127-133.

10   Sommerfeld M, Bourloutski E, Broeder D. Euler/Lagrange calculations of bubbly flows with consideration of bubble coalescence. *Can J Chem Eng*. 2003;81:508-518.

11   Sommerfeld M. Validation of a stochastic Lagrangian modeling approach for inter-particle collisions in homogeneous isotropic turbulence. *Int J Multiphas Flow*. 2001;27:1829-1858.

List of publications

1. Sungkorn R, Derksen JJ, Khinast JG. Modeling of turbulent gas-liquid bubbly flows using stochastic Lagrangian model and lattice-Boltzmann scheme. Accepted for publication in *Chemical Engineering Science* (2011).

2. Sungkorn R, Derksen JJ, Khinast JG. Euler-Lagrange modeling of a gas-liquid stirred reactor with consideration of bubble breakage and coalescence. Submitted to *AIChE Journal* (2011).

3. Sungkorn R, Derksen JJ, Khinast JG. Modeling of aerated stirred tanks with non-Newtonian liquids. Submitted to *International Journal of Multiphase Flow* (2011).

About the author

Radompon Sungkorn was born on October tenth, 1981 in Songkhla, Thailand. He grew up in Bangkok and completed his secondary school education at Suankularb wittayalai school in 1999 and becomes an old Suankularb (OSK 118) alumnus. During the period between 1999 and 2003, he studied chemical engineering at Chulalongkorn University.

After the completion of his bachelor study, Radompon started his MSc study in mechanical engineering (Maschinenbau) at the Leibniz University of Hanover, Germany. During his MSc study, he carried out projects on the subject of multiphase flow in screw pump numerically and experimentally at the Institute for Process Engineering of Professor Dieter Mewes and completed his MSc in August 2007.

In September 2007, Radompon started as a PhD student in the group of Professor Johannes Khinast at the Institute of Process and Particle Engineering, Graz University of Technology, Austria. During his PhD, Radompon conducted various industrial researches with close collaboration with number of pharmaceutical companies. In the fall of 2009, Radompon was selected to participate the Novartis Biotechnology Leadership Camp 2009 in Basel, Switzerland. In the fall of 2010, Radompon visited the group of Professor Jos Derksen at the Department of Chemical and Materials Engineering, University of Alberta, Canada. His research visiting was supported by the short time academic research program (KUWI) granted by Graz University of Technology. Radompon also collaborated with Dr. Benjamin Ahrenholz of the Institute for Computational Modeling in Civil Engineering at the Technische Universität Braunschweig, Germany, on the subject of solid-liquid flow modeling using lattice-Boltzmann scheme.

In July 2011 he started his post-doctoral research at the group of Professor Jos Derksen at the University of Alberta, Canada. His research topic is in the area of lattice-Boltzmann method for multiphase large-scale flows.